Antarctic sea ice : a seasonal perspective

Kenza Himmich

THESE DE DOCTORAT DE SORBONNE UNIVERSITE

Ecole Doctorale : 129 - Sciences de l'Environnement d'Ile de France

Spécialité : Océanographie Physique

réalisée au

Laboratoire d'Océanographie et du Climat: Expérimentations et Approches Numériques

présentée par

Kenza Himmich

pour obtenir le grade de

Docteur de Sorbonne Université

Titre de la thèse

Antarctic Sea Ice: a Seasonal Perspective

Soutenance prévue le 25 avril 2024 devant le jury composé de :

Rapportrice	Cecilia Bitz	University of Washington
Rapporteur	Alexander Haumann	Alfred Wegener Institute
Président du jury	Damien Cardinal	LOCEAN, Paris
Examinatrice	Rym Msadek	CERFACS, Toulouse
Directeur de thèse	Martin Vancoppenolle	LOCEAN, Paris
Directeur de thèse	Gurvan Madec	LOCEAN, Paris

Abstract

Antarctic sea ice has undergone an abrupt reduction in 2016, following more than four decades of a slow increase. This could have wide-ranging consequences given the importance of Antarctic sea ice for climate, ocean, and local ecosystem. Yet, climate models fail to capture this observed evolution, leaving considerable uncertainty regarding its origin, impacts and future evolution. Models failure relates, but not only, to a poor understanding of fundamental Antarctic sea ice processes. In this thesis, we contribute to progress understanding of Antarctic sea ice, adopting a seasonal perspective. We investigate the drivers of seasonal sea ice edge advance and retreat, analyzing the roles of thermodynamic preconditioning, air-ice-sea heat fluxes and sea ice dynamics. We show that, in the mean state, timings of ice edge advance and retreat are largely controlled by thermodynamics, via preconditioning from mixed layer heat content and sea ice thickness, respectively. Variations in air-ice-sea heat fluxes and sea ice dynamics have a significant but secondary importance. This conclusion is supported by a simple thermodynamic model, observational analyses and the NEMO ice-ocean model. We also show that recent changes in sea ice seasonality are mainly driven by thermodynamics, similar to the mean state. The reduction in Antarctic sea ice following 2016 coincides with nearly circumpolar earlier retreat and later advance of the ice edge. Our analysis links these changes to thinner ice in winter, faster melt in spring and warmer upper ocean in summer, in line with ice-albedo feedback processes. Based on the circumpolar footprint of these changes, we argue that they likely have an oceanic origin.

Keywords: Antarctic sea ice, Southern Ocean, sea ice retreat, sea ice advance, seasonal cycle, recent changes, ice-ocean interactions.

Résumé

La banquise antarctique a subi une réduction brutale en 2016, après plus de quatre décennies d'une lente augmentation. Une telle évolution pourrait avoir de larges conséquences, compte tenu de l'importance de la banquise antarctique pour le climat, l'océan et l'écosystème marin polaire local. Pourtant, les modèles climatiques ne parviennent pas à reproduire les changements observés, laissant planer une incertitude considérable quant à leur origine et à leurs conséquences. Cette déficience des modèles est en partie due à une mauvaise compréhension des processus fondamentaux liés à la banquise antarctique. Dans cette thèse, nous contribuons à faire progresser cette compréhension, en adoptant une perspective saisonnière. Les processus moteurs de l'avancée et du retrait saisonniers de la banquise sont explorés. En particulier, les rôles possibles d'un préconditionnement thermodynamique, des flux de chaleur air-glace-mer et de la dynamique de la banquise sont étudiés. Nous montrons, dans l'état moyen, que les dates d'avancée et de retrait de la banquise sont largement contrôlées par des processus thermodynamiques, à travers un préconditionnement respectif du contenu thermique de la couche de mélange et de l'épaisseur de la banquise. Les variations des flux de chaleur air-glace-mer et la dynamique de la banquise ont une importance significative mais secondaire. Ces conclusions sont étayées par un modèle thermodynamique simple, des analyses d'observations et un modèle glace-océan (NEMO). Nous montrons également que les changements récents dans la saisonnalité de la banquise sont principalement dus à des processus thermodynamiques, comme pour l'état moyen. La réduction de la banquise antarctique suivant l'année 2016 coïncide avec un recul plus précoce et une avancée plus tardive de la banquise, à l'échelle quasi-circompolaire. Notre analyse relie ces changements à une glace plus fine en hiver, une fonte plus rapide au printemps et un océan de surface plus chaud en été, en accord avec les processus de la rétroaction glace-albédo. L'empreinte circumpolaire de ces changements leur suggère une cause océanique.

Mots-clés: Banquise antarctique, Océan Austral, retrait de la banquise, avancée de la banquise, cycle saisonnier, changements récents, interactions océan-banquise.

Ph.D. Retrospective

Publications in peer-reviewed scientific journals

Goosse, H., Allende Contador, S., Bitz, C. M., Blanchard-Wrigglesworth, E., Eayrs, C., Fichefet, T., **Himmich, K.**, Huot, P.-V., Klein, F., Marchi, S., Massonnet, F., Mezzina, B., Pelletier, C., Roach, L., Vancoppenolle, M., and van Lipzig, N. P. M. (2023). Modulation of the seasonal cycle of the Antarctic sea ice extent by sea ice processes and feedbacks with the ocean and the atmosphere, *The Cryosphere, 17, 407–425,* . doi: 10.5194/tc-17-407-2023,

Himmich, K., Vancoppenolle, M., Madec, G., Sallée, J.-B., Holland, P. R., & Lebrun, M. (2023). Drivers of Antarctic sea ice advance. *Nature Communications*, 14(1). doi: 10.1038/s41467-023-41962-8

Himmich, K., Vancoppenolle, M., Stammerjohn S., Bocquet M., Madec G., Sallée, J.-B. & Fleury S. (*in revision in JGR Oceans*). Thermodynamics Drive Changes in the Antarctic Sea Ice Seasonal Cycle Following 2016.

Meiners K. M., Vancoppenolle M., Massom R. A., **Himmich K.**, Wongpan P., Lannuzel D., Flores H., *et al.* (*in preparation*). Perspective: Implications of sea-ice change for Southern Ocean ecosystems and biogeochemical cycles.

International Conferences

Himmich, K., Vancoppenolle, M., Madec, G., Sallée, J.-B., Lebrun, M. . Changes in Antarctic sea ice seasonality over the last 4 decades. EGU General Assembly 2021, held online.

Himmich, K., Vancoppenolle, M., Madec, G., Sallée, J.-B., Lebrun, M., Holland P. . Drivers of Antarctic sea ice advance. Ocean Science Meeting 2021, held online.

Himmich, K., Vancoppenolle, M., Madec, G., Sallée, J.-B., Lebrun, M., Holland P. . Drivers of Antarctic sea ice advance. EGU General Assembly 2022, held in Vienna (Austria).

Himmich, K., Stammerjohn S., Vancoppenolle, M., Madec, G. . Understanding recent changes in Antarctic sea ice seasonality. EGU General Assembly 2023, online presentation.

Himmich, K., Vancoppenolle, M., Stammerjohn, S., Madec, G. . Understanding recent changes in Antarctic sea ice seasonality. IGS Symposium 2023, held in Bremerhaven (Germany).

Seminars

Himmich, K., Vancoppenolle, M., Madec, G. (2022). Drivers of Antarctic sea ice advance. Earth & Climate research group at UCLouvain (Louvain-la-Neuve, Belgium).

Himmich, K., Vancoppenolle, M., Madec, G. (2022). Drivers of Antarctic sea ice advance. Earth & Climate research group at UCLouvain (Louvain-la-Neuve, Belgium).

Himmich, K., Vancoppenolle, M., Madec, G. (2022). Seasonal cycle of Antarctic sea ice. Paleo and Polar Climate Section research group at NCAR (Boulder, CO, USA).

Himmich, K., Vancoppenolle, M., Madec, G. (2023). Understanding recent changes in Antarctic sea ice seasonality. Antarctic Sea Ice and Southern Ocean Seminars, held online.

Fellowships

SCAR INSTANT (“Instabilities and Thresholds in Antarctica") Fellowship. Funding to visit Sharon Stammerjohn at UC Boulder’s INSTAAR lab.

Oceanographic cruises

December 2022 - March 2023, PS134. 11 weeks on board on the Polarstern. Cape Town - Neumayer (Antarctica) - Bellingshausen Sea - Puntas Arenas. Oceanographic moorings deployment and retrieval. Sediment coring.

Courses

Seminar "Impacts du changement climatique", ED129 (21h)

Seminar "Changement climatique : sciences, sociétés, politique", ENS (24h)

Course "Modélisation statistique - application de l’analyse en Composante Principale", ED129 (40h)

Seminar "JDD: Journées des doctorants 2023" (15h)

Activities in the Laboratory

Took part in the implementation of a monitoring committee within the lab aimed at ensuring the smooth progress of PhD students .

Acknowledgements

First, I would like to thank each jury members of this PhD. Thank you, Cecilia Bitz and Alexander Haumann, for accepting to review this thesis. I am also grateful to Rym Msadek for serving as an examiner, and to Damien Cardinal for presiding over the jury.

I would also like to thank all the people involved in any way in my PhD, and without whom the work presented here would not have been possible.

I am deeply grateful to Martin Vancoppenolle and Gurvan Madec, for their great supervising. I could not have imagined better PhD supervisors. Martin, merci pour tout ! Pour ton implication et ta disponibilité sans pareilles, pour tous tes précieux conseils, pour les nombreuses relectures et surtout, pour tes fameuses blagues qui ont rendu ma thèse bien plus marrante. Je te suis particulièrement reconnaissante de m'avoir poussée et aidée à partir en visite, de l'autre côté de l'Atlantique, et en mer, en Antarctique. Gurvan, merci d'avoir été présent à chaque fois que j'en avais besoin, de m'avoir conseillée et partagé tes idées de génie.

I am grateful to Sharon Stammerjohn, for her warm welcome at UC Boulder and her great scientific inputs. Thank you, Sharon, for all the enriching discussions, the orchid lighting up my desk for a few weeks, and for John's book, which gave me a beautiful teaser of the Antarctic wonders.

Merci à mon comité de suivi, à Casimir de Lavergne, Jean-Baptiste Sallée et François Massonnet pour toutes les discussions scientifiques qui ont largement enrichi ma thèse. Je te suis aussi profondément reconnaissante, JB, de m'avoir permis d'aller en mer (et pas n'importe où !) et de finir ma thèse sereinement, plus tard que prévu.

Je souhaite également remercier Hugues Goosse, de m'avoir accueillie à Louvain et d'avoir si gentiment partagé ses simulations avec moi. Merci aussi à Christian Ethé, pour ton aide et ta patience, sans lesquelles mes propres simulations n'auraient jamais tourné.

Finally, I would like to thank all the people who have contributed to making this PhD such a great journey.

I am grateful to all the people of the PS134 expedition. To Johannes Klages, and to all the geology team, thank you for "adopting me" as your own, and showing me the muddy wonders of the ocean's bottom. Antonio, je repense avec beaucoup de nostalgie aux quelques jours passés au milieu de caisses en bois, à visser, dévisser, porter, assembler, rythmés par la houle (du jamais vu, ces « big storms ») et la musique de Novos Baianos. Merci pour ta patience, ta

bonne humeur ; pour tous nos rires et tes belles histoires !

Au bureau 431, que je n'aurais échangé pour aucun autre, même plus lumineux et moins poussiéreux, mille merci. À Chab et aux GG, aux plus vrais des faux-amis, sans vous, mes premières années au LOCEAN auraient été bien mornes (et sûrement plus productives). Merci d'avoir égayé mes journées. Merci aussi pour le soutien, les farces, les rires et j'en passe. À Margaux, Mathieu, Matthias et Hervé, merci d'avoir supporté mon silence ennuyeux pendant cette dernière année de thèse, et de m'avoir fait rire et fourni en chocolat quand le moral était bas.

Merci aux plus anciens doctorants, à Antoine, Batoul, Clara, Clovis, Clément, Diego, Gaston, Linus, Matthis, Robin, qui ont perdu du temps avec moi, à rire et à refaire le monde, pendant de (trop) longues pauses café. Antoine, Clément, Gaston et Linus, je ne vous remercierai jamais assez de m'avoir accueillie, écoutée et supportée, dans votre bureau, à chaque fois que j'en avais marre.

Et merci aux plus jeunes et à tous les nouveaux arrivants qui ont réussi à égayer encore plus les couloirs du LOCEAN.

À mes parents, merci de toujours m'encourager et me soutenir, même si c'est pour me retrouver loin de vous, au bout du monde. À Valentin, merci d'avoir été là, tout le temps, même de loin. Merci pour l'écoute, le réconfort, les encouragements à chaque fois que j'en avais besoin et pour tout le reste.

Contents

General Introduction

On February 21st, 2023, I was on board of the Polarstern icebreaker, navigating through uncharted iceless waters close to the west Antarctic ice shelves. These regions had been inaccessible in previous years due to year-round sea ice coverage. It soon became evident that I was witnessing a historic minimum for Antarctic sea ice cover, unprecedented since the start of satellite observations in the late 1970s. This record low marks the third in a series since 2016, abruptly placing Antarctic sea ice into a low-extent state after over 40 years of gradual increase. One year later, as I write these words, the summer Antarctic sea ice cover remains notably low, well below its average extent.

The recent reductions in Antarctic sea ice have drawn significant attention from the general public, nearly overshadowing concerns for the rapid decline of Arctic sea ice. However, unlike the Arctic, where the decrease in sea ice is a clear consequence of increased atmospheric CO_2, it remains uncertain whether recent reductions in Antarctic sea ice can be attributed to climate change. This uncertainty is partly due to the complexity and limited understanding of fundamental Antarctic sea ice processes, notably those driving seasonal sea ice growth and decay. The main aim of my thesis is to progress this understanding.

1 Importance of Antarctic Sea Ice

Encircling the Antarctic continent and extending to 30-35°S, the Southern Ocean stands as the largest ocean on Earth and a major component of global ocean circulation and climate. Unrestricted by any continental barriers, it connects the Pacific, Atlantic and Indian oceanic basins, distributing heat, salt and carbon among them through the global overturning circulation. It is also a region of substantial vertical exchanges, linking the surface and deep layers of the ocean. Through these processes, the Southern Ocean represents a major sink of atmospheric carbon and heat, accounting for 40% of anthropogenic CO2 and 75% of heat uptake by the ocean (Frölicher et al., 2015).

The Southern Ocean, similar to its northern counterpart in the Arctic, is covered by sea ice – a thin layer of frozen seawater that floats on the ocean surface (Figure 1). The Antarctic sea ice cover can reach around 19 million square kilometers in winter. However, most of it vanishes by summer. Only about 3 million square kilometers of perennial ice remain near the Antarctic coasts (Parkinson, 2019). Antarctic sea ice thus exhibits a pronounced seasonal cycle, resulting from a number of processes involving the ocean and the atmosphere. Sea ice grows from seawater freezing, when the ocean surface layer is cooled down to the freezing temperature (~ - 1.8°C) (Talley et al., 2011; Thompson et al., 2020), and decays through melting, under heat inputs from both the ocean and the atmosphere. In addition to thermodynamics, sea ice dynamics can also contribute to its seasonal variations (e.g. Holland & Kimura, 2016), as sea ice is continuously moved around by winds and currents.

Despite covering up only a small fraction of the Earth's surface (~4% in winter), Antarctic sea ice and related seasonal processes have a substantial influence on ocean circulation and climate, and are crucial for the Antarctic marine ecosystem and continental ice.

First, Antarctic sea ice influences Southern Ocean dynamics and biogeochemical processes, thus affecting its ability to absorb atmospheric heat and carbon. Sea ice acts as a physical barrier for the Southern Ocean, constraining air-sea transfers of carbon (Shadwick et al., 2021), heat (Turner et al., 2013) and momentum (McPhee, 1992). Seasonal sea ice growth and melt releases dense brine or light freshwater into the underlying ocean. These processes modify the Southern Ocean's stratification (Pellichero et al., 2017), and ultimately drive the formation of key water masses contributing to the global ocean overturning circulation (Abernathey et al., 2016; Jacobs, 2004; Pellichero et al., 2018) and to the uptake of heat and carbon (e.g. Marshall & Speer, 2012). Finally, Antarctic sea ice contributes to primary production and resulting biological carbon pump, as an efficient iron conveyor (Person et al., 2021).

Second, Antarctic sea ice has an impact on the local and global climate. Sea ice influences the surface energy budget. In winter, it insulates, via its low conductivity (Pringle et al., 2007), the cold atmosphere from the warmer underlying ocean. In summer, the high albedo of the sea ice surface (Perovich et al., 2002) prevents a significant portion of solar radiation from penetrating into the ocean. At larger scales, Antarctic sea ice also influences the Earth's energy budget through a number of radiative feedbacks involving sea ice (Goosse et al., 2018; Riihelä et al., 2021). In addition, climate models suggest that changes in Antarctic sea ice may affect the global atmospheric circulation (Ayres & Screen, 2019; Aiken & England, 2008; Ayres et al., 2022).

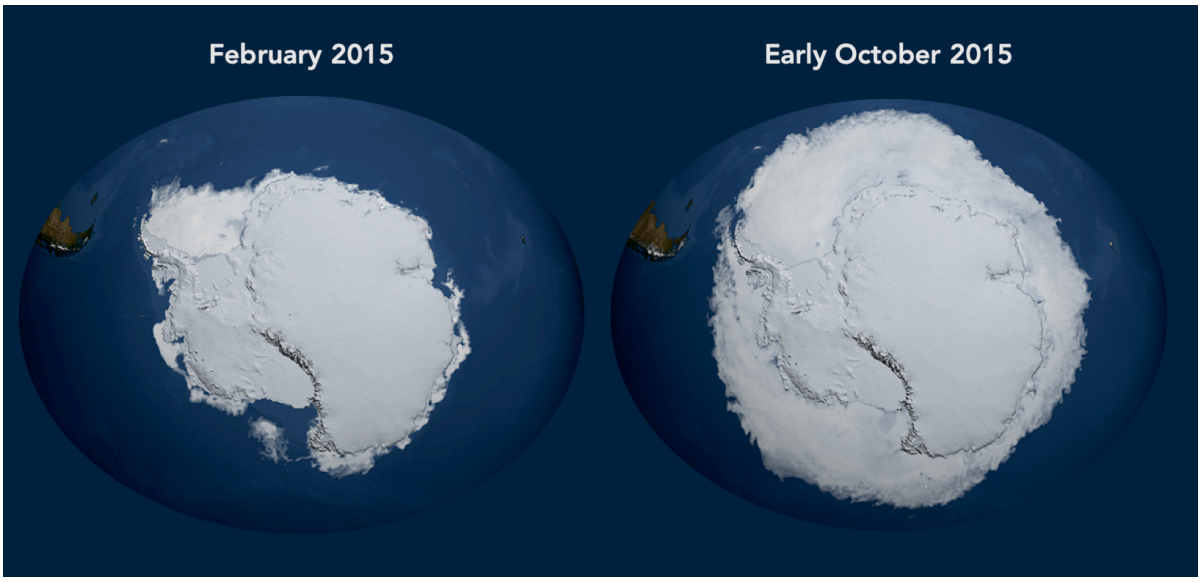

Figure 1: **The Antarctic sea ice extent seasonal cycle.** Antarctic sea ice in February and Early October 2015, adapted from NASA's Goddard Space Flight Center Scientific Visualization Studio. Source: https://svs.gsfc.nasa.gov/.

Last, sea ice serves as a protective barrier for ice shelves against swell (Massom et al., 2018, 2010). Furthermore, Antarctic sea ice is a habitat for endemic species, from algae to marine mammals. It also influences the underlying marine ecosystem. Sea ice forms a habitat for ice algae (Lizotte, 2001) and releases important nutrients (e.g. iron) during the melt season, fertilizing phytoplankton (Person et al., 2021; Smith & Nelson, 1986). Furthermore, many species depend on Antarctic sea ice for shelter, breeding and food (Bester et al., 2017). The 2022 large breeding failure in western Antarctic penguin colonies, caused by an abrupt in sea ice reduction in spring, highlights this critical dependency (Fretwell et al., 2023).

Based on the previous arguments, changes in Antarctic sea ice in the context of rising atmospheric CO_2 could have wide-ranging consequences. Hence, understanding recent Antarctic sea ice changes and anticipating future ones is crucial. However, observed changes are complex, and Earth System Models struggle to accurately reproduce them, resulting in low confidence in their projections of the future.

2 Recent and Future Antarctic Sea Ice Changes

2.1 Recent changes

Sea ice extent has been monitored on a near-daily basis since 1979, using satellite passive-microwave retrievals of sea-ice concentration. The resulting time series are shown in Figure 2. Unlike Arctic sea ice which has steadily decreased since 1979, Antarctic sea ice extent has slowly increased over 1979-2016 and then abruptly decreased after 2016. Regional changes are generally consistent with integrated ones, except for the Amundsen-Bellingshausen Seas, where the sea ice extent has decreased until 2007 then increased (Comiso et al., 2017; Parkinson, 2019). In the context of rising global temperature and rapid decline of Arctic sea ice, such behaviour of the Antarctic sea ice cover is puzzling for the scientific community. Previous studies have nonetheless investigated the causes of these recent Antarctic sea ice changes, suggesting a role for both atmospheric and oceanic processes.

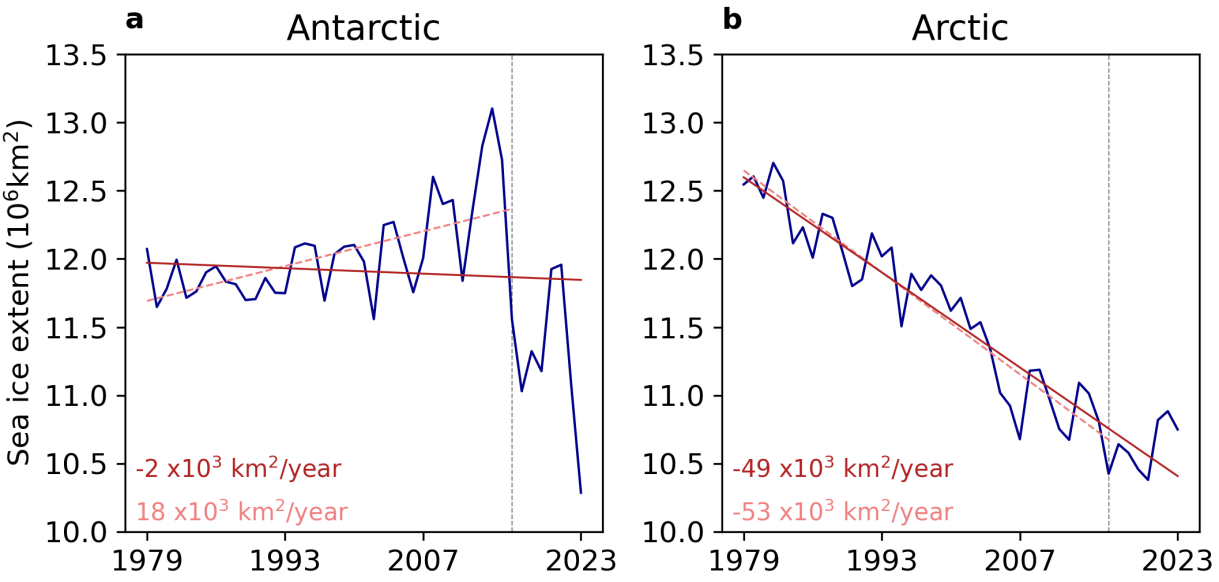

Figure 2: **Evolution of the sea ice extent over the satellite period era.** Timeseries of **a**, Antarctic and **b**, Arctic annual sea ice extent over 1979-2023, based on OSI SAF Sea Ice Index v2.2 (Ocean and Sea Ice Satellite Application Facility., 2023). Trend lines are obtained using a linear least squares fit regression over 1979-2023 (red) and 1979-2016 (pink). Corresponding trend lines slopes are shown.

Atmospheric processes impacting sea ice at the interannual timescale are linked to Southern Ocean wind changes, often driven by variability in the Amundsen Sea Low (ASL) (Clem & Fogt, 2013; Holland & Kwok, 2012; Hosking et al., 2013) or various climate modes such as El Niño Southern Oscillation (ENSO) (Yuan, 2004) and the Southern Annular Mode (SAM) (Stammerjohn et al., 2008). Notably, wind anomalies may have contributed to the abrupt sea ice extent decrease following 2016. Anomalous southward winds produced by tropical

teleconnections (Meehl et al., 2019) and a negative phase of the SAM (Schlosser et al., 2018; Turner et al., 2017) have transported warm air and surface waters southward, and kept sea ice confined to southern regions (Stuecker et al., 2017; Turner et al., 2017). In the longer term, however, the role of atmospheric modes in driving Antarctic sea ice trends remains unclear. Previous studies have notably attributed the overall sea ice extent increase until 2016 to positive SAM-driven eastward wind anomalies, resulting in cooler sea surface temperature and northward sea ice transport, expanding the sea ice cover (Thompson et al., 2011; Zhang, 2014). Yet, Simpkins et al. (2012) found no statistically significant link between the trends in sea ice area. On the regional scale, the sea ice decrease in the Amundsen and Bellingshausen Seas has been attributed to ASL-driven southward wind anomalies, warming the sea surface and limiting sea ice growth (Holland & Kwok, 2012).

The Southern Ocean has also been changing over the last decades, possibly contributing to sea ice variability. The positive trend in sea ice extent before 2016 has been linked to observed ocean surface cooling (Fan et al., 2014) and freshening (Durack & Wijffels, 2010), itself possibly driven by an increase in precipitation (Liu & Curry, 2010), in melt water inputs (Bintanja et al., 2013; Pauling et al., 2016; Swart & Fyfe, 2013) or by changes in sea ice transport (Haumann et al., 2016). Furthermore, the decline in sea ice extent following 2016 coincides with a warming of the ocean subsurface within the sea ice zone, suggesting that subsurface warming has played a role in the recent sea ice changes (Meehl et al., 2019; Purich & Doddridge, 2023; Zhang et al., 2022). Subsurface warming has been attributed to wind-driven suction of warm relatively deep waters towards the surface (Ferreira et al., 2015; Kostov et al., 2017; Meehl et al., 2016), and to increased stratification limiting the ventilation of the subsurface (Haumann et al., 2020). Nevertheless, the mechanism through which this warming has affected sea ice remains unclear.

Observational limitations, notably regarding sea ice thickness and Southern Ocean hydrography, contribute to complicate the understanding of observed Antarctic sea ice changes (Macalady & Thomas, 2017). First, to comprehensively characterize sea ice changes, both ice area and thickness should be examined. However, large-scale monthly estimates of sea ice thickness, provided by satellite altimetry, have several limitations. Being relatively recent, these estimates come with significant uncertainties, due to unreliable measurements of snow depth and sea ice and snow densities (Giles et al., 2008; Kern & Spreen, 2015). Additionally, the time series from altimetry missions (e.g. ERS-1, ERS-2, Envisat, and CryoSat) are individually too brief to capture the long-term variability of ice thickness. The work of Bocquet (2023) has recently addressed this limitation by inter-calibrating and merging time series back to 1993 from the different altimetry missions (Figure 3a). Second, Antarctic sea ice changes are linked to the underlying ocean, for which hydrographic measurements are historically sparse

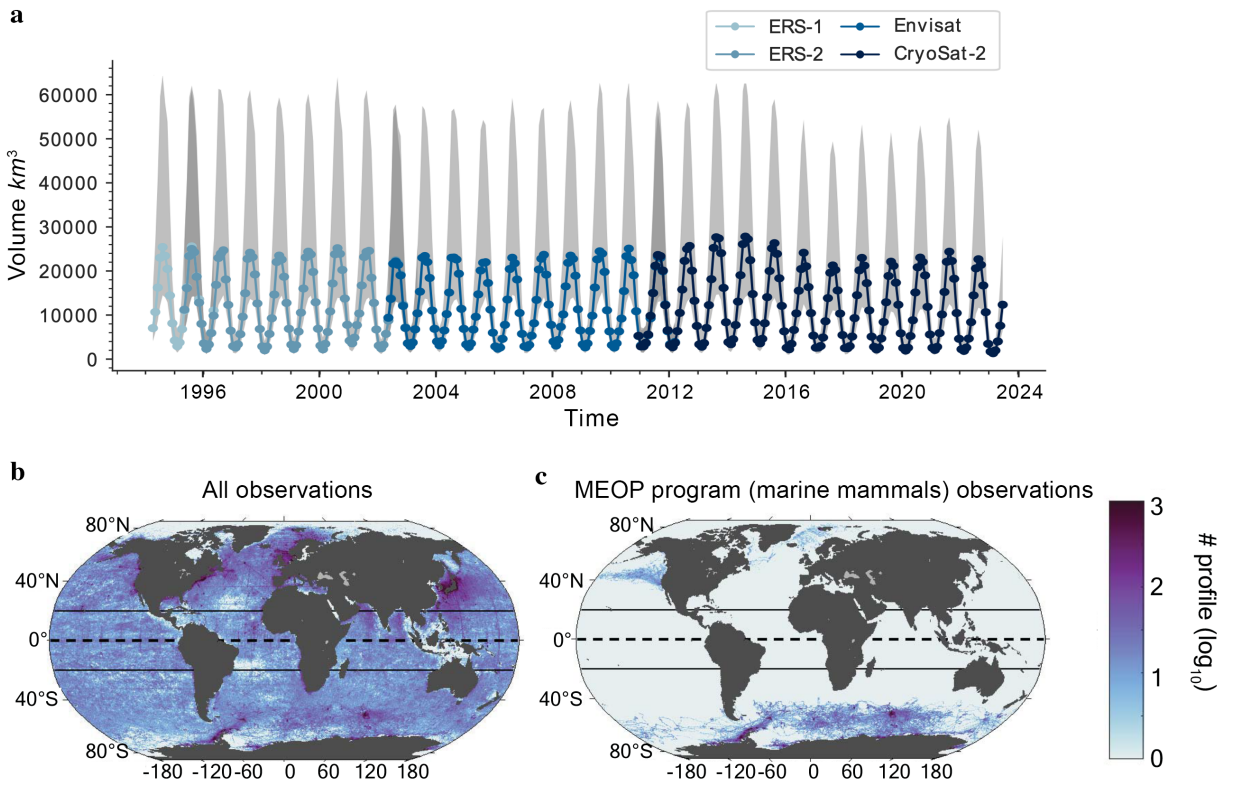

Figure 3: **Illustration of recent observational progresses in observing hydrography and sea ice thickness in the Southern Ocean.** **a**, Antarctic sea ice volume derived from passive microwave sea ice concentration and merged time series of ice thickness from four altimetry missions (Envisat-CCI, CryoSat-2-DCCI, ERS1 and ERS2). Grey shading in **a** shows the associated 5-95% ensemble quantiles. Number of mixed layer estimates in 1° × 1° longitude–latitude bins from **b**, all available observation sources (ships, Argo floats and marine mammals profiles) and **c**, from instrumented marine mammal observations. Figures from Bocquet (2023) (**a**) and Sallée et al. (2021) (**b**, **c**).

compared to other regions (Figure 3b). This prevents a comprehensive and reliable assessment of regional and vertical variability in ocean state. However, extensive observations by international programs since 2000 (e.g. Argo, MEOP), notably via elephant seal-borne sensors and automated floats (Figure 3c) have facilitated the development of monthly climatological maps of key hydrographic properties within the sea ice zone (Pellichero et al., 2017; Sallée et al., 2021). These datasets may help progress the understanding of ice-ocean interactions.

2.2 Future changes

Earth System Models provide valuable tools to understand climate variability and project future climate change. The Coupled Model Intercomparison Project (CMIP), enables the assessment of different climate models by establishing a common protocol for model experiments. Yet, regarding Antarctic sea ice, the latest CMIP models (CMIP6) have not been able to reproduce the observed changes. Most CMIP6 models simulate a decrease in sea ice extent over 1979-2018 (Roach et al., 2020), contrasting with observations.

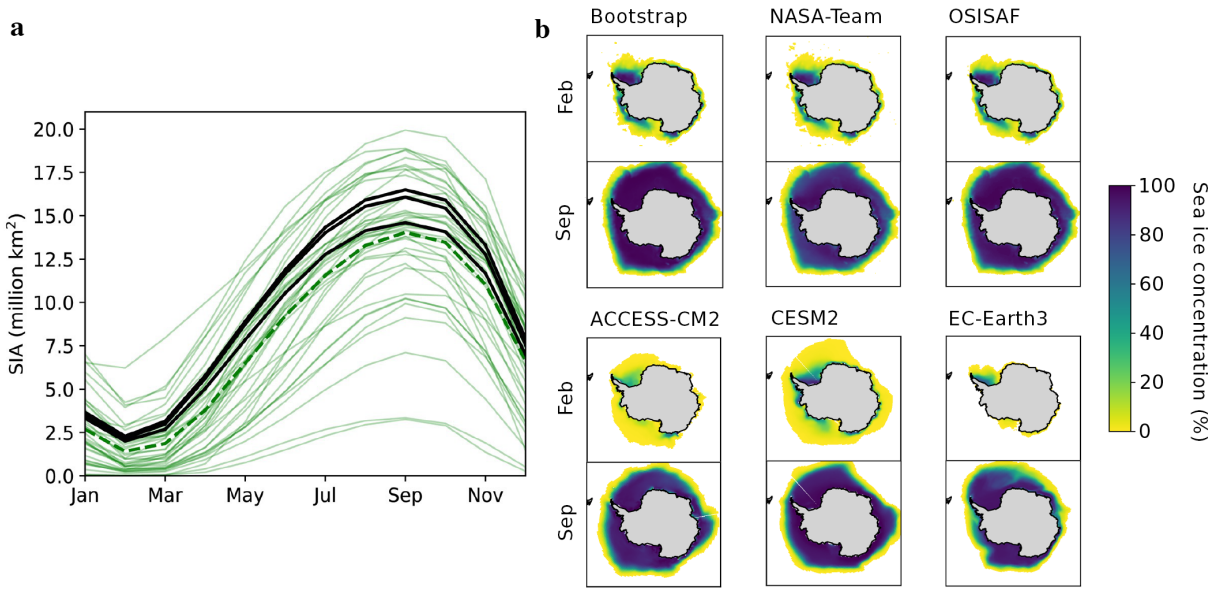

Figure 4: **Antarctic sea ice in global climate models.** **a**, Mean seasonal cycle in Antarctic sea ice area (SIA) over 1979–2014 for individual CMIP6 models (faint green lines), the CMIP6 multi-model mean (thick green dashed line), and three observational products (Bootstrap, NASA-Team, and OSI-SAF; black lines). Mean 1979-2014 September (**e-f**; **k-m**) and February (**e-d**; **h-j**) Antarctic sea ice concentration for observations (black frames) and three selected CMIP6 models (green frames). Figures from Roach et al. (2020).

Various reasons for this mismatch emerge from previous work. The observed changes could fall within the range of internal variability (Polvani & Smith, 2013; Zhang et al., 2019; Zunz et al., 2013; Singh et al., 2019). Other studies point to model biases and the lack of representation of specific processes. For instance, reducing biases in the Southern Ocean's sea surface temperature and winds reconciles observed and modelled trends (Blanchard-Wrigglesworth et al., 2021; Roach et al., 2023). Furthermore, CMIP6 models improperly represent (if at all) glacial meltwater inputs to the ocean. Such inputs could contribute to cooling the surface ocean and hence, to increasing the sea ice extent (Bintanja et al., 2013; Roach et al., 2023; Schloesser et al., 2019).

In addition, climate models feature substantial problems in simulating the Antarctic sea ice mean state, potentially contributing to their inability to replicate observed sea ice changes. CMIP6 models exhibit considerable intermodel spread in simulating the mean seasonal cycle of sea ice extent, with the multimodel mean consistently lower than observed throughout the year and several models completely loosing summer ice (Figure 4a) (Roach et al., 2020). The processes driving the Antarctic sea ice seasonal cycle thus differ across models, and may not be realistic. Regionally, the discrepancy is also evident: the spatial distribution of sea ice concentration in CMIP6 models significantly differs from observations, for both winter and summer (Casagrande et al., 2023). These difficulties are highlighted in Figures 4b-m, for

three widely used CMIP6 models. The simulated SIC field presents large differences from observations and among models, in particular during summer. These discrepancies provide another illustration of model issues in simulating seasonal sea ice processes, coming down to limitations in our understanding.

Considering the inadequately simulated Antarctic sea ice within CMIP6 models, particularly at regional scales, the latest Intergovernmental Panel on Climate Change report (IPCC-AR6) concluded that "there is low confidence in model simulations of future Antarctic sea ice decrease, and lack of decrease", in response to increasing atmospheric CO_2 (Fox-Kemper et al., 2021).

In this thesis, I hypothesize that improving our process-scale understanding can contribute to reduce the uncertainty in Antarctic sea ice. In particular, I address the limitations in the understanding of the processes shaping the sea ice seasonal cycle, as illustrated by the disagreement between models and observations regarding seasonal patterns (Figure 4). While the nature of these processes is well-known, how they act in synergy and drive Antarctic sea ice seasonality and its related changes at the local scale remains to be established.

3 Antarctic Sea Ice Seasonality

3.1 Seasonal sea ice processes: from circumpolar to local scale

Sea ice extent. Many previous studies have explored the processes shaping the mean seasonal cycle of Antarctic sea ice extent, notably its asymmetric behavior of a slow advance followed by a fast retreat (Figure 4a). The seasonal cycle of incoming solar radiation has been identified as the main contributor to this asymmetric behavior (Roach et al., 2022), with a possible contribution of wind-driven sea ice transport (Eayrs et al., 2019; Enomoto & Ohmura, 1990) and oceanic heat input (Gordon, 1981). In addition, a series of model-based sensitivity experiments was performed by Goosse et al. (2023) to examine the influence of specific processes on this mean seasonal cycle. Their findings suggest that the evolution of the sea ice extent, respectively during the advance and retreat seasons, is strongly dependent on the initial summer ocean and winter sea ice conditions. Hence, initial sea ice and ocean conditions, heat fluxes and sea ice drift have been identified as important drivers of the mean-state sea ice extent seasonality. Nonetheless, these previous studies all adopted a circumpolar approach, overlooking regional specificities which are essential to fully understand sea ice seasonality.

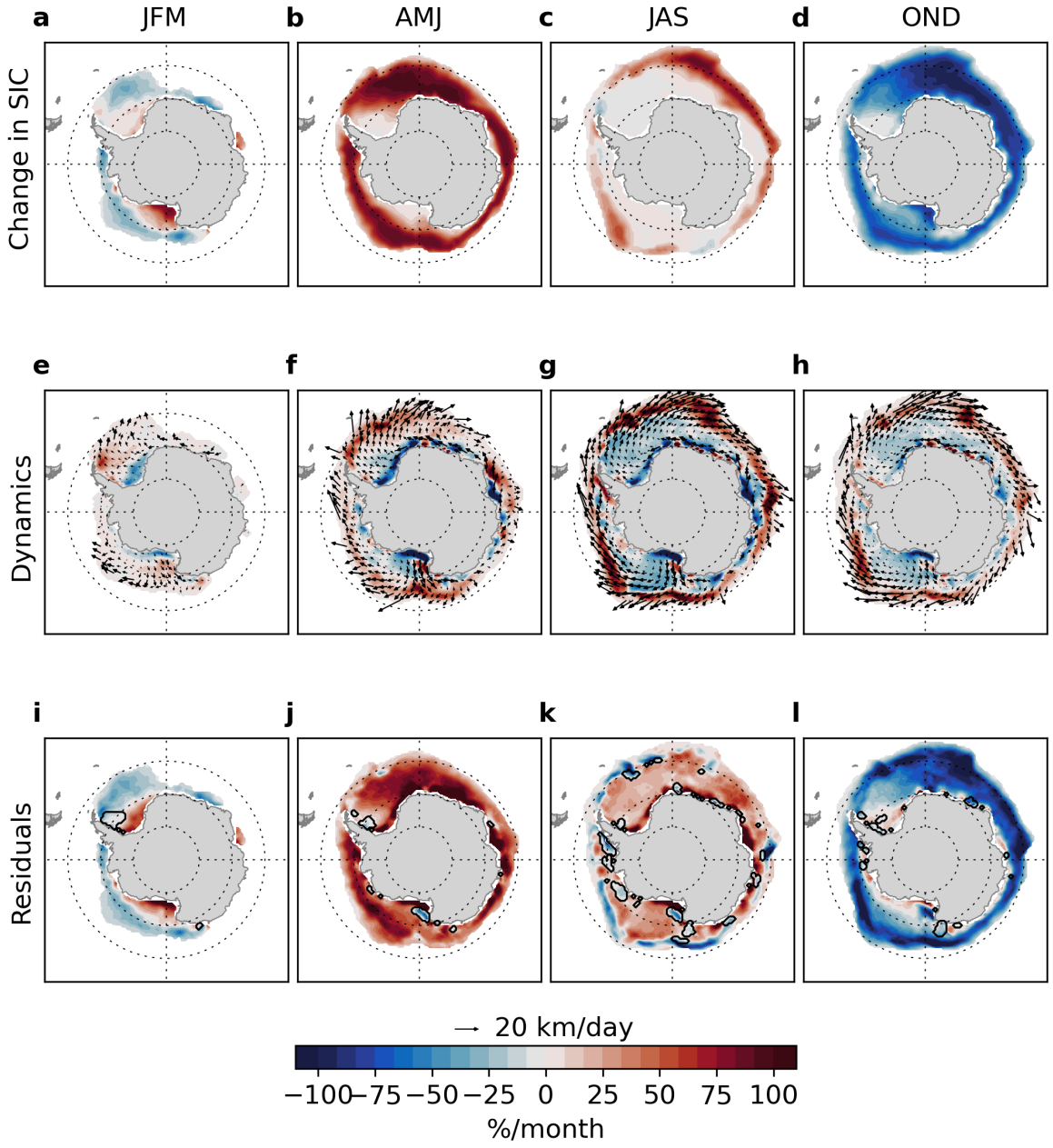

Figure 5: **Drivers of seasonal sea ice concentration variations.** Seasonal mean changes in sea ice concentration (**a-d**; SIC) over summer (JFM), autumn (AMJ), winter (JAS) and spring (OND) and corresponding dynamic (i.e. advection and divergence; **e-h**) and residual (i.e. freezing/melting and mechanical redistribution; **i-l**) contributions, obtained from a sea ice concentration budget. See equation (1) and related explanation for a more detailed description. Seasonal mean ice drift vectors are overlaid on top of **e-h**. Black contours in **i-l** encircle areas where mechanical redistribution may dominate the residual according to the criteria of negative residual, convergent ice drift, and concentration 90%. We adapted this figure from Figure 3 of (Holland & Kimura, 2016), using OSI-SAF mean sea ice concentration (Lavergne et al., 2019) and drift (Lavergne & Down, 2023) over 1992-2020.

Sea ice concentration budget. In practice, drivers of sea ice seasonality operate at the local scale, altering the sea ice concentration, defined as the fractional sea ice coverage in a grid cell. Seasonal changes in Antarctic sea ice extent ultimately integrate local variations in sea ice concentration, driving the sea ice edge to advance or retreat. The governing equation for sea ice concentration (Holland & Kwok, 2012) describes these variations, and allows to isolate their thermodynamic and dynamic contributions, based on sea ice concentration (C) and drift (u) fields:

$$\frac{\partial \mathrm{C}}{\partial t} = \nabla.(\boldsymbol{u}\ \mathrm{C}\ ) + \text{residual} \tag{1}$$

The ice concentration flux divergence represents the effects ice transport (advection and divergence) whereas the residual term primarily reflects thermodynamic processes (melting and freezing) but also includes local effects of sea ice deformation (ridging and rafting). These contributions can be easily retrieved from passive-microwave observations of sea ice concentration and drift. A climatology of each contribution was first retrieved by Holland and Kimura (2016), using observations over 2003-2010. Figure 5 shows an updated version of this analysis, which I reprocessed using more recent observations available over a longer time period (1992-2020). How seasonal sea ice thermodynamics and dynamics operate can be easily retraced based on this climatology and on seasonal cycles of sea ice concentration, thickness, mixed layer temperature and depth, evaluated at a selected grid point in the Weddell Sea (Figure 6).

Thermodynamics. At the start of autumn, most of the Southern Ocean is ice-free and cools down, mainly because of the drop of solar radiation. This also deepens the mixed layer as the density of salt water increases upon cooling toward the freezing point (see, e.g., Talley et al., 2011). Once the full ocean mixed layer approaches the freezing point, freezing starts (Talley et al., 2011; Thompson et al., 2020). Freeze onset is thus determined by the amount of heat to be evacuated from the mixed layer and the rate of cooling, set by the net heat fluxes into the mixed layer. First free-floating frazil ice crystals nucleate, then they consolidate into sea ice, more or less rapidly, depending on sea state and wave activity. During the ice growth season (Figures 5j, k), freezing progressively expands the sea ice cover northward. Once a stable ice cover is established, the ice thickens from its base by upward conductive heat loss and snow-ice formation. In spring, because of the increase in solar radiation and of snow ice formation, ice warms, which decreases the inner conduction and sea ice growth. Ultimately, when the net heat flux at the ice base reverses, melting starts (Figure 5l). In practice, the melt rate is set by the solar input to the mixed layer via open water. The open water fraction is largely set by the melting of thin ice, which depends on the thickness distribution (Holland et al., 2006) and strongly relates to the pixel-mean thickness.

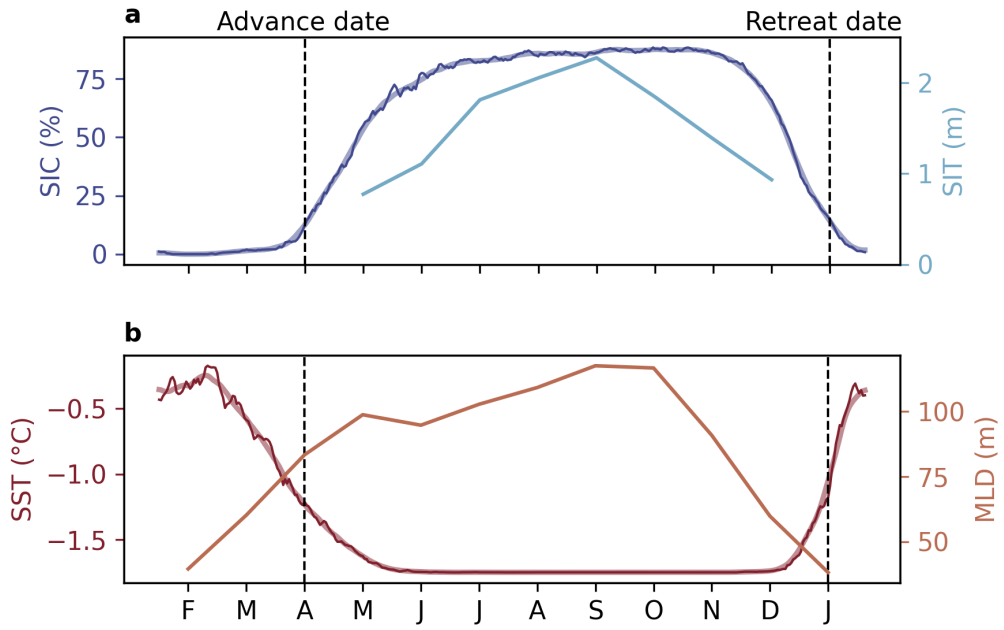

Figure 6: **Local seasonal cycles of climatological sea ice and ocean characteristics at a selected grid point in the seasonal ice zone.** **a**, 1979-2022 daily sea ice concentration (SIC) from (Lavergne et al., 2019) and 1994-2022 monthly sea ice thickness (SIT) from (Bocquet, 2023). **b**, 1982-2018 daily sea surface temperature (SST) from (Paul et al., 2021) and 1970-2018 monthly mixed layer depth (MLD) from (Sallée et al., 2021). For SIC and SST, light colored lines show 15-day filtered data overlaid on dark colored unfiltered data. The selected grid point is located in the Ross Sea (68.6°S, 137.1°W).

Dynamics. In addition, sea ice moves under the influence of winds and currents, and can reach drift speeds of up to 20 kilometers per day. Induced ice transport or deformation can influence the position of the ice edge through three main processes (Figures 5e-h). First, sea ice area is mainly advected northward (Holland & Kimura, 2016), where the ocean is ice free. This process occurs year round; however, the intensity and location of the import varies seasonaly. Northward advection can either induce sea ice melt (Holland & Kimura, 2016) or increase the sea ice extent (Holland & Kwok, 2012), if the underlying ocean is cold enough. Second, sea ice divergence also occurs regardless of the season (Holland & Kimura, 2016), and can open leads within the ice pack, decreasing the surface albedo and triggering the ice albedo-feedback in summer (Ohshima et al., 1998). This enhances the melt rate and accelerate the sea ice edge retreat (Nihashi & Cavalieri, 2006). Third, convergence within the ice pack can cause sea ice to deform and pile up, through ridging and rafting (e.g. Weeks et al., 1989; Granberg & Leppäranta, 1999). This locally increases ice thickness (Figures 5i-l) (Holland & Kimura, 2016).

Dates of sea ice advance and retreat. Seasonal alterations in sea ice concentration are thus driven by a variety of processes, depending on the region and the season of interest. This emphasizes the importance of examining drivers of sea ice seasonality at the local scale, and at distinct key moments. For this purpose, mapping the timings of the sea ice edge advance and

retreat was found useful by previous studies (Holland et al., 2017; Lebrun et al., 2019; Massom et al., 2008; Stammerjohn et al., 2012, 2008). The dates of sea ice advance and retreat are defined as the first day in the year when sea ice concentration exceeds or falls below 15% (Figure 6), locally marking the start and end of the ice season. Yearly dates of advance and retreat are computed from daily passive-microwave, at each grid-point of the seasonal ice zone. Climatological maps (Figures 7a, b), anomalies (not shown) and trends (Figure 8) can then be derived from these yearly dates. Furthermore, these metrics are robust across different observational sea ice concentration products, which is not the case of the more commonly used sea ice extent metric (Figure 4a). Indeed, the mean standard deviations in the advance and retreat dates, derived from "OSI-SAF" (Lavergne et al., 2019), "Nasa Team" (Markus & Cavalieri, 2000) and "Bootstrap" (Comiso, 2017) products is less than 2 days over the seasonal ice zone (Figures 7c, d).

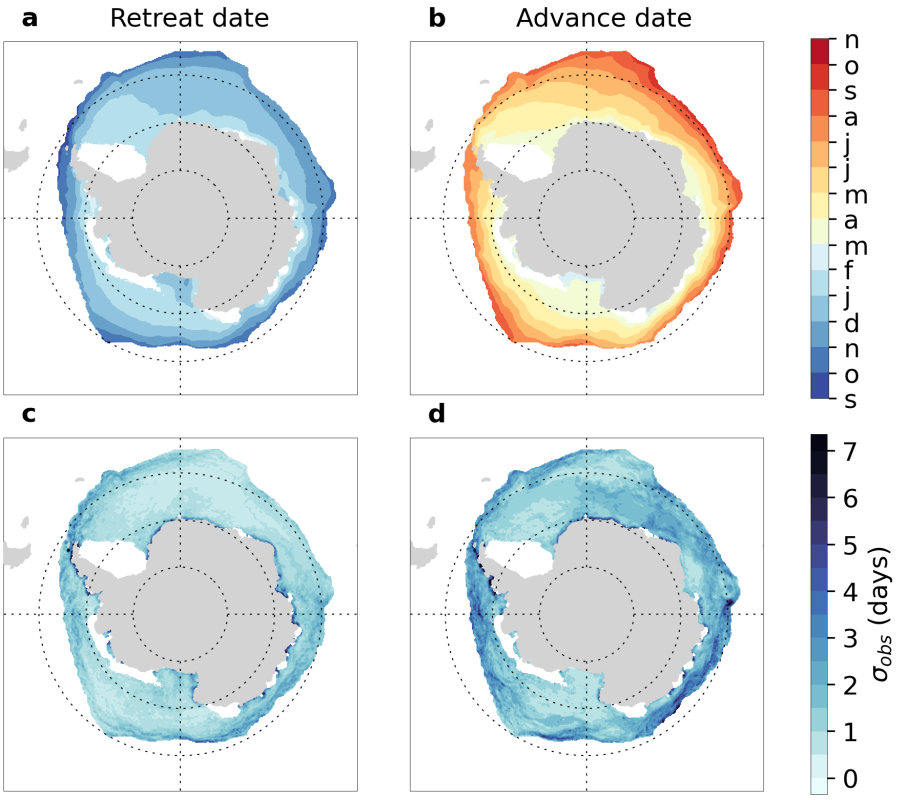

Figure 7: **Local markers of Antarctic sea ice seasonality.** 1979-2022 climatology in **a**, sea ice retreat and **b**, advance dates. Standard deviation over different sea ice concentration products (σ_{obs}; OSI-SAF (Lavergne et al., 2019), Nasa-Team (Markus & Cavalieri, 2000) and Bootstrap (Comiso, 2017), in climatological **c**, retreat and **d**, advance dates. White patches indicate regions out of the seasonal ice zone.

3.2 Drivers of the sea ice edge retreat and advance?

The timing of sea ice retreat and advance is likely determined by the thermodynamic and dynamic processes described in section 3.1. These processes include thermodynamic constraints (mixed layer heat content for advance, and sea ice thickness for retreat), heat fluxes (rate of mixed layer cooling for advance, and of sea ice warming, for retreat) and sea ice drift processes. However, the specific contributions of each of these processes in setting these dates remains unclear. While a number of previous studies have examined the dates of sea ice advance and retreat, subtantial knowledge gaps persist, hindering our fundamental understanding of Antarctic sea ice seasonality.

Building a strong understanding of sea ice seasonality first requires examining the mean state. However, the drivers of the climatological timing of sea ice retreat and advance remain unexplored in both observations and models. Consequently, the underlying processes of the mean-state sea ice edge advance and retreat, and how they are represented in models are currently uncertain.

Previous work on Antarctic sea ice retreat and advance dates has mainly focused on recent changes, highlighting the significant role of thermodynamic constraints (ocean heat uptake) and sea ice transport. Long-term changes have been well documented over 1979-2013, with the largest trends occurring in the west Antarctic sector and reaching 2-3 days per year (Holland et al., 2017; Simpkins et al., 2013; Stammerjohn et al., 2012, 2008). Over this period, the sea ice season has been shortening in the Amundsen and Bellingshausen Seas, due to later advance and earlier retreat, and lengthening in the Ross Sea, due to earlier advance and later retreat (Figures 8a, b). These regional trends have been attributed to SAM-driven wind variability and resulting ice transport (Stammerjohn et al., 2008). Additionally, ice-albedo feedback processes have also presumably contributed to the changes in advance date, in response to changes in the preceding retreat date (Holland et al., 2017; Stammerjohn et al., 2012). Indeed, earlier sea ice retreat increases solar radiation uptake by the ocean during the open water season (Perovich et al., 2007). In turn, the upper ocean takes more time to cool down to the freezing point, delaying sea ice advance. These findings thus provide insights on how sea ice transport and thermodynamic constraints drive recent changes in sea ice seasonality. However, these need to be updated because trends have been evolving since 2013 (Figures 8c, d), especially in the context of the abrupt sea ice decrease following 2016.

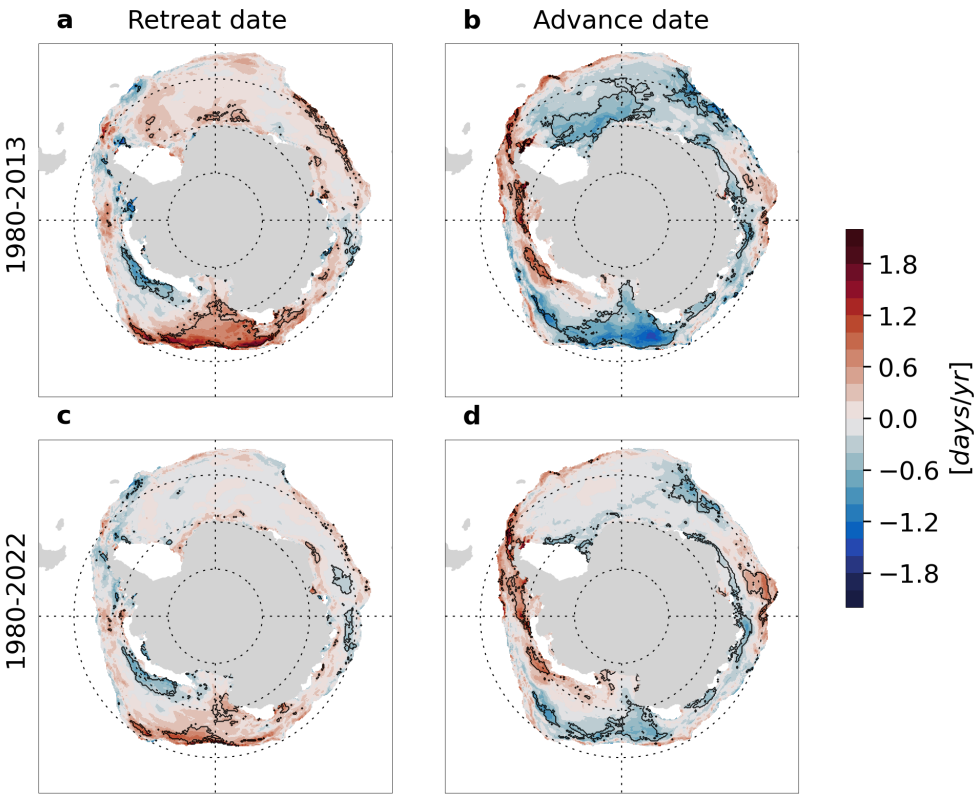

Figure 8: **Observed changes in Antarctic sea ice seasonality since 1979.** Trends in the sea ice retreat date (**a, c**) and advance date (**b, d**) season duration over 1979-2016 and 1979-2022, derived from OSI-SAF passive microwave sea ice concentration (Lavergne et al., 2019). Positive (negative) trends signify later (earlier) retreat / advance. The black contour delimits where trends are statistically significant to the 95% level. White patches indicate regions out of the seasonal ice zone. Trends are calculated using a linear Least-Square method.

4 Thesis Aim and Outline

Based on what precedes, there is a need to improve our understanding of Antarctic sea ice processes and changes, refine their representation in climate models, and potentially reduce the uncertainties regarding how Antarctic sea ice responds to increasing CO_2. In this thesis, I address a crucial dimension of this pressing challenge: **what drives Antarctic sea ice seasonality and its recent changes?**

I adopt the local approach described in section 3, and specifically examine local markers of sea ice seasonality, namely the dates of sea ice retreat and advance. Several knowledge gaps have emerged from the state-of-the-art on these sea ice seasonality diagnostics, setting the stage for the subsequent chapters of this thesis. These gaps and ensuing questions may be summarized as follows:

1. **What drives the timing of Antarctic sea ice advance and retreat in the mean state?** Fundamental understanding of Antarctic sea ice seasonality remains limited. In particular, the roles of potential thermodynamic constraints, heat fluxes and sea ice dynamics in setting the dates of sea ice retreat and advance in the mean state have not been investigated.

2. **What insights can retreat and advance dates provide regarding the representation of seasonal Antarctic sea ice processes in ice-ocean models?** Ice-ocean models can be used as tools to understand specific sea ice seasonality processes that are not captured by available observations. However, their effectiveness relies on accurately representing these processes. Model evaluation could benefit from analyses of key markers of sea ice seasonality.

3. **What are the recent changes in the timing of Antarctic sea ice retreat and advance, and their drivers?** Since 2016, Antarctic sea ice has experienced an abrupt decline, the causes of which remain ambiguous. Potential coinciding shifts in the seasonal cycle of Antarctic sea ice have not been investigated. Yet, addressing those changes with a seasonal perspective might bring a new light on the drivers of the recent sea ice decrease.

I address these questions in the subsequent chapters of this thesis, based on a number of observational data sets and relevant configurations of the NEMO ice-ocean model. My observational approach notably relies on recent improvements in observations of sea ice thickness (Bocquet, 2023) and Southern Ocean hydrography (Sallée et al., 2021), and on several sea ice concentration budget analyses following the method of Holland and Kimura (2016).

Chapters I and II are mainly focused on progressing the understanding of the mean-state sea ice seasonality while Chapter III explores the recent changes. In Chapter I, we use climatological observations to establish the necessary foundational understanding for the two following chapters. We highlight a strong thermodynamic control of sea ice advance (Chapter 1.1) and retreat dates (Chapter 1.2) respectively by summer ocean mixed layer heat content and winter sea ice thickness. We also find that sea ice dynamics plays a regional role. These findings provide an analytical framework to examine the processes driving both the mean-state sea ice seasonality in an ice-ocean model and the observed recent changes. In Chapter II, we apply this framework to evaluate different NEMO simulations. We then assess, in the model, how sea ice dynamics and heat fluxes influence the thermodynamic constraints on retreat and advance dates, which cannot be achieved solely based on observations. In Chapter III, we adapt the same analytical framework to document and explain the changes in sea ice seasonality occurring after 2016, using interannual observations. I finally conclude with a summary of the key findings of this thesis and perspectives for further work.

CHAPTER

I Drivers of Antarctic Sea Ice Seasonality

In the General Introduction, I presented the processes expected to shape the seasonal cycle of Antarctic sea ice. Freezing and melting contribute to start and conclude the sea ice season. How they proceed relates to the thermodynamic state of the ice-ocean system (primarily the ice thickness and ocean heat content) and air-ice-sea heat fluxes. Additionally, sea ice drift may hasten or delay the sea ice edge advance and retreat. These drivers of Antarctic sea ice seasonality are therefore well identified; yet, how they shape the seasonal cycle of Antarctic sea ice remains incompletely understood.

Previous work has investigated the effects of some of these processes on the Antarctic-integrated sea ice coverage (either area or extent) and found a prominent role for insolation (Eayrs et al., 2019; Roach et al., 2022). In a sensitivity study with a regional climate model, Goosse et al. (2023) highlighted a preconditioning role for summer ocean and winter sea ice thickness on the minima and maxima of sea ice coverage, respectively. Additionally, the impact of sea ice dynamics on sea ice extent was found greater during the retreat season compared to the advance season. Eayrs et al. (2019) added that the ice-albedo feedback (Holland et al., 2006) driving the melting process can be amplified by the divergent nature of the ice drift. Most of these studies adopt an integrated perspective, however, which overlooks processes at a more local scale. Satellite-based analyses of the Antarctic sea ice area budget (e.g. Holland & Kwok, 2012; Holland & Kimura, 2016; Kimura et al., 2023) somehow address this issue, indicating large spatial and seasonal variations in the respective importance of thermodynamic and dynamic processes in the ice concentration budget. A separate stream of studies by Stammerjohn et al. (2012, 2008) proposed advance and retreat dates as insightful local markers of the Antarctic seasonal ice cycle. The drivers of their evolution were not fully disentangled, mostly because there was not much information on either ice thickness or oceanic heat content available by then. As a result, the physical drivers of ice advance and retreat dates remain largely unexplored.

In this chapter, we develop theoretical and analytical frameworks to examine how the thermodynamic state of the ice-ocean system, heat fluxes and sea ice drift processes shape the mean-state Antarctic advance and retreat dates. We base our analyses on satellite and in situ observations, taking advantage of recently released observational datasets of sea ice thickness (Bocquet, 2023) and hydrography (Sallée et al., 2021), covering the entire Antarctic sea ice zone. Our main focus is to explain the spatial distributions of climatological sea ice advance and retreat dates. First, we use the sea ice concentration budget technique (Holland & Kimura, 2016; Holland & Kwok, 2012), to identify the regions where dynamics dominate changes in sea ice concentration at the time of sea ice advance and retreat. Second, we evaluate the role of

thermodynamic preconditioners (ocean heat content and ice thickness) by crossing them with advance and retreat dates. Ultimately, we assess to which extent the processes explaining the spatial variations in the mean state can also explain interannual anomalies.

The drivers of sea ice retreat and advance are different and correspond to different types of observations; they were therefore treated separately, in two sub-chapters. Chapter I.1 focuses on the drivers of the sea ice advance date, and is published in *Nature Communications* (Himmich et al., 2023). Chapter I.2 is more exploratory, and examines the drivers of the sea ice retreat date.

1 Drivers of Antarctic Sea Ice Advance

nature communications

Article

https://doi.org/10.1038/s41467-023-41962-8

Drivers of Antarctic sea ice advance

Received: 12 January 2023

Accepted: 22 September 2023

Published online: 05 October 2023

Check for updates

Kenza Himmich[1] ✉, Martin Vancoppenolle[1], Gurvan Madec[1,2], Jean-Baptiste Sallée[1], Paul R. Holland[3] & Marion Lebrun[1,4]

Antarctic sea ice is mostly seasonal. While changes in sea ice seasonality have been observed in recent decades, the lack of process understanding remains a key challenge to interpret these changes. To address this knowledge gap, we investigate the processes driving the ice season onset, known as sea ice advance, using remote sensing and in situ observations. Here, we find that seawater freezing predominantly drives advance in the inner seasonal ice zone. By contrast, in an outer band a few degrees wide, advance is due to the import of drifting ice into warmer waters. We show that advance dates are strongly related to the heat stored in the summer ocean mixed layer. This heat is controlled by the timing of sea ice retreat, explaining the tight link between retreat and advance dates. Such a thermodynamic linkage strongly constrains the climatology and interannual variations, albeit with less influence on the latter.

The Antarctic sea ice seasonal wax and wane is one of the most spectacular, climate-related signals, with large consequences for the global ocean water mass structure and circulation[1–3], the Earth's energy budget[4], and marine ecosystems[5,6].

The seasonal cycle of Antarctic sea ice is marked by two key transitions between open water and ice-covered conditions: advance and retreat. Advance or retreat are defined as the first day in the year when smoothed-in-time sea ice concentration exceeds or falls below 15%[7–9]. Over the last 40 years, changes in the timing of Antarctic sea ice advance and retreat have been documented from satellite-based passive microwave sensors[7,10]. The changes, highly variable regionally, were attributed to wind-driven changes in ice transport and seasonal thermodynamic ice-ocean feedbacks[7,11–15]. Yet interpretation is complicated: strong interannual variability dominates the trends in the last two decades[16] and drivers involve multiple oceanic and atmospheric processes[7,10,17,18], in a context of limited understanding of the drivers of sea ice advance and retreat.

Sea ice advance and retreat are influenced by different processes implying specific observational needs and problems. In this paper, we focus on the fundamental drivers of the sea-ice advance date and on links to the sea-ice retreat date. Sea-ice advance can be controlled either by the freezing of seawater or by sea-ice drifting from already frozen areas[19–22]. Freezing starts ultimately once the entire mixed layer, having warmed up from solar absorption in spring and summer then cooled down through fall, approaches the freezing temperature[23,24]. Close to the winter sea ice edge, freezing can, however, be inhibited by entrained[25] or advected[20] oceanic heat into the mixed layer.

As such, one can hypothesize that the date of sea ice advance is controlled by the upper ocean heat content, surface fluxes, sea ice thermodynamics and drift. To understand these contributions, we relate climatological dates of sea ice advance derived from passive-microwave sea ice concentration[26] to recently available observational datasets. They include passive microwave-based sea ice concentration budget diagnostics that split sea ice changes into dynamic (i.e., drift-related) and thermodynamic (i.e., related to freezing) process contributions[22]; thermal infra-red radiance satellite sea surface temperature[27] (SST); compilations of in situ hydrographic measurements[28] which now provide a detailed climatological view of the upper oceanic thermohaline structure under Antarctic sea ice, thanks to animal-borne sensor records[29]. Combining these sources, we highlight a strong overarching contribution of upper ocean thermodynamics in setting the climatological date of sea ice advance and an important role for ice drift in an outer band, with a width of a few degrees of latitude. We then provide evidence that these mechanisms also contribute to a certain extent to observed interannual changes in the timing of sea ice advance.

[1]Sorbonne Université, Laboratoire d'Océanographie et du Climat, CNRS/IRD/MNHN, Paris, France. [2]Université Grenoble Alpes, Inria, CNRS, Grenoble INP, LJK, 38000 Grenoble, France. [3]British Antarctic Survey, Cambridge, UK. [4]Takuvik, Université de Laval, Québec, QC, Canada.
✉e-mail: kenza.himmich@locean.ipsl.fr

Sea ice advance: local freezing or import of remote ice?

The satellite-based sea ice concentration budget, based on sea ice drift and coverage retrievals from AMSR-E products over 2003–2010[11,18], is used to assess how thermodynamic (i.e., freezing of seawater) and dynamic (i.e., import of sea ice) processes control the spatial variability of climatological dates of advance (d_a) (Fig. 1a). The sea-ice concentration budget cannot be evaluated prior to d_a, when the processes leading to sea ice advance take place, because of missing ice drift data and large sea ice concentration errors in the low-concentration ice near the ice edge. Instead, we evaluate the thermodynamic (Th) and dynamic (Dy) contributions to the total sea ice concentration tendency over the 30 days following d_a, as well as their ratio (Dy/Th) (Fig. 2; see Methods), which delineates regions where transport or freezing dominates sea ice concentration changes.

Following sea ice advance, freezing (Th > 0; Fig. 2a) dominates sea ice concentration tendencies (|Dy/Th| < 1; Fig. 2c) in most of the seasonal ice zone except in a circumpolar band close to the sea ice edge where ice import (Dy > 0, Fig. 2b) takes over freezing (|Dy/Th| > 1) or where net melting occurs (Th < 0). This is consistent with previous work, based on sea ice concentration or volume budget decomposition, which showed that the wintertime ice edge is sustained by ice transport rather than freezing[20,22,30]. We refer to the region south of the |Dy/Th| = 1 contour, as the inner zone and north of this contour, as the outer zone. The latter represents 32% of the seasonal ice zone area. These zones are robust to the choice of the time window over which the budget is integrated following d_a, being weakly sensitive to the window size from 15 to 60 days (Supplementary Fig. 1). We retain a time window of 30 days as a compromise between the needs to be close enough to the time of advance and to maximize the number of useable observations (Supplementary Fig. 1).

We find the inner and outer zones hydrographically differ at the time of advance. Indeed, the sea surface temperature at the date of advance (SST_{da}), evaluated from an infrared satellite SST climatology (2003–2010)[27], is consistent with our analysis of the sea ice concentration budget (Fig. 2d). First, similar spatial structures are seen, which is remarkable since both sources are independent. In particular, SST_{da} is significantly warmer than the freezing temperature (T_f) in the outer zone (median +/− IQR: 0.6 +/− 0.3 °C). Also, the 5% highest values of SST_{da}- T_f (i.e., >1°C and higher than the uncertainty of the SST product, Supplementary Fig. 2), are found in or very close to the outer zone contour (Fig. 2d). The median SST_{da}- T_f is lower in the inner zone (0.4 +/− 0.2 °C) than in the outer zone, however this difference is not

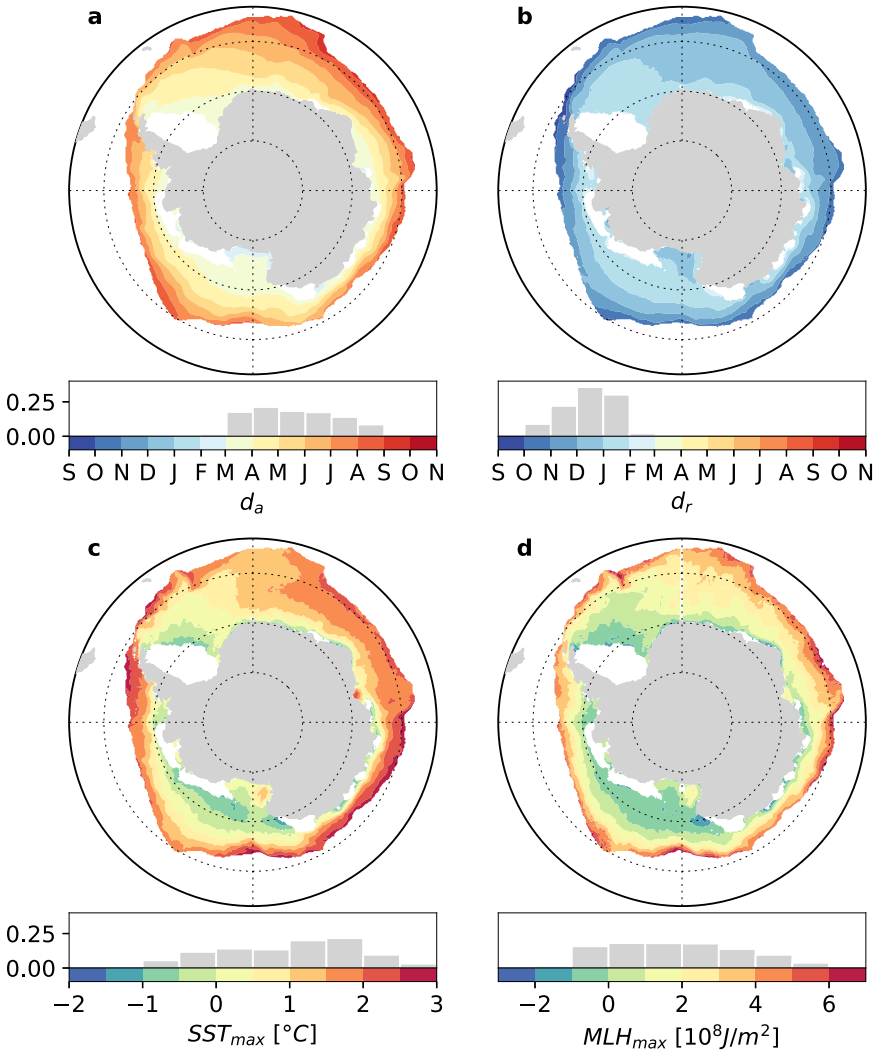

Fig. 1 | Climatological maps of key variables (1982-2018). Dates of sea ice **a** advance (d_a) and **b** retreat (d_r) derived from passive microwave sea ice concentration; seasonal maxima of **c** sea surface temperature (SST_{max}) and **d** mixed layer heat content (MLH_{max}) from a climatology of thermal infra-red radiance satellite sea surface temperature and a climatology of mixed layer depths, constructed from in situ observations. Corresponding frequency histograms are shown under each map. White patches indicate regions out of the seasonal ice zone. Source data are provided as a Source data file.

https://doi.org/10.1038/s41467-023-41962-8

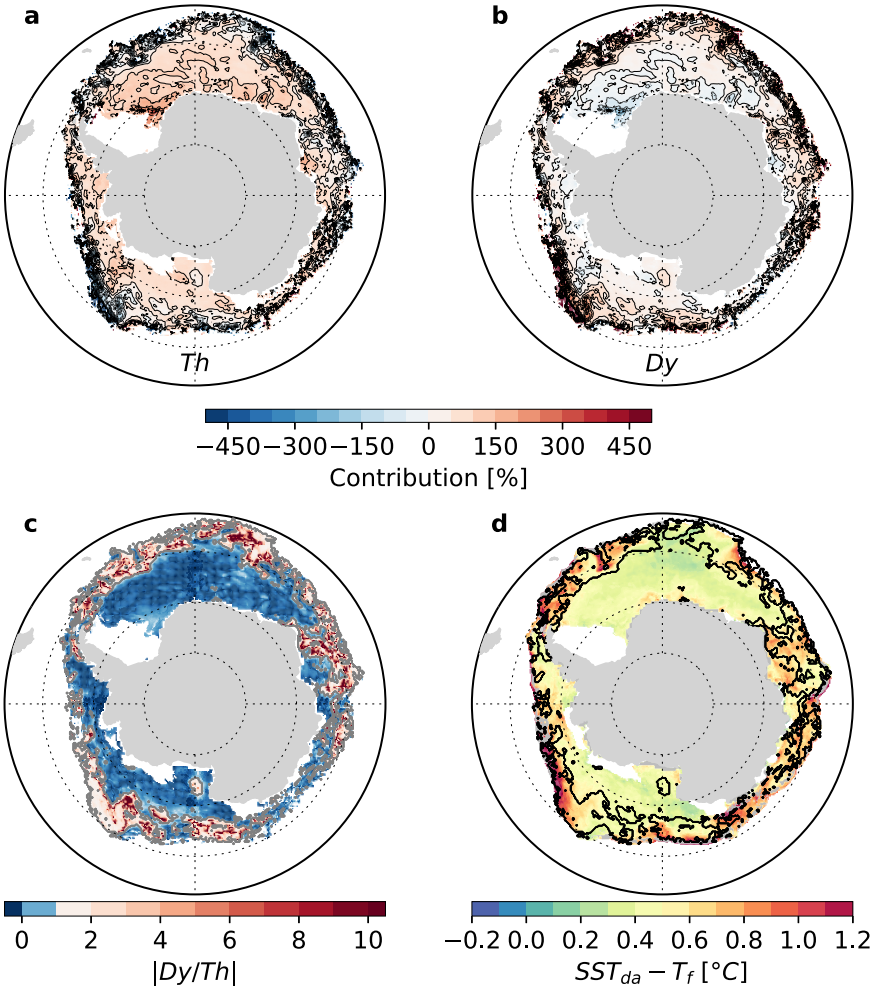

Fig. 2 | Maps of passive microwave-based sea ice concentration budget terms and infra-red radiance satellite sea surface temperature, near the date of sea ice advance, averaged over 2003–2010. The thermodynamic (Th, **a**) dynamic (Dy, **b**) contribution to the total sea ice concentration tendency over the 30 days following the date of advance and their absolute ratio (|Dy/Th|, **c**), all evaluated over a one-month window following the sea ice advance date. **d** Sea surface temperature at the date of advance referenced to freezing temperature (SST_{da} -T_f, with T_f assumed constant at −1.8 °C). Superimposed contour in **d** indicates |Dy/Th| = 1 which defines the limit between the inner and outer zones. White patches indicate regions out of the seasonal ice zone and gray patches (in **d**), where the sea ice concentration budget is not defined because of missing ice drift data. Source data are provided as a Source data file.

significant, which may reflect uncertainties in the exact position of the inner-outer zone boundary, or in SST_{da}. Nevertheless, these findings are robust to the choice of alternative SST products (satellite[31]and in situ; Supplementary Figs. 2 and 3) and to the choice of a longer considered time period (1982–2018 instead of 2003–2010; Supplementary Fig. 2). Finally, a last element of interest is that the temperature profile at the base of the mixed layer is thermally unstable in the outer zone during the first three months of the advance season, according to an in situ hydrographic climatology[28] (Supplementary Fig. 4). Taken together, we argue that the outer zone corresponds to where drifting ice encounters sufficiently warm waters for net basal melting to occur on the day of advance. The contrast is arguably reinforced by an unstable water column, which could lead to entrainment of warm waters into the mixed layer, opposing sea ice growth. Previous studies have also highlighted the role of oceanic heat supply as a spatial constraint to sea ice advance in the winter ice edge region[20,25].

In conclusion, the sea ice concentration budget, satellite SST and in situ hydrography observations consistently suggest the climatological date of advance in the inner and the outer zones is controlled by different processes. While the onset of freezing controls the date of advance in the inner zone, a more complex balance between ice import and oceanic heat supply driving basal melting primarily controls the date of advance in the outer zone. We next investigate the physical processes controlling the onset of freezing.

Control of sea ice advance from ice-ocean thermodynamic processes

In the inner zone, where freezing is the main driver of sea ice advance, we expect the climatological d_a to be strongly linked to the climatological heat content of the mixed layer, as well as the mixed layer cooling rate during the open water season. In this section, we explore the strength of these links. We find that the spatial pattern of d_a relates to the spatial pattern of the seasonal satellite-based[27] SST maximum (SST_{max}). Maps of climatological d_a and SST_{max}, shown respectively in Fig. 1a and c, indicate that waters with lower seasonal SST maximum freeze earlier. Moreover, a linear model attributes a large part of the spatial variance in d_a to SST_{max} ($R^2 = 0.81$), suggesting that SST_{max} could be a proxy of the mixed layer heat gained in spring and summer, which is then lost before sea ice advance. However, a nonlinearity in the relationship appears when representing the spatial distributions of d_a anomalies versus SST_{max} anomalies on a 2D histogram (Fig. 3a). Using a monthly climatology of mixed layer depths[28], we find that this non-linearity is most

https://doi.org/10.1038/s41467-023-41962-8

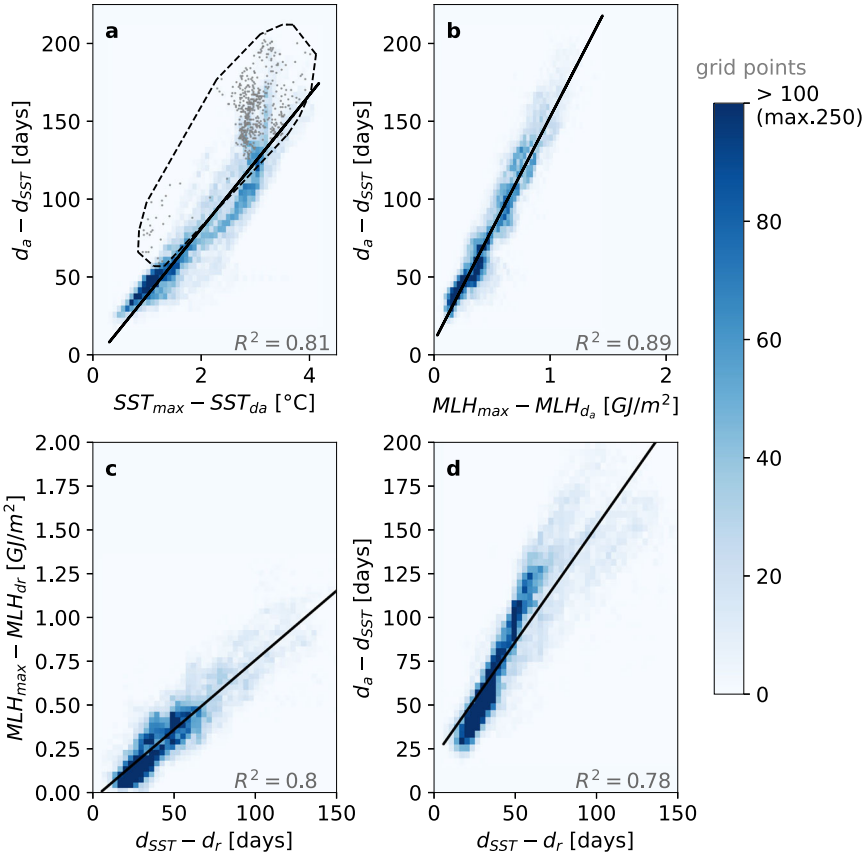

Fig. 3 | Selected inner zone spatial relationships between the 1982–2018 climatological maps of variables displayed in Fig. 1, plotted as 2D histograms. **a** Advance dates (d_a) vs seasonal maximum of sea surface temperature (SST_{max}), **b** d_a vs seasonal maximum of mixed layer heat content (MLH_{max}), **c** MLH_{max} vs retreat dates (d_r) and **d** d_a vs d_r. Anomalies are used, tailored to best showcase the relevant relationships (see Methods). d_a (d_r) anomalies refer to the date of maximum sea surface temperature (d_{SST}) such that positive anomalies indicate later advance (retreat). In **b** (**c**), MLH_{max} anomalies refer to the mixed layer heat content value at sea ice advance (retreat) date, which is close to but not exactly zero, because the sea surface temperature is a few tenths of degree above freezing (see Supplementary Figs. 2 and 3). Only grid points from the inner zone were retained. Color gives the number of points in each pixel of the 2D histogram space. In **a**, the black polygon highlights high mixed layer depths, enclosing grid points with a mixed layer deeper than 80 m on average over the open water season; the gray dots refer to the corresponding grid points. A Least Square linear regression was performed for each plot; the corresponding regression line (significant at 99%), and corresponding coefficients of determination (R^2) are shown. Source data are provided as a Source data file.

obvious for the deepest mixed layers. In Fig. 3a, the non-linearity is confined in the black polygon enclosing all grid points with an averaged mixed layer depth over the open water season, greater than 80 m. This suggests that the SST insufficiently characterizes the mixed layer heat content (MLH), and that the heat content over the entire mixed layer depth, which itself has a spatial variability, must be considered.

Based on the climatological mixed layer depth and SST_{max}, we define an observational estimate of the climatological seasonal maximum of MLH (MLH_{max}; see Methods):

$$MLH_{max} \approx \rho c_p MLD_{d_{SST}}.SST_{max} \quad (1)$$

where MLD_{dSST} is the mixed layer depth evaluated in the month of d_{SST}, the climatological date of maximum SST. MLH_{max} accounts for the variability in both SST and mixed layer depth (Fig. 1d). Strikingly, the 2D histogram of d_a anomalies versus MLH_{max} anomalies does not show any evident non-linearity (Fig. 3b). MLH_{max} also explains a larger part of the spatial variance in d_a ($R^2 = 0.89$) than SST_{max} does ($R^2 = 0.81$, Fig. 3a). The observed relationship between MLH_{max} and d_a can be understood in the framework of a mixed layer heat budget model[9] (see Methods). Integrating this budget for each (x,y) grid point over the open ocean cooling period, a direct link between d_a and MLH_{max} anomalies arises:

$$d_a(x,y) - d_{SST}(x,y) = \frac{MLH_{max}(x,y) - MLH_{da}(x,y)}{<Q^-(x,y)>} \quad (2)$$

where:

$$MLH_{da} \approx \rho c_p MLD_{da}.SST_{da}. \quad (3)$$

where MLD_{da} is the mixed layer depth evaluated in the month of d_a. The average net heat loss during the cooling period <Q-> sets the rate of mixed layer heat loss between the date of maximum SST and d_a. A linear MLH_{max}-d_a relationship over the whole seasonal ice zone would then suggest spatially uniform <Q->, which seems to hold overall (Fig. 3b). The scatter associated with this relationship indicates that <Q-> varies but is equally distributed around the mean, without altering the linearity of the relationship. Thus, the spatial variability of <Q-> only has a minor influence on d_a in the inner zone. Applying Eq. (1) to the slope of the MLH_{max}-d_a linear regression model (Fig. 3b), we estimate the average net heat loss <Q-> to 80 W/m^2. This number integrates all mixed layer heat budget contributors (entrainment, advection, diffusion and air-sea fluxes) but is likely dominated by air-sea fluxes[32]. Such net air-sea heat loss is consistent with reanalysis-

based estimates of net surface fall heat loss in Antarctic ice-free waters (e.g., ref. 33).

The date of advance in the inner zone is therefore controlled by the heat that accumulates in the mixed layer during the ice-free season. This heat is tightly related to the net radiative energy input at the ocean surface (turbulent fluxes are much weaker than radiative fluxes in the sea-ice zone[34]; Supplementary Fig. 5), which is itself constrained by the presence of sea ice and hence, by the date of sea ice retreat (d_r). Consistently, we find a remarkably strong linear link between climatological d_r and MLH_{max} ($R^2 = 0.80$; Fig. 3c). This suggests that MLH_{max} is mostly set by the timing of sea ice retreat and weakly influenced by the spatial variability of net heat fluxes warming the mixed layer during the ice-free season (see Methods). Therefore, by controlling amount of heat accumulating in the mixed layer over the ice-free period, the timing of ice retreat indirectly controls the timing of ice advance. Comparing the climatology of d_r with that of d_a consistently indicates that later d_r is associated with earlier d_a, with a significant and strong linear relationship ($R^2 = 0.78$, Fig. 3d). Previous work has already linked interannual anomalies in d_a to anomalies in d_r[7]. Here, we show that this link holds for the spatial variability of climatological retreat and advance dates, and is controlled by the upper ocean heat content.

The statistical relationships between d_r, MLH_{max}, and d_a are also strong in the outer zone, but generally not as much as in the inner zone (Supplementary Fig. 6). The MLH_{max}-d_a link is weaker in the outer zone ($R^2 = 0.83$) than in the inner zone ($R^2 = 0.89$), but still explains a large part of the d_a variance. Similarly, the d_r-MLH_{max} link is weaker ($R^2 = 0.72$, $p < 0.01$) in the outer zone than in the inner zone ($R^2 = 0.80$). This general weakening and the associated larger regression errors might reflect a larger spatial variability in net heat fluxes in the outer zone (see Methods), possibly linked to the entrainment of warm waters into the mixed layer (Supplementary Fig. 4). The departure from the linear relationship occurs in regions of the outer zone that differ between the d_r-MLH_{max} and the MLH_{max}-d_a relationships (Supplementary Fig. 7). This spatial mismatch affects the d_r-d_a relationship, which is therefore weaker than the two others in the outer zone ($R^2 = 0.61$), and does not explain as much of the d_a variance there.

In summary, the climatological d_r strongly affects the climatological d_a in the inner zone only. By contrast, the climatological MLH_{max} determines the climatological d_a throughout the seasonal ice zone, regardless of the processes (freezing or ice import) increasing sea ice concentration at that time.

From spatial to interannual variability

Thermodynamic processes in ice-free waters provide strong constraints to the climatological date of advance. Whether such mechanisms also apply at interannual time scales is not straightforward. Stammerjohn et al.[7] disclosed significant correlations between detrended dates of retreat and subsequent advance over 1980–2010. An ice-ocean thermodynamic feedback was hypothesized to explain this link. The same mechanism was also identified in the Arctic[7–9,35]. However, observations and CMIP5 model analyses suggest that thermodynamic processes are less effective at explaining interannual variations than they are for the mean state[8,9]. Based on what precedes, we question to which extent our findings on the mean state can be applied to interannual variations.

We expect the ice-ocean thermodynamic feedback to operate in agreement with our d_r-MLH_{max}-d_a framework: an earlier retreat on a given year would lead to a higher maximum MLH and a later advance. We examine these links at the interannual time scale, using the SST as a proxy for the MLH, due to the limited spatial coverage of interannual mixed layer depth data. Based on detrended time series over 1982-2018, we find significant and relatively strong negative links between anomalies of d_r and subsequent SST_{max} ($p < 0.05$ and $r = -0.6 +/- 0.2$; Fig. 4a), and positive links between anomalies of SST_{max} and subsequent d_a ($p < 0.05$ and $r = 0.5 +/- 0.2$; Fig. 4b) in large parts of the seasonal ice zone. As a result of the thermodynamic linkage between d_r, SST_{max}, and d_a, we also find relatively strong correlations between detrended anomalies of sea ice retreat and subsequent advance date ($p < 0.05$ and $r = -0.5 +/- 0.2$; Fig. 4c), consistently with Stammerjohn et al.[7]. However, those correlations are weak or statistically insignificant close to the seasonal ice zone edge and also in the East Antarctic and Maud Rise sectors, which indicates that processes distinct from the ice-ocean feedback are also strongly involved (Fig. 4a–c).

The mean state-based decomposition between an inner and outer zone seems relevant to better constrain the role of ice transport and melt processes at the interannual time scale. To explore this idea, we examine the interannual standard deviation in the date of advance. We find that interannual variability is highest within or close to the outer zone (Fig. 4d). This suggests that high interannual variability in the timing of advance is due to variability in either sea ice drift, which relates to variability in winds[11] or in ocean heat input[20], or both. By contrast, the lower variability in d_a in the inner zone could relate to a more prevalent control of thermodynamics on the date of advance. Spatial patterns of detrended correlations between d_r, SST_{max} and d_a are also generally in line with the inner-outer zones decomposition. The largest correlations are found in the inner zone (Fig. 4a–c), consistently with thermodynamic processes driving sea ice advance there. However, one difference with our findings related to mean state is that drift and melt processes may also considerably contribute to interannual variability in the date of advance in the inner zone, as indicated by locally existing weak and low significance d_r-SST_{max}-d_a correlations there (Fig. 4a, b). For instance, close to Maud Rise, the correlations between d_r and d_a are significant (Fig. 4c) but not between d_r and SST_{max} (Fig. 4a) and between SST_{max} and d_a (Fig. 4b). The effects of oceanic heat entrainment[36,37] and advection[14,15] might be more suited to explain the variability in this region, despite being located in the inner zone. We therefore surmise that the inner-outer zones boundary may not be as clear for interannual variations in the date of advance than it is for the climatology.

Ultimately, the drivers of the spatial variability in the climatological date of advance also contribute to a certain extent to the interannual variability. Nonetheless, heat fluxes and transport processes exert a stronger influence on the timing of advance at the interannual time scale, compared to the mean state. Future work may help to clarify the exact role of such processes.

Discussion

Our findings progress the understanding of the climatological timing of sea ice advance while providing valuable insights on the drivers of interannual changes. We now discuss their implications regarding long-term Antarctic sea ice changes.

Projected future Antarctic sea ice changes vary widely amongst current climate models[38] because of persistent biases and poorly represented physical processes in climate projections, particularly problematic in the Southern Ocean[39]. Our results can be used to evaluate the model representation of the processes driving sea ice seasonality in the Southern Ocean against observations. Primarily, the inner-outer zone decomposition provides a specific approach to validate the ice concentration budget during the ice advance season. Additionally, an examination of the different relations embedded in the d_r-MLH_{max}-d_a framework can serve as a robust approach to verify the existence of the thermodynamic control of sea ice advance by the ocean.

Furthermore, our results provide important constraints on future long-term Antarctic sea ice changes. Given how strong the d_r-MLH_{max}-d_a relationships are in the recent mean state, it can be argued that these will still hold for the future Antarctic sea ice mean state, providing helpful constraints to project long-term future changes. Indeed, the

https://doi.org/10.1038/s41467-023-41962-8

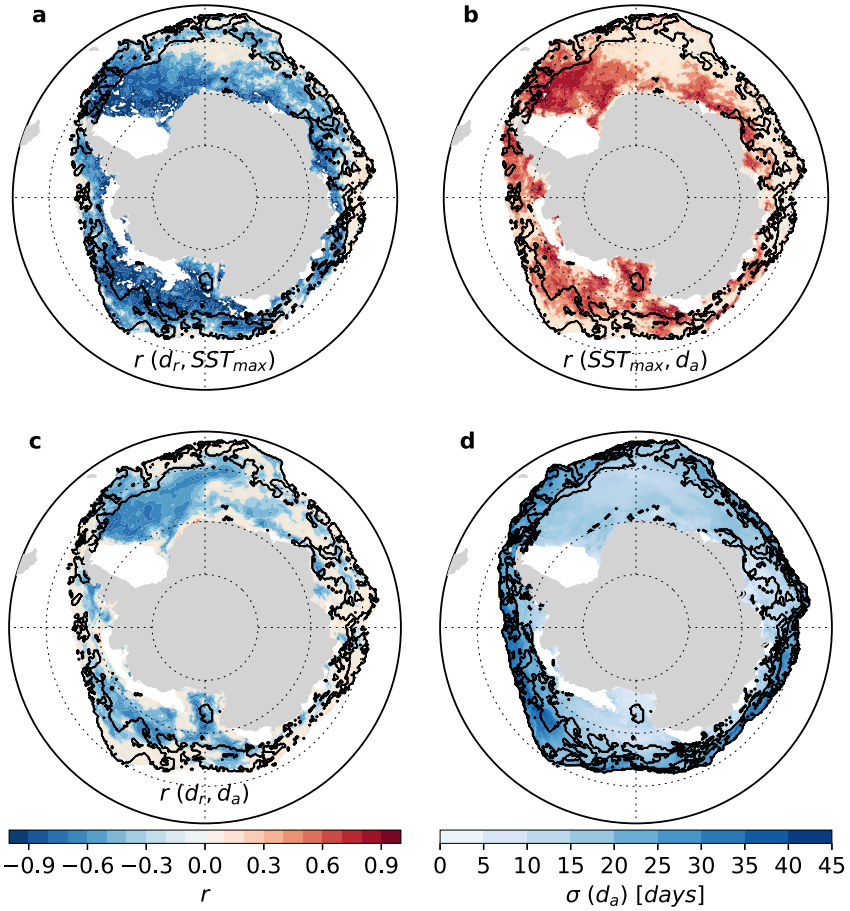

Fig. 4 | Interannual variability in passive-microwave (1982–2018) date of advance and how it relates to variability in date of retreat and seasonal maximum of sea surface temperature (1982–2018). Correlation coefficients (r) between detrended timeseries of **a** annual dates of retreat (d_r) and subsequent seasonal sea surface temperature maximum (SST_{max}), **b** annual SST_{max} and subsequent dates of advance (d_a), and **c** annual d_r and subsequent d_a. **d** Standard deviation (σ) in the date of advance. Beige shading in **b**–**d** indicates where correlations are not statistically significant at the 95% level. The black contour delimits the inner-outer zone limit derived from the sea ice concentration budget and shown in Fig. 2d. White patches indicate regions out of the seasonal ice zone. Source data are provided as a Source data file.

increased skill of the MLH_{max}-d_a relationship, compared to SST_{max}-d_a (Fig. 3a, b) emphasizes the importance of considering changes not only in the mixed layer temperature but also in mixed layer depth to fully understand long-term changes. Arguably global warming will be associated with earlier retreat and warmer surface waters, providing more heat to the mixed-layer in summer, delaying sea ice advance. However, changes in mixed layer stratification are also operating and might compete with the effects of the temperature increase. The increase in freshwater input to the subpolar Southern Ocean through increased precipitation[40] and ice sheet mass loss[41], increases the regional upper ocean stratification[28,42,43] potentially reducing the mixed-layer heat content and act against warming by allowing for earlier date of advance, even with an increased surface heat uptake. More work will be needed to understand how temperature and stratification processes drive and respond to long-term sea ice seasonality changes.

Methods

Observational data sources

We assess the relationships between the date of sea ice advance and the state of the underlying ocean based on a number of observational data sets. We use daily passive microwave sea ice concentration (SIC) from the EUMETSAT Ocean and Sea Ice Satellite Application Facility[26] (OSI SAF) over 1982–2018 (OSI-450 from January 1982 to April 2015, and OSI-430-b after April 2015). For the sea surface temperature (SST), we use a daily satellite product available from 1982, based on thermal infra-red radiance measurements, and taken from the global L4 (gap-free, gridded) European Space Agency (ESA) SST Climate Change Initiative (CCI) analysis with a resolution of 0.05°[27], provided with an estimate of the analysis uncertainty on the SST.

We also use a gap-filled monthly 1979–2018 climatology of mixed layer depth and stratification, based on in situ observations[28]. Conductivity–temperature–depth (CTD; 1970–2018), Argo floats (Argo international programme[44]; 2000–2018) and marine mammal-borne sensor profiles (Marine Mammals Exploring the Oceans Pole to Pole programme[45]; 2004–2018) were included. Generalized least squares linear-regressions of individual in situ profiles are performed around each grid point to produce gridded maps of climatological mean fields.

Other datasets are used to support our analysis. To evaluate the radiative heat fluxes during the open water season, we derive a daily climatology of surface shortwave and longwave radiative fluxes from the FH-series data of the International Satellite Cloud Climatology Project[46,47], available over 1982-2016 (ISCCP). Finally, we use NOAA Advanced very High Resolution Radiometer (AVHRR) Optimum Interpolation (OI) 0.25° daily SST v2.0 analysis data[31], also referred to as Reynolds' SST, to ensure the robustness of our analysis.

All data were interpolated on the OSI-SAF Equal-Area Scalable Earth 2 (EASE2) 25 km grid.

Diagnostics of sea ice and ocean seasonality

Climatological mean dates of sea ice retreat (d_r) and sea ice advance (d_a) were derived from OSI SAF sea ice concentration, on which we applied a 15-day temporal filter to avoid retaining any d_a or d_r reflecting short events[9]. These dates are defined consistently with previous work[7,9,16,48]. d_r is defined as the first day filtered sea ice concentration drops below 15% while d_a is the first day filtered sea ice concentration exceeds 15%. To ensure d_r and subsequent d_a of the same yearly seasonal cycle are retained, we looked for d_a (d_r) starting on a month where no sea ice advance (retreat) occurs, on average over 1982–2018. We selected January 1 of the current year as the start date for d_a, and May 1 of the previous year for d_r, since the majority (>99%) of d_a and d_r occurs after those dates.

To obtain a meaningful 1982–2018 climatological average of d_a and d_r, a missing value is assigned where the number of years with undefined d_a and d_r (corresponding to year-round ice-free or ice-covered grid points) is less than one third of the total number of years in the considered period, following ref. 9.

Other climatological diagnostics were calculated to diagnose the seasonality of upper ocean thermodynamics, using the ESA CCI satellite SST over 1982–2018. For each year, the seasonal maximum of SST, SST_{max} and date when this maximum is reached, d_{SST} were identified during the open water season, between d_r and d_a of the corresponding year. We also calculated the yearly SST on the days of advance (SST_{da}) and retreat (SST_{dr}). Then, the 1982–2018 average of each of the four ocean seasonality diagnostics was obtained following the same method as for climatological d_r and d_a.

Decomposition of sea ice concentration budget at the time of advance

To explore the respective role of ice dynamics and thermodynamics in setting d_a, we evaluate the dynamic and thermodynamic contributions to the sea ice concentration budget at the time of advance. We identify regions of ice import/export, ice melt/growth and regions of dominant dynamic/thermodynamic contributions. We use the sea ice concentration budget decomposition outputs from ref. 22 available at daily frequency between 2003 and 2010. We also use a 2003–2010 climatology of d_a, for temporal consistency. These outputs are obtained based on the technique developed by ref. 11 from daily sea ice concentration (NASA Team algorithm[49]) and ice drift fields derived from AMSR-E brightness temperature by a cross-correlation algorithm[50,51]. The governing equation for the sea ice concentration, is decomposed between a dynamic term and a residual:

$$\frac{\partial \mathrm{SIC}}{\partial t} = \nabla.(u\mathrm{SIC}) + \mathrm{residual} \tag{4}$$

The ice concentration flux divergence represents the effects of advection and divergence of sea ice caused by ice drift. The residual term includes both thermodynamic processes (melting/freezing) and mechanical redistribution through ridging and rafting. However, mechanical redistribution should not intervene in the budget at the time of sea ice advance, as it usually occurs for high sea ice concentration. Thus, we consider the residual as purely thermodynamic.

Evaluating the different terms of the previous equation at the time of advance requires analyzing the output of the sea ice concentration budget for sea ice concentration below 15%. However, the budget is not defined at such low sea ice concentration because of missing ice drift data and large sea ice concentration errors near the ice edge. To overcome this limitation, we diagnose total sea ice concentration increase (ΔSIC), as well as percent dynamic (Dy) and thermodynamic (Th) contributions to sea ice concentration tendency during a period on length Δt following d_a.

The diagnostics are defined as such:

$$\Delta\mathrm{SIC} = \int_{d_a}^{d_a+\Delta t} \frac{\partial \mathrm{SIC}}{\partial t}\, dt \tag{5}$$

$$\mathrm{Dy} = \frac{1}{\Delta\mathrm{SIC}} \int_{d_a}^{d_a+\Delta t} \nabla.(u\mathrm{SIC})\, dt \tag{6}$$

$$\mathrm{Th} = \frac{1}{\Delta\mathrm{SIC}} \int_{d_a}^{d_a+\Delta t} \mathrm{residual}\, dt \tag{7}$$

To choose the most suitable upper bound of integration, the sensitivity to Δt of the contours delimiting our regions of interest (Th = 0, Dy = 0 and |Dy/Th| = 1) was assessed (Supplementary Fig. 1). For varying Δt from 15 to 60 days, we find that the Th = 0 and |Dy/Th| = 1 contours vary only little. More precisely, regions of sea ice melt (Th <0) and dominant dynamic contribution (|Dy/Th| > 1) are consistent both in location and percentage of total seasonal ice zone area, strengthening our confidence that they are a close representation of the sea ice concentration budget prior to d_a. Hence, our regions of interest should be at similar location and have a similar area at the time of sea ice advance than in any of the time periods Δt within the 2 months following d_a. We choose Δt = 30 days as a compromise between a low proportion of missing values in the considered seasonal ice zone and the proximity in time to d_a.

The d_r-MLH_{max}-d_a relationship in a simple heat budget model framework

The mathematical description of the simple thermodynamic framework used to explain spatial variations in the timing of advance is an updated version of the framework developed by ref. 9 in the context of Arctic sea ice, based on the heat budget in the mixed layer. We define the heat stored in the mixed layer, termed mixed layer heat content (MLH) as:

$$\mathrm{MLH} = \rho c_p h T \tag{8}$$

where h is the mixed layer depth, T, the mixed layer temperature, ρ, the reference density of seawater, and c_p, the specific heat of seawater.

The model is based on the temperature balance equation[52], which writes as:

$$\frac{\partial \mathrm{MLH}}{\partial t}(t,x,y) = Q_t(t,x,y) \tag{9}$$

with Q_t, the total net heat flux in the mixed layer, accounting for surface heat fluxes, entrainment, diffusion and advection. Now, integrating the MLH budget during mixed layer heating (from d_r to d_{MLH}) and cooling (from d_{MLH} to d_a) periods we get:

$$d_a(x,y) - d_{SST}(x,y) = \frac{\mathrm{MLH}_{\max}(x,y) - \mathrm{MLH}_{\mathrm{da}}(x,y)}{<Q^-(x,y)>} \tag{10}$$

$$\mathrm{MLH}_{\max}(x,y) - \mathrm{MLH}_{\mathrm{dr}}(x,y) = <Q^+(x,y)>(d_{MLH}(x,y) - d_r(x,y)) \tag{11}$$

where d_{MLH} is the date of maximum MLH. $<Q+>$ and $<Q->$ are respectively the mean total net heat flux during the heating and the cooling periods:

$$<Q^-(x,y)>.\left[d_a(x,y) - d_{MLH}(x,y)\right] = \int_{d_{MLH}}^{d_a} Q_t(t,x,y)dt \tag{12}$$

$$<Q^+(x,y)>.\left[d_{MLH}(x,y) - d_r(x,y)\right] = \int_{d_r}^{d_{MLH}} Q_t(t,x,y)dt \tag{13}$$

Combining Eqs. (12) and (13), we obtain a relationship between d_r and d_a:

$$d_a(x,y) - d_{MLH}(x,y) = \frac{<Q^+(x,y)>}{<Q^-(x,y)>} r_{MLH}\left[(d_{MLH}(x,y) - d_r(x,y))\right] \quad (14)$$

with:

$$r_{MLH}(x,y) = \frac{\mathrm{MLH_{max}} - \mathrm{MLH_{da}}}{\mathrm{MLH_{max}} - \mathrm{MLH_{dr}}}.$$

If T is at the freezing point on d_r and d_a, then $\mathrm{MLH_{da}} \approx \mathrm{MLH_{dr}}$ and $r_{MLH} \approx 1$.

Perfectly linear relationships between climatological d_a and $\mathrm{MLH_{max}}$ anomalies, $\mathrm{MLH_{max}}$ and d_r anomalies would respectively suggest uniform spatial distributions of $<Q->$ and $<Q+>$. Resultingly, the relationship between d_a and d_r anomalies would also become linear (if $r_{MLH} \approx 1$).

Definition of the observational MLH

Using the monthly climatology of mixed layer depth from ref. 28 and the ESA CCI SST diagnostics (e.g., $\mathrm{SST_{max}}$, $\mathrm{SST_{dr}}$, $\mathrm{SST_{da}}$), we estimated the observational MLH for any date, t, during the open water season as:

$$\mathrm{MLH}(t) \approx \rho c_p \mathrm{MLD_t}.\mathrm{SST} \quad (15)$$

where $\mathrm{MLD_t}$ is the monthly mixed layer depth evaluated on the month of the given date, t (e.g., $\mathrm{MLD_{dSST}}$ is evaluated on the month of climatological seasonal maximum of SST, d_{SST}). The SST is in degrees Celsius. Using this observational estimation of the MLH, we obtain:

$$\mathrm{MLH_{dr}} \approx \rho c_p \mathrm{MLD_{dr}}.\mathrm{SST_{dr}};$$
$$\mathrm{MLH_{max}} \approx \rho c_p \mathrm{MLD_{d_{SST}}}.\mathrm{SST_{max}};$$
$$\mathrm{MLH_{da}} \approx \rho c_p \mathrm{MLD_{da}}.\mathrm{SST_{da}}.$$

Data availability

The present analyses are mostly based on publicly available observational data. OSI-SAF sea ice concentration data are available from https://osi-saf.eumetsat.int/products. Sea ice concentration budget decomposition outputs are available upon request. Sea surface temperature data are available from https://cds.climate.copernicus.eu/cdsapp#!/home for the ESA CCI product and from https://www.ncei.noaa.gov/products/avhrr-pathfinder-sst for the NOAA AVHRR product. ISCCP radiative surface heat fluxes are available from https://isccp.giss.nasa.gov/projects/flux.html. Climatological fields of mixed layer depth and stratification are available from https://zenodo.org/record/4073174#.YA_jsC2S3XQ. Source data are provided with this paper.

Code availability

All scripts used for generating the plots in this paper are available from the corresponding author upon request.

References

1. Stössel, A., Kim, S.-J. & Drijfhout, S. S. The impact of Southern Ocean Sea Ice in a global ocean model. *J. Phys. Oceanogr.* **28**, 1999–2018 (1998).
2. Goosse, H. & Fichefet, T. Importance of ice-ocean interactions for the global ocean circulation: a model study. *J. Geophys. Res. Oceans* **104**, 23337–23355 (1999).
3. Pellichero, V., Sallée, J.-B., Chapman, C. C. & Downes, S. M. The southern ocean meridional overturning in the sea-ice sector is driven by freshwater fluxes. *Nat. Commun.* **9**, 1789 (2018).
4. Frey, W. R., Morrison, A. L., Kay, J. E., Guzman, R. & Chepfer, H. The combined influence of observed Southern Ocean clouds and sea ice on top-of-atmosphere Albedo. *J. Geophys. Res. Atmos.* **123**, 4461–4475 (2018).
5. Labrousse, S. et al. Winter use of sea ice and ocean water mass habitat by southern elephant seals: the length and breadth of the mystery. *Prog. Oceanogr.* **137**, 52–68 (2015).
6. Moreau, S., Boyd, P. W. & Strutton, P. G. Remote assessment of the fate of phytoplankton in the Southern Ocean sea-ice zone. *Nat. Commun.* **11**, 3108 (2020).
7. Stammerjohn, S., Massom, R., Rind, D. & Martinson, D. Regions of rapid sea ice change: an inter-hemispheric seasonal comparison. *Geophys. Res. Lett.* https://doi.org/10.1029/2012GL050874 (2012).
8. Stroeve, J. C., Crawford, A. D. & Stammerjohn, S. Using timing of ice retreat to predict timing of fall freeze-up in the Arctic. *Geophys. Res. Lett.* **43**, 6332–6340 (2016).
9. Lebrun, M., Vancoppenolle, M., Madec, G. & Massonnet, F. Arctic sea-ice-free season projected to extend into autumn. *Cryosphere* **13**, 79–96 (2019).
10. Stammerjohn, S. E., Martinson, D. G., Smith, R. C., Yuan, X. & Rind, D. Trends in Antarctic annual sea ice retreat and advance and their relation to El Niño–Southern Oscillation and Southern Annular Mode variability. *J. Geophys. Res. Oceans* https://doi.org/10.1029/2007JC004269 (2008).
11. Holland, P. R. & Kwok, R. Wind-driven trends in Antarctic sea-ice drift. *Nat. Geosci.* **5**, 872–875 (2012).
12. Holland, P. R. The seasonality of Antarctic sea ice trends. *Geophys. Res. Lett.* **41**, 4230–4237 (2014).
13. Holland, M. M., Landrum, L., Raphael, M. & Stammerjohn, S. Springtime winds drive Ross Sea ice variability and change in the following autumn. *Nat. Commun.* **8**, 731 (2017).
14. Bushuk, M. et al. Seasonal prediction and predictability of regional Antarctic Sea Ice. *J. Clim.* **34**, 6207–6233 (2021).
15. Holland, M. M., Blanchard-Wrigglesworth, E., Kay, J. & Vavrus, S. Initial-value predictability of Antarctic sea ice in the Community Climate System Model 3. *Geophys. Res. Lett.* **40**, 2121–2124 (2013).
16. Simpkins, G. R., Ciasto, L. M. & England, M. H. Observed variations in multidecadal Antarctic sea ice trends during 1979–2012. *Geophys. Res. Lett.* **40**, 3643–3648 (2013).
17. Meehl, G. A. et al. Sustained ocean changes contributed to sudden Antarctic sea ice retreat in late 2016. *Nat. Commun.* **10**, 14 (2019).
18. Eayrs, C., Li, X., Raphael, M. N. & Holland, D. M. Rapid decline in Antarctic sea ice in recent years hints at future change. *Nat. Geosci.* **14**, 460–464 (2021).
19. Kimura, N. & Wakatsuchi, M. Processes controlling the advance and retreat of sea ice in the Sea of Okhotsk. *J. Geophys. Res. Oceans* **104**, 11137–11150 (1999).
20. Bitz, C. M., Holland, M. M., Hunke, E. C. & Moritz, R. E. Maintenance of the sea-ice edge. *J. Clim.* **18**, 2903–2921 (2005).
21. Stevens, R. P. & Heil, P. The interplay of dynamic and thermodynamic processes in driving the ice-edge location in the Southern Ocean. *Ann. Glaciol.* **52**, 27–34 (2011).
22. Holland, P. R. & Kimura, N. Observed concentration budgets of Arctic and Antarctic Sea ice. *J. Clim.* **29**, 5241–5249 (2016).
23. Thompson, L. et al. Frazil ice growth and production during katabatic wind events in the Ross Sea, Antarctica. *Cryosphere* **14**, 3329–3347 (2020).
24. Talley, L. D., Pickard, G. L., Emery, W. J. & Swift, J. H. in *Descriptive Physical Oceanography (Sixth Edition)* (eds Talley, L. D., Pickard, G. L., Emery, W. J. & Swift, J. H.) 29–65 (Academic Press, 2011).
25. Su, Z. Preconditioning of Antarctic maximum sea ice extent by upper ocean stratification on a seasonal timescale. *Geophys. Res. Lett.* **44**, 6307–6315 (2017).

26. Lavergne, T. et al. Version 2 of the EUMETSAT OSI SAF and ESA CCI sea-ice concentration climate data records. *Cryosphere* **13**, 49–78 (2019).
27. Merchant, C. J. et al. Satellite-based time-series of sea-surface temperature since 1981 for climate applications. *Sci. Data* **6**, 223 (2019).
28. Sallée, J.-B. et al. Summertime increases in upper-ocean stratification and mixed-layer depth. *Nature* **591**, 592–598 (2021).
29. Roquet, F. et al. Delayed-mode calibration of hydrographic data obtained from animal-borne satellite relay data loggers. *J. Atmos. Ocean. Technol.* **28**, 787–801 (2011).
30. Haumann, F. A., Gruber, N., Münnich, M., Frenger, I. & Kern, S. Sea-ice transport driving Southern Ocean salinity and its recent trends. *Nature* **537**, 89–92 (2016).
31. Reynolds, R. W. et al. Daily high-resolution-blended analyses for sea surface temperature. *J. Clim.* **20**, 5473–5496 (2007).
32. Pellichero, V., Sallée, J.-B., Schmidtko, S., Roquet, F. & Charrassin, J.-B. The ocean mixed layer under Southern Ocean sea-ice: seasonal cycle and forcing. *J. Geophys. Res. Oceans* **122**, 1608–1633 (2017).
33. Tamura, T., Ohshima, K., Nihashi, S. & Hasumi, H. Estimation of surface heat/salt fluxes associated with sea ice growth/melt in the Southern Ocean. *Sci. Online Lett. Atmos.* **7**, 17–20 (2011).
34. Yu, L., Jin, X. & Schulz, E. W. Surface heat budget in the Southern Ocean from 42°S to the Antarctic marginal ice zone: four atmospheric reanalyses versus icebreaker *Aurora Australis* measurements. *Polar Res.* https://doi.org/10.33265/polar.v38.3349 (2019).
35. Perovich, D. K. et al. Increasing solar heating of the Arctic Ocean and adjacent seas, 1979–2005: attribution and role in the ice-albedo feedback. *Geophys. Res. Lett.* https://doi.org/10.1029/2007GL031480 (2007).
36. Beckmann, A., Timmermann, R., Pereira, A. F. & Mohn, C. The effect of flow at Maud Rise on the sea-ice cover – numerical experiments. *Ocean Dyn.* **52**, 11–25 (2001).
37. Gordon, A. L. & Huber, B. A. Southern ocean winter mixed layer. *J. Geophys. Res. Oceans* **95**, 11655–11672 (1990).
38. Roach, L. A. et al. Antarctic Sea ice area in CMIP6. *Geophys. Res. Lett.* **47**, e2019GL086729 (2020).
39. Beadling, R. L. et al. Representation of Southern Ocean properties across coupled model intercomparison project generations: CMIP3 to CMIP6. *J. Clim.* **33**, 6555–6581 (2020).
40. Liu, J. & Curry, J. A. Accelerated warming of the Southern Ocean and its impacts on the hydrological cycle and sea ice. *Proc. Natl Acad. Sci. USA* **107**, 14987–14992 (2010).
41. Paolo, F. S., Fricker, H. A. & Padman, L. Volume loss from Antarctic ice shelves is accelerating. *Science* **348**, 327–331 (2015).
42. Li, G. et al. Increasing ocean stratification over the past half-century. *Nat. Clim. Chang.* **10**, 1116–1123 (2020).
43. Yamaguchi, R. & Suga, T. Trend and variability in global upper-ocean stratification since the 1960s. *J. Geophys. Res. Oceans* **124**, 8933–8948 (2019).
44. Wong, A. P. S. et al. Argo data 1999–2019: two million temperature-salinity profiles and subsurface velocity observations from a global array of profiling floats. *Front. Mar. Sci.* https://doi.org/10.3389/fmars.2020.00700 (2020).
45. Treasure, A. et al. Marine mammals exploring the oceans pole to pole: a review of the MEOP Consortium. *Oceanography* **30**, 132–138 (2017).
46. Rossow, W. B. & Schiffer, R. A. Advances in understanding clouds from ISCCP. *Bull. Am. Meteorol. Soc.* **80**, 2261–2288 (1999).
47. Zhang, Y., Rossow, W. B., Lacis, A. A., Oinas, V. & Mishchenko, M. I. Calculation of radiative fluxes from the surface to top of atmosphere based on ISCCP and other global data sets: refinements of the radiative transfer model and the input data. *J. Geophys. Res. Atmos.* https://doi.org/10.1029/2003JD004457 (2004).
48. Parkinson, C. L. Spatial patterns in the length of the sea ice season in the Southern Ocean, 1979–1986. *J. Geophys. Res. Oceans* **99**, 16327–16339 (1994).
49. Cavalieri, D. J., Markus, T. & Comiso, J. C. *AMSR-E/Aqua Daily L3 12.5 km Brightness Temperature, Sea Ice Concentration, & Snow Depth Polar Grids, Version 3* (NSIDC, 2014).
50. Kimura, N. & Wakatsuchi, M. Large-scale processes governing the seasonal variability of the Antarctic sea ice. *Tellus A* **63**, 828–840 (2011).
51. Kimura, N., Nishimura, A., Tanaka, Y. & Yamaguchi, H. Influence of winter sea-ice motion on summer ice cover in the Arctic. *Polar Res.* https://doi.org/10.3402/polar.v32i0.20193 (2013).
52. Dong, S., Gille, S. T. & Sprintall, J. An assessment of the Southern Ocean mixed layer heat budget. *J. Clim.* **20**, 4425–4442 (2007).

Acknowledgements

The authors acknowledge Casimir de Lavergne and François Massonnet for their helpful suggestions. J.-B.S. has received funding from the European Union's Horizon 2020 research and innovation program under grant agreement no. 821001.

Author contributions

Analysis for this paper was performed by K.H. and supervised by M.V. and G.M. K.H. and M.V. wrote the initial manuscript. G.M., J.-B.S., P.R.H., and M.L. contributed to interpreting the results and improving the paper.

Competing interests

The authors declare no competing interests.

Additional information

Supplementary information The online version contains supplementary material available at https://doi.org/10.1038/s41467-023-41962-8.

Correspondence and requests for materials should be addressed to Kenza Himmich.

Peer review information *Nature Communications* thanks Cecilia Bitz and the other, anonymous, reviewers for their contribution to the peer review of this work. A peer review file is available.

Supplementary Information

Drivers of Antarctic sea ice advance

Kenza Himmich, Martin Vancoppenolle, Gurvan Madec, Jean-Baptiste Sallée, Paul R. Holland, Marion Lebrun

Supplementary Text

Analysis of the Supplementary Figures

The sea ice concentration budget at the date of advance (d_a) has large uncertainties, hence we integrate it in time over a time window spanning part of the sea ice season. In Supplementary Fig.1, we find that the sea ice concentration budget-derived limit between the inner and outer zones does not strongly depend on the size of the time integration window, suggesting it is robust enough for the present analysis.

In Supplementary Fig. 2, we evaluate the robustness of the sea surface temperature at date of advance (SST_{da}) across time periods and SST products. We find that SST_{da} slightly differs according to the averaging period (2003-2010 or 1982-2018) or the product (ESA CCI or Reynolds'). However, the effect of the inner-outer zone limit is always visible. Hence, the SST-based inner-outer zone limit is also robust, we reckon. Furthermore, SST_{da} - T_f (where T_f is the freezing temperature) is generally higher than uncertainty, and even more so in the outer zone. This is consistent with a higher SST_{da} in the outer zone compared to the inner zone. In the inner zone, higher than uncertainty (SST_{da} - T_f) could be due to a spatial averaging effect: a 15% ice covered grid point of 25 km^2 is not necessarily at the freezing point over its full surface.

In Supplementary Fig. 3, we test whether available in-situ hydrographic records support satellite-based findings regarding the SST at the date of advance. In-situ SST measurements are from float (2000-2020) and marine mammal-borne sensors (2004-2020, see Methods). In situ SSTs were collocated with the passive-microwave dates of sea ice advance for the corresponding sampling year. Only 28 records correspond to an available date of advance within 3 days in the corresponding satellite pixel. We find the histograms of Supplementary Fig. 2 from these 28 in situ records and their satellite counterparts (ESA CCI) SST_{da} to be compatible.

In Supplementary Fig. 4, we examine the temperature contribution to the stratification at the base of the mixed layer during the sea ice advance season (N_T^2). N_T^2 is proportional to the vertical temperature gradient at the base of the mixed layer and defined as: $N_T^2 = g\alpha \frac{\partial T_b}{\partial z}$, where T_b is the temperature at the base of the mixed layer, α, the thermal expansion coefficient at constant pressure: $\alpha = -\frac{1}{\rho}\frac{\partial \rho}{\partial t}$ and g, the gravity acceleration. $N_T^2 < 0$ ($N_T^2 > 0$) indicates a negative (positive) temperature gradient and an unstable (stable) temperature profile at the base of the mixed layer.

We find that, in the outer zone, the temperature profile at the base of the mixed layer is unstable during the three first months of the advance season ($N_T^2 < 0$), indicating a possible entrainment of warm waters into the mixed layer during these months. This entrainment might contribute to the excess of heat causing the high SST_{da} and the resulting melting in the outer zone.

In Supplementary Fig. 5, we show a strong correspondence between the seasonal maximum of mixed layer heat content (MLH_{max}) and the net radiative flux absorbed by the ocean. The latter is itself constrained by the date of sea ice retreat, which suggests a large control of MLH_{max} by radiative heating of the upper ocean and explains why MLH_{max} is tightly linked to the date of sea ice retreat (d_r) (see Figure 3c).

In Supplementary Fig. 6, we test the strength of the d_r-MLH_{max}-d_a linear relationships in the outer zone. We find that these relationships are significantly weaker in the outer zone than in the inner zone (see Fig. 3), according to Fisher's Z-test at a 0.01 significance level. However, the MLH_{max}-d_a relation still explains a large part (83%) of the variance in the climatological date of advance. By contrast, the d_r-d_a relation is weaker than the d_r-MLH_{max} and the MLH_{max}-d_a relations, in the outer zone.

In Supplementary Fig. 7, we show that the weaker d_r-d_a relation in the outer zone might be due to different spatial distributions of the errors in the d_r-MLH_{max} and the MLH_{max}-d_a linear regressions.

Supplementary Figures

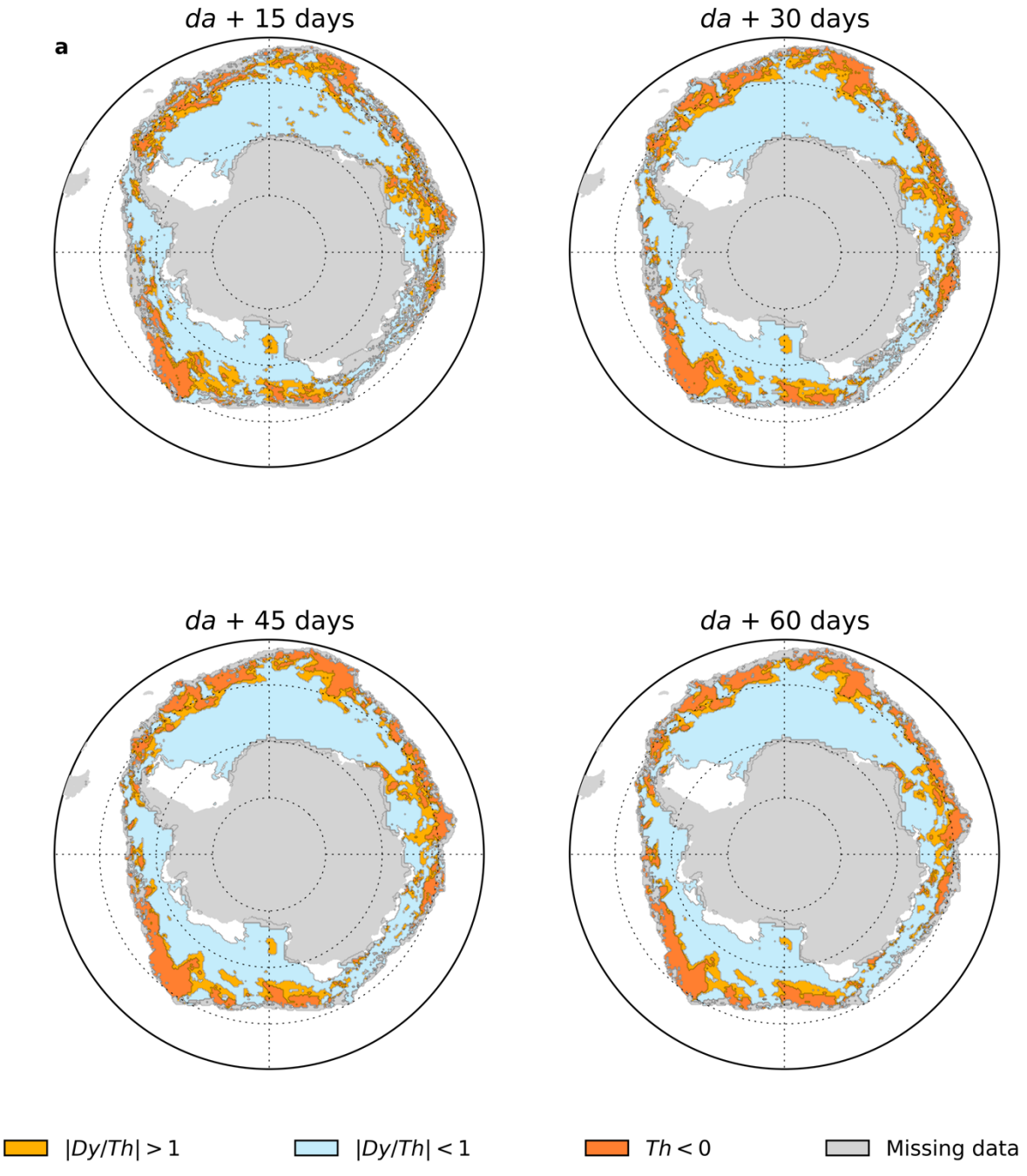

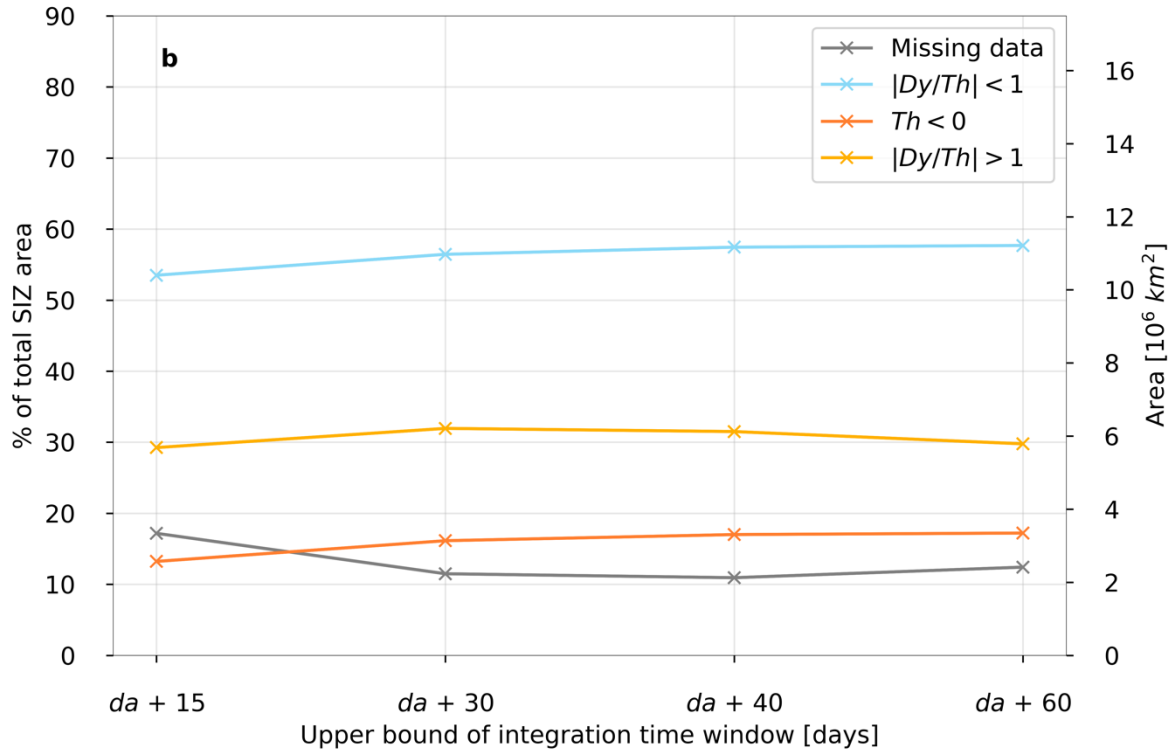

Supplementary Figure 1 | Sensitivity of the sea ice concentration-budget-based regions to the time-integration window. a shows the spatial distribution of three regions defined based on the budget: melting (Th < 0; orange), dominant dynamics (|Dy/Th| > 1; yellow and orange), dominant thermodynamics (|Dy/Th| < 1; blue). The budget is averaged after the date of sea ice advance (d_a), over a time window of unconstrained duration, which influence is tested here (values of 15, 30, 40 and 60 days). Grid points where the budget is not defined because of missing ice drift data are in grey and the perennial ice zone in white. **b** shows the fractional area of the aforementioned regions (in % of the seasonal ice zone), for the different integration time windows.

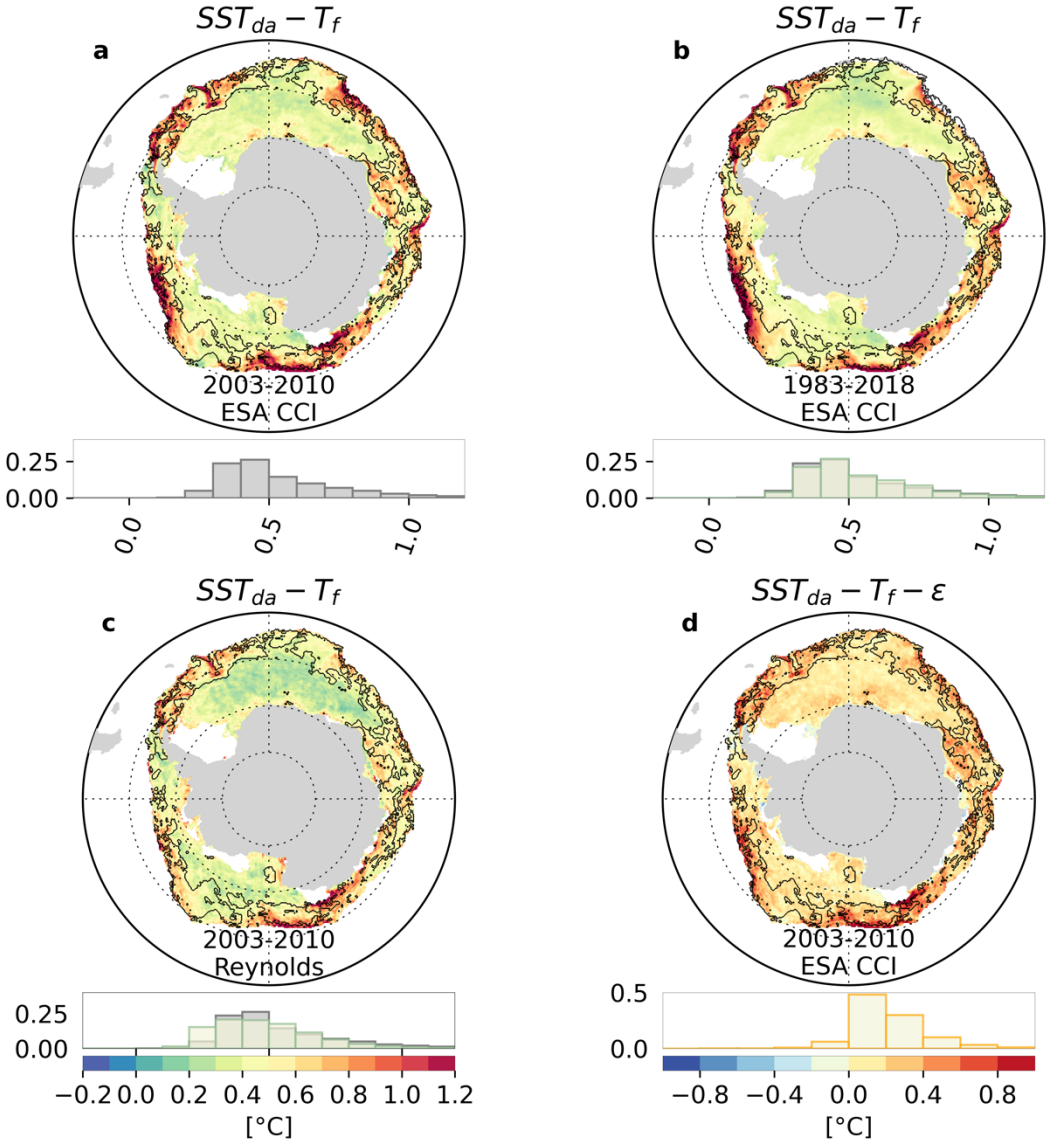

Supplementary Figure 2 | Robustness of the inner-outer zone limit across time periods and sea surface temperature (SST) products. SST at the date of advance (SST_{da}) referenced to freezing temperature (T_f, assumed constant at -1.8°C), based on **a** ESA CCI SST, averaged over 2003-2010; **b** ESA CCI SST, averaged over 1982-2018; and **c** Reynolds' SST, averaged over 2003-2010. **d** Difference between SST_{da} and T_f and the uncertainty (ε) on the ESA CCI SST analysis, averaged over 2003-2010. Corresponding frequency histograms are shown under each map in grey (**a**) or beige (**b**, **c**, **d**). In **b** and **c**, the grey histogram is the same as in **a** and used as a reference distribution. The black contour defines the limit between the inner and outer zones. White patches indicate regions out of the seasonal ice zone.

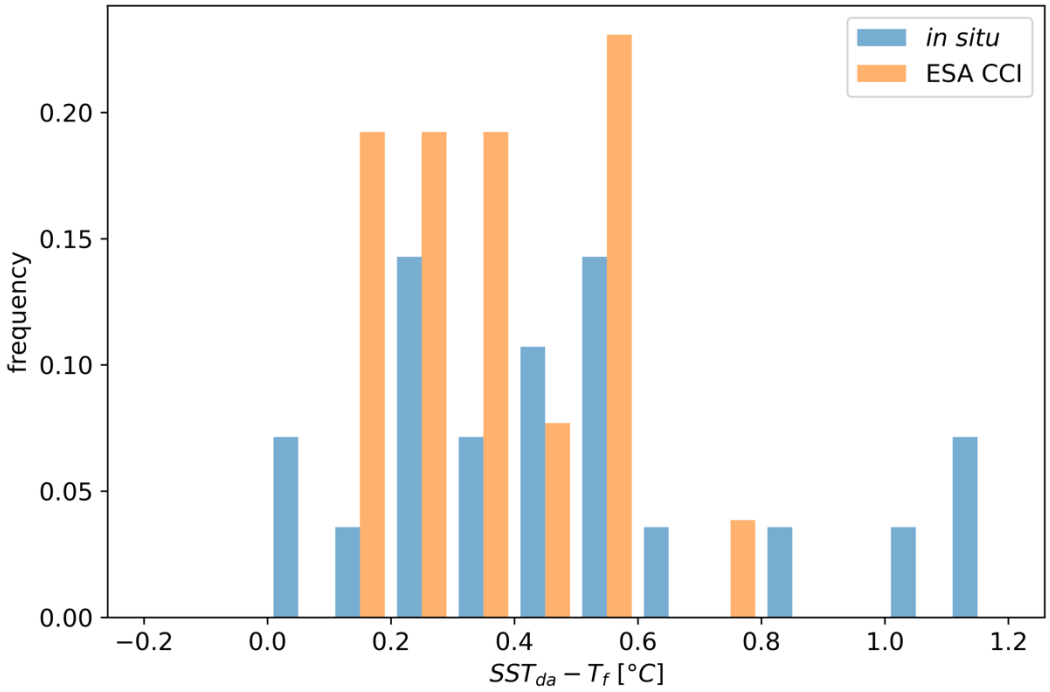

Supplementary Figure 3 | Comparison of satellite and in situ sea surface temperature on the day of advance (SST_{da}). Frequency histograms of SST at the date of advance referenced to freezing temperature (T_f, assumed constant at -1.8°C), derived from satellite (ESA CCI) and from in situ SST.

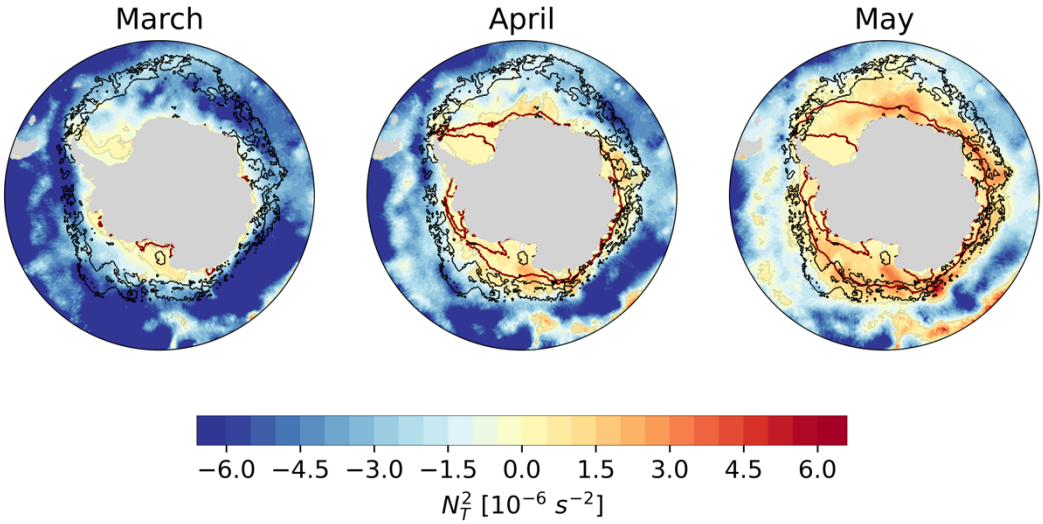

Supplementary Figure 4 | Monthly temperature contribution to the stratification at the base of the mixed layer (N_T^2) during the sea ice advance season. Maps are climatological, and constructed from in situ observations over 1979-2018. Red contours define the monthly climatology (over 1982-2018) of sea ice extent of the corresponding month, derived from passive microwave data. The black contour defines the limit between the inner and outer zones.

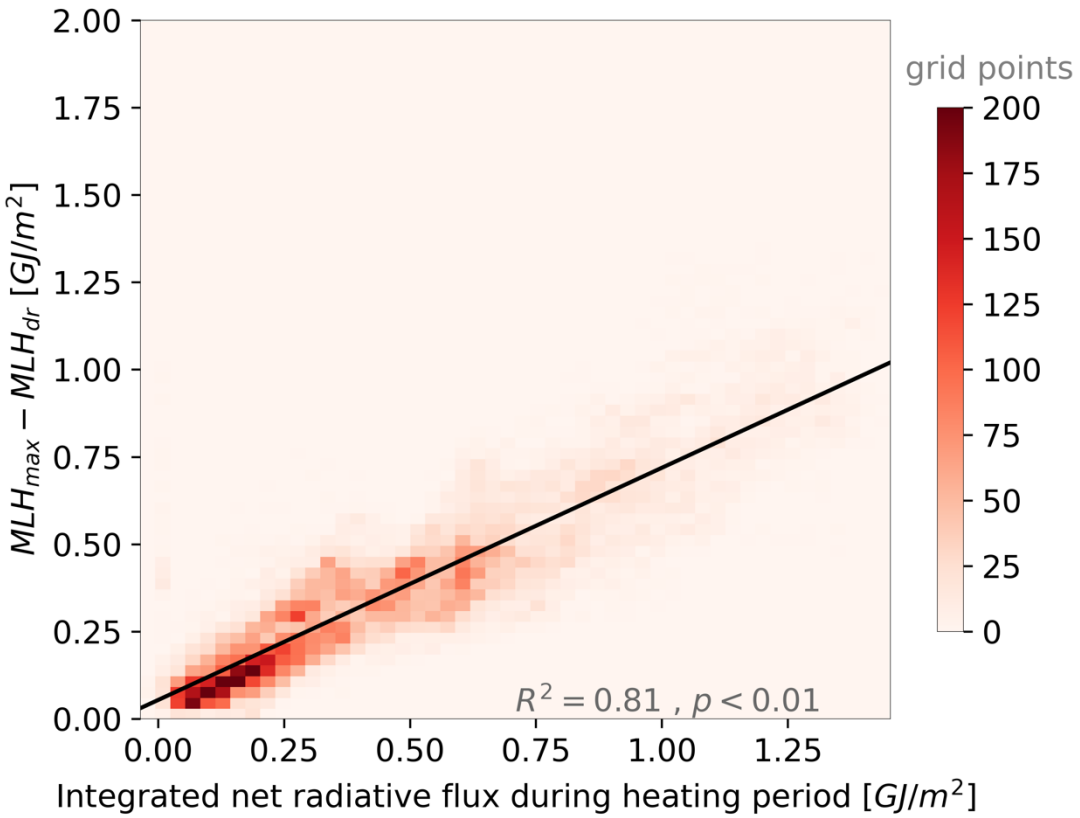

Supplementary Figure 5 | Spatial relationship between the increase in the mixed-layer heat content (MLH) and the total surface radiative heating over the ocean heating period (from the date of retreat to the date of seasonal maximum MLH). The sources used include: the climatological MLH derived from thermal infrared radiance satellite sea surface temperature (ESA CCI) and a climatology of mixed layer depths (1979-2018); the ISCCP observed climatological net radiative flux (1984-2016). The relationship is represented as a 2D histogram showing grid points from the inner zone only. Color gives the number of points in each pixel of the 2D histogram space. A Least Square linear regression was performed and the corresponding regression line, R^2 and p-values are shown.

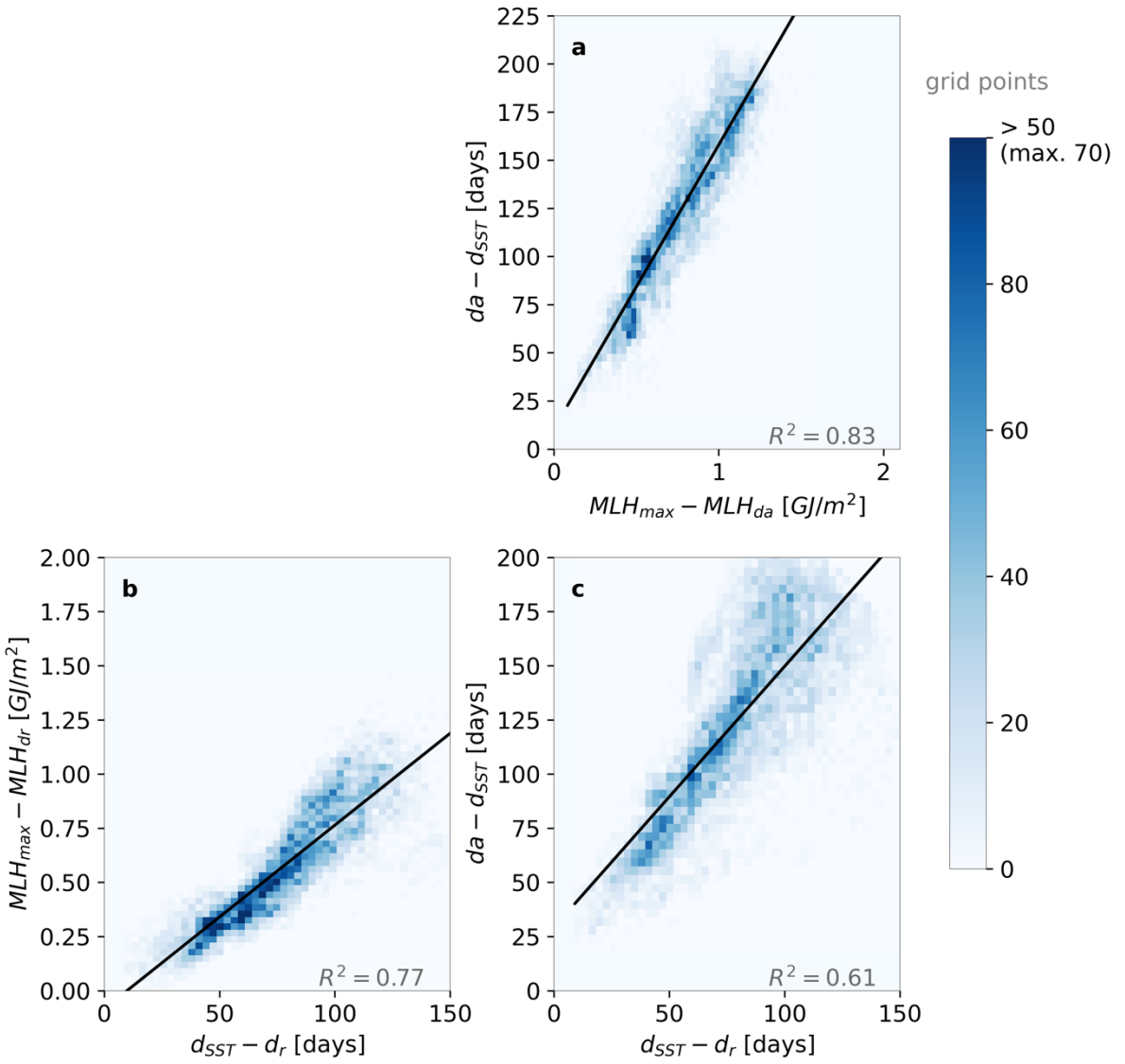

Supplementary Figure 6 | Selected outer zone spatial relationships between the 1982-2018 climatological maps of key variables displayed in Fig. 1, plotted as 2D histograms. a, date of advance (d_a) vs seasonal maximum of mixed layer heat content (MLH_{max}), **b**, MLH_{max} vs date of retreat (d_r) and **c**, d_a vs d_r. Anomalies are used, tailored to best showcase the relevant relationships (see Methods). d_a (d_r) anomalies refer to the date of maximum sea surface temperature (d_{SST}) such that positive anomalies indicate later advance (retreat). In **a** (**b**), MLH_{max} anomalies refer to the mixed layer heat content value at sea ice advance (retreat) date, which is close to but not exactly zero, because the sea surface temperature is a few tenths of degree above freezing (see Supplementary Figure 2). Only grid points from the outer zone are shown. Color gives the number of points in each pixel of the 2D histogram space. A Least Square linear regression was performed for each plot; the corresponding regression line (significant at 99%), and corresponding R^2 are given.

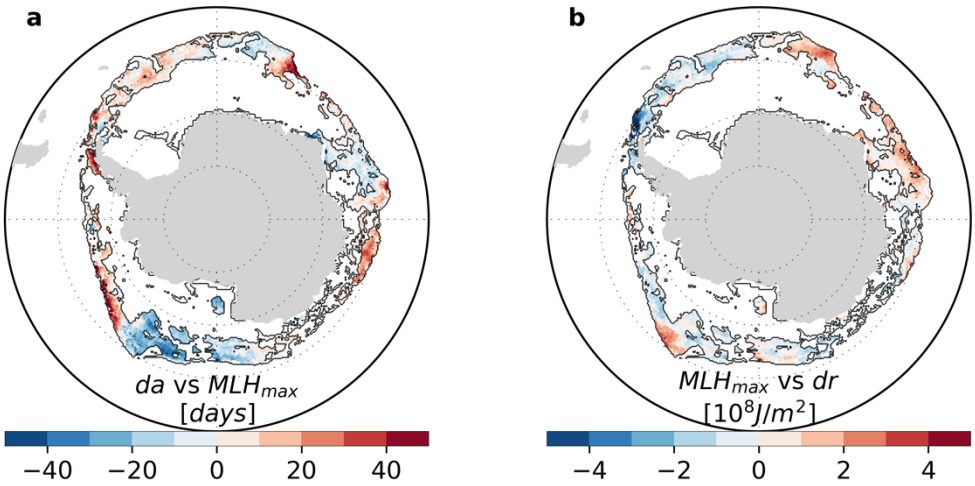

Supplementary Figure 7 | Spatial distribution of errors in the d_r-MLH$_{max}$-d_a linear regressions, in the outer zone. Error are defined as the residuals of **a**, the date of advance (d_a) vs seasonal maximum of sea surface maximum (MLH$_{max}$) and **b**, the MLH$_{max}$ vs date of retreat (d_r) linear regressions (Supplementary Figure 6). Residuals are calculated as the difference between the actual value at a given grid point and the predicted value based on the model fit. Only grid points located in the outer zone are displayed.

2 Drivers of Antarctic Sea Ice Retreat

Kenza Himmich, Martin Vancoppenolle, Marion Bocquet, Gurvan Madec

The Antarctic sea ice cover undergoes a rapid retreat in spring. Here, we explore the roles of ice melt, export and thickness in setting, locally, the climatological dates of sea ice retreat. Our findings reveal that retreat is driven by sea ice melt in most of the seasonal ice zone, being strongly constrained by sea ice thickness at the onset of the melt season. Ice export is the dominant driver of sea ice retreat only locally, in regions of coastal polynyas formation. The link between ice thickness and retreat date holds for interannual anomalies at the circumpolar scale but is significantly weaker at the local level.

2.1 Introduction

Within a year, the Antarctic sea ice cover undergoes a fast retreat from September to February, followed by a slower advance (e.g. Gordon, 1981; Roach et al., 2022). Dates of sea ice retreat and advance, defined as the first day in the year when smoothed-in-time sea ice concentration exceeds or falls below 15% (Lebrun et al., 2019; Stammerjohn et al., 2012; Stroeve et al., 2016), allow to track these seasonal variations at any given location.

The processes setting the date of sea ice advance have been investigated in Chapter I.1 (Himmich et al., 2023). Notably, we found that the climatological date of advance is tightly linked to the heat stored in the summer mixed layer, itself controlled by the climatological date of retreat. However, what sets the date of retreat still has to be examined to fully understand the mean state of seasonal Antarctic sea ice.

Previous studies have investigated the rapid seasonal decrease in Antarctic sea ice extent, offering insights into the drivers of sea ice retreat. This decrease has been linked to the large intensity of incoming solar radiation during summer (Roach et al., 2022), suggesting that solar-induced melting sets the pace of the seasonal sea ice extent reduction. Solar radiation influences sea ice melt through the ice-albedo feedback: any decrease in sea ice concentration enhances solar radiation uptake, basal melting and further loss of sea ice (Maykut & McPhee, 1995; Maykut & Perovich, 1987; Vivier et al., 2016). The creation of open water early on in the season, triggering the ice-albedo feedback, can also be promoted by thinner sea ice, which is removed more efficiently upon melting (Holland et al., 2006) or caused by wind-induced ice divergence (Eayrs et al., 2019; Nihashi & Cavalieri, 2006). Hence, sea ice melting, thickness and transport may all contribute to set the date of sea ice retreat.

In this exploratory study, we outline how these processes drive the climatological dates of sea ice retreat, as derived from passive-microwave sea ice concentration. Following a similar approach as Himmich et al. (2023), we evaluate the contributions of ice melting and transport to the total ice area removal leading to sea ice retreat, using passive microwave-based sea ice concentration budget diagnostics. We also investigate the potential link between the date of sea ice retreat and the ice thickness at the start of the melt season, using altimetry-based ice thickness retrievals. Lastly, we assess the extent to which anomalies in sea ice thickness contribute to the interannual variability in the timing of retreat.

2.2 Methods

2.2.1 Calculation of relevant diagnostics

We assessed the relationships between climatological mean sea ice thickness at the beginning of the melt season and the retreat date, using satellite observations.

The climatological date of sea ice retreat was derived as in Himmich et al. (2023) using daily passive microwave sea ice concentration from the EUMETSAT Ocean and Sea Ice Satellite Application Facility (OSI-SAF, Lavergne et al., 2019) over 1994-2022 (OSI-450 from January 1994 to April 2015, and OSI-430-b after April 2015).

Climatological sea ice thickness at the start of the melt season was approximated by the monthly mean September ice thickness, given its proximity to the spring equinox. We utilized altimetry-based ice thickness retrievals over 1994-2022 resulting from a decade of developments at LEGOS (Laboratoire d'Etudes en Géophysique et Océanographie Spatiales) in the group of Sara Fleury. This dataset, described in the recently defended thesis of Marion Boquet (Bocquet, 2023), and integrates year-round 12.5 km gridded L1B time series from ERS-1, ERS-2, Envisat, and CryoSat-2 missions. These different missions are inter-calibrated, leveraging mission overlap. Ice thickness is derived from radar freeboard following the methodology outlined by (Laxon et al., 2003). Ku-band radar freeboards are employed, with a correction applied to account for the varying speed of light in snow (Mallett et al., 2020). The density of ice (875-920 kgm^3) and snow (320-350 kgm^3) includes specified seasonal variations (Kurtz & Markus, 2012; Maksym & Markus, 2008). Snow depth is taken from a climatology of radiometer-based estimation developed for SI-CCI (Paul et al., 2021). In a submitted manuscript to JGR-oceans (Bocquet, 2024), the resulting ice thickness dataset was evaluated against independent data, namely the ASPeCt visual estimates (Worby et al., 2008), upward-looking sonar data from AWI moorings in the Weddell Sea (Behrendt et al., 2013), and Operation Ice Bridge air-based estimates (Kurtz et al., 2013), showing reasonable agreement. The study also highlights a possible overall high bias, consistent with suggestions by (Kacimi & Kwok, 2020). Overall, as this dataset is fairly recent, it must be considered as significantly uncertain.

All mentioned data were interpolated on the OSI-SAF Equal-Area Scalable Earth 2 (EASE2) 25 km grid.

2.2.2 Sea ice concentration budget

To explore the respective role of ice dynamics and thermodynamics in setting the date of sea ice retreat, we computed a sea ice concentration budget decomposition from OSI-SAF daily fields of ice concentration (Lavergne et al., 2019) and drift (Lavergne & Down, 2023). The OSI-SAF sea ice drift is retrieved using different methods according to the season. In winter, from April to September, ice drift is retrieved using a maximum cross correlation algorithm applied to brightness temperature from a number of sensors (SSM/I, SSMIS, AMSR-E and AMSR2). In summer, from November to February, a free-drift model based on the ERA5 wind fields (Hersbach et al., 2020) is used. In October and March, drift fields are derived from both the free-drift model and satellite-based retrievals. This dataset is available over 1991-2020, with a resolution of 75 km.

The governing equation for the sea ice concentration is decomposed into dynamic and residual terms (Holland & Kwok, 2012):

$$\frac{\partial \text{SIC}}{\partial t} = \nabla.(\boldsymbol{u}\ \text{SIC}\ ) + \text{residual} \tag{I.2}$$

The ice concentration flux divergence represents the effects of advection and divergence of sea ice caused by ice drift. The residual term includes both thermodynamic processes (melting / freezing) and local mechanical redistribution through ridging and rafting. To compute each contribution to the above budget, we applied the exact methodology of Holland and Kimura (2016) on OSI-SAF sea ice concentration and drift data. Sea ice concentration fields are interpolated on the 75-km grid of ice drift. A 7x7 cell square-window smoothing filter is then applied to the ice drift fields in order to avoid noise in the dynamic term. The time derivative in ice concentration is calculated as a central difference in time of sea ice concentration fields at a daily frequency. Advection and divergence terms are calculated as central differences in space then averaged over 3-days periods to synchronize with time derivatives. The resulting time series (1991-2020) are more than three times longer than the original product of Holland and Kimura (2016) (2003-2010). They were carefully evaluated by reproducing Figure 3 of Holland and Kimura (2016), showing the seasonal evolution of the climatological terms of the SIC budget, with negligible differences (see Figure 5 in General Introduction).

Adapting the method of Himmich et al. (2023), we finally evaluated the total dynamic and thermodynamic contributions to the sea ice concentration budget from September 15th to the date of retreat, which approximates the melt season. We diagnosed the total sea ice concentration decrease (ΔSIC), as well as the dynamic (Dyn) and residual (Res) contributions to sea ice concentration tendency over the melt season as follow:

$$\begin{aligned}
\Delta\text{SIC} &= \int_{15Sep.}^{d_r} \frac{\partial \text{SIC}}{\partial t} dt, \\
\text{Dyn} &= \frac{1}{\Delta\text{SIC}} \int_{15\text{Sep.}}^{d_r} \nabla.(\boldsymbol{u}\text{SIC}) dt, \\
\text{Res} &= \frac{1}{\Delta\text{SIC}} \int_{15Sep.}^{d_r} \text{residual}\ dt.
\end{aligned} \tag{I.3}$$

2.3 Results and Discussion

Sea ice retreat, local melting or export? We investigate how local ice export and melt control the spatial variability in the sea ice retreat date, based on the ice transport (Dyn) and residual (Res) contributions to the total sea ice concentration decrease over the melt season (Figure 1). We hypothesize that the residual ice removal is generally dominated by melting, as ice deformation is limited to small regions and would predominantly occur at the onset of the melt season, when sea ice concentration is still high (Holland & Kimura, 2016). First examining the dynamic contribution (Figure 1a), we find that sea ice is exported from the inner seasonal ice zone ($Dyn < 0$) towards a thin circumpolar band, close to the winter ice edge ($Dyn > 0$). These spatial patterns resemble the ones of the dynamic contribution evaluated during the advance

season by Himmich et al. (2023). Next, examining the thermodynamic contribution, we find that melting occurs ($Res < 0$; Figure 1b) and dominates ice removal during the melt season in 93% of the seasonal ice zone area ($|Dyn/Res|$; Figure 1c < 1). In the remaining 7%, mostly located near the coast, sea ice growth occurs ($Res > 0$) and ice removal is dominated by ice export ($|Dyn/Res| > 1$). These regions correspond to areas of polynya formation (Nihashi & Cavalieri, 2006), where sea ice is continuously growing and advected off the coast at the start of spring (Nakata & Ohshima, 2022). Hence, our analysis suggests sea ice melt controls the timing of retreat everywhere in the seasonal ice zone but in regions where polynyas can form.

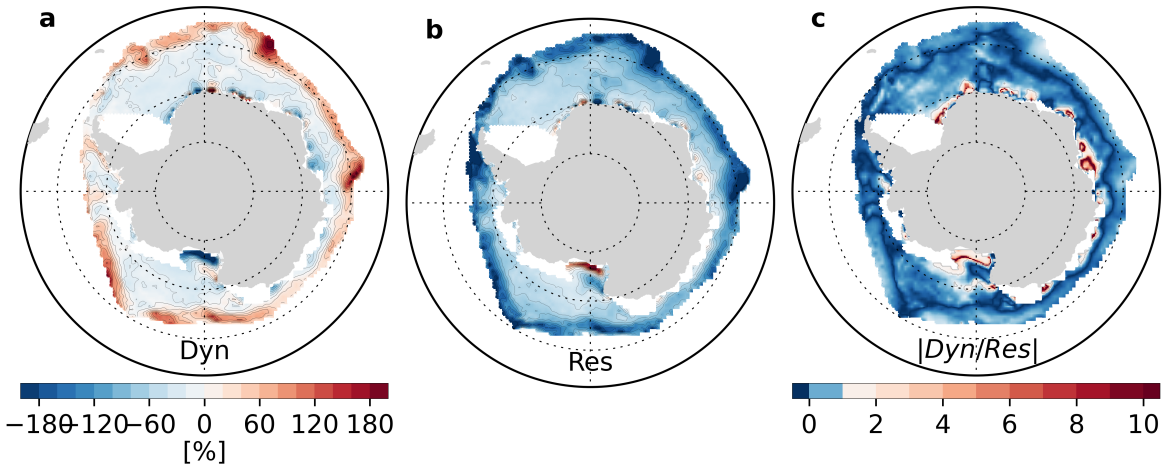

Figure I.1: **Maps of passive microwave-based sea ice concentration budget terms preceding the date of sea ice retreat, averaged over 1991-2020.** The dynamic (Dyn, **a**) and residual (Res, **b**) contribution to the total sea ice concentration tendency and their absolute ratio ($|Dyn/Res|$, **c**), all evaluated over the melting period, from September 15 to the date of retreat. White patches indicate regions out of the seasonal ice zone.

Control of sea ice retreat from thermodynamic processes. In the case of a melt-driven sea ice retreat, a relationship between the timing of retreat and the sea ice thickness at the melt onset (SIT_{mo}) arises when integrating, from the sea ice melt onset (d_{mo}) to the date of retreat (d_r), the heat budget in sea ice (Lebrun et al., 2019; Semtner, 1976), neglecting snow, sensible heat and salt contents:

$$d_r(x,y) - d_{mo}(x,y) = \rho L \frac{SIT_{mo}(x,y)}{< Q_{ice}(x,y) >} \tag{I.4}$$

where ρ is the ice density and L is the sea ice latent heat of fusion and $< Q_{ice} >$, the mean net heat flux to sea ice over the melt season. We subsequently explore the strength of this link, using climatological distributions of ice retreat date and September thickness over 1994-2022. Maps of the climatological sea ice retreat date (Figure 2a) and September thickness (Figure 2b) indicate that thicker sea ice retreats later, reflecting a robust linear relationship ($p < 0.05$; Figure 3a). Specifically, 65% of the spatial variance in the retreat date is attributed to September ice thickness, based on a linear model (Figure 3a). Ice thickness therefore strongly contributes to setting the climatological timing of sea ice retreat. This is consistent with simulations conducted by Goosse et al. (2023), highlighting that the pace of the spring sea ice extent decrease is modulated by initial September thickness.

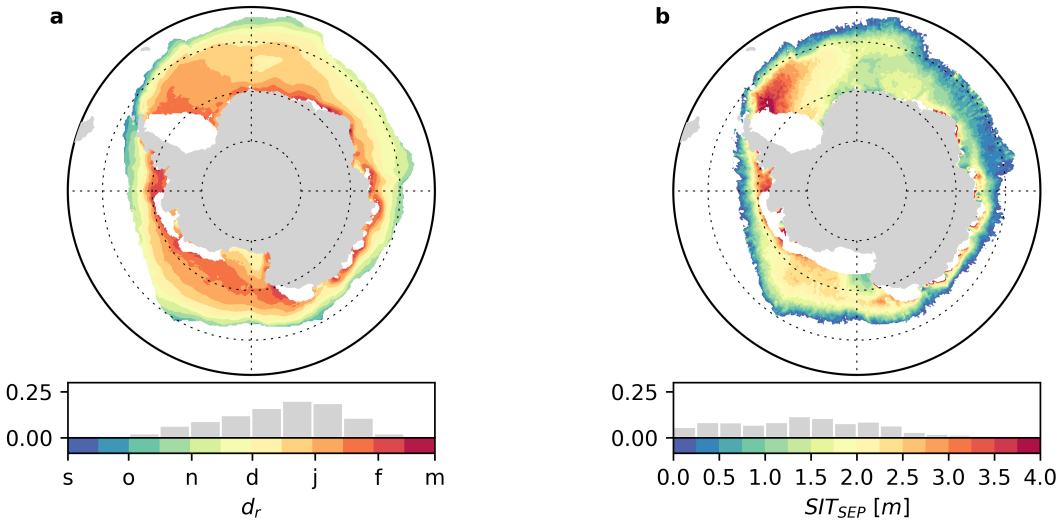

Figure I.2: **Climatological maps of key variables (1994-2022). a**, retreat dates derived from passive microwave sea ice concentration and **b**, altimetry-based mean September sea ice thickness. Corresponding frequency histograms are shown under each map. White patches indicate regions out of the seasonal ice zone.

Nonetheless, one third of the spatial variance in retreat dates remains unexplained by sea ice thickness, as illustrated by the scatter around the linear relationship (Figure 3a). We next discuss the potential causes of this scatter. Based on equation (3), a perfectly linear relationship between ice thickness and retreat date would indicate spatially uniform $< Q_{ice} >$. This suggests that the spatial variability of $< Q_{ice} >$ explains, at least in part, the remaining variance in retreat date. In addition, observed sea ice export and resulting concentration decrease during the melt season (Figure 1a) could contribute to this spatial variability by locally increasing solar heat uptake and triggering the ice-albedo feedback (Eayrs et al., 2019; Nihashi & Cavalieri, 2006). Consistently, the dispersion in the retreat date-thickness diagram decreases by thickness where considering only regions where melting dominates ice removal (R^2 = 72%; Figure 3b) than in the entire the seasonal ice zone (R^2 = 65%; Figure 3a) or where ice export prevails (R^2 = 28%; Figure 3c). Last, uncertainties related to ice thickness, including observational errors (Bocquet, 2023) and using the mean September value as a proxy of the ice thickness at the melt onset, could contribute to the scatter around the thickness-retreat relationship. In summary, heat fluxes, sea ice dynamics and observational uncertainties could explain the remaining spatial variance in climatological retreat dates; however, their relative contribution cannot be untangled from observations alone. Models may be more suitable for that purpose.

From spatial to interannual variability. Lastly, we evaluate possible interannual links between anomalous September sea ice thickness and timing of sea ice retreat. Regressing mean detrended anomalies over the seasonal ice zone, we find that ice thickness explains 50% of the interannual variance in retreat dates (Figure 4a). This suggests that, at the scale of the ice pack, interannual anomalies in retreat dates are partly caused by anomalies in ice thickness.

Next, examining the strength of this link at the grid-point scale on a correlation map (Figure 4b), we find statistically significant correlations between detrended anomalies in ice

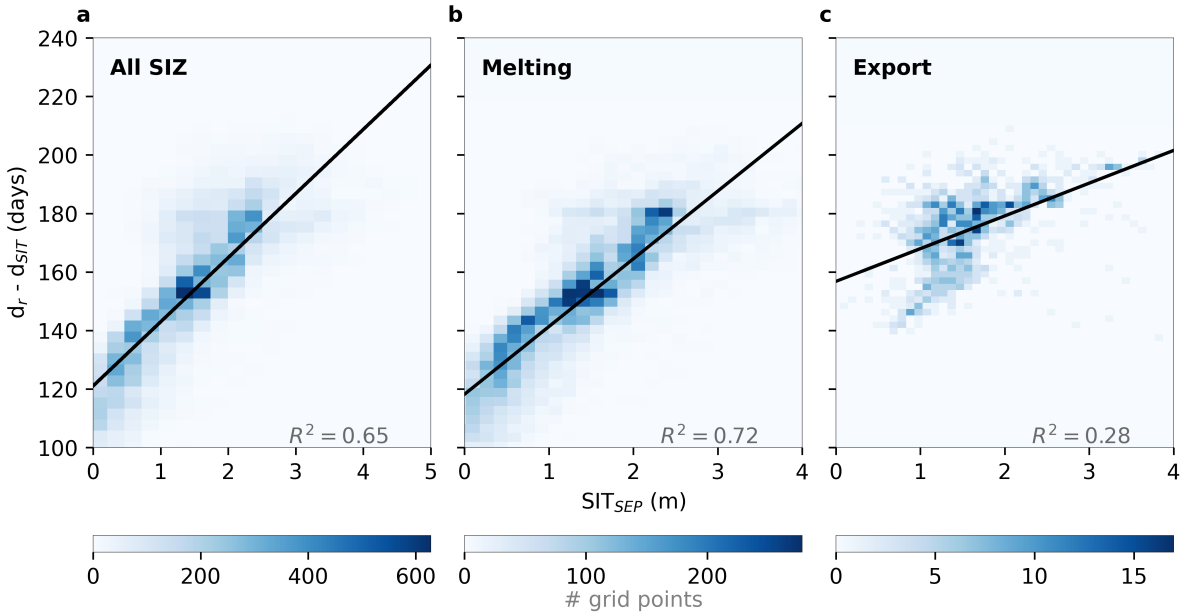

Figure I.3: **Spatial relationships between September sea ice thickness (SIT_{SEP}) and the date of sea ice retreat (d_r).** Relationships are plotted as 2D histograms over **a**, the entire seasonal ice zone and over regions where the dominant ice removal process preceding ice retreat is **b**, melting and **c**, export (see Figure 1). d_{SIT} refers to September 15th. Color gives the number of points in each pixel of the 2D histogram space. A Least Square linear regression was performed for each plot; the corresponding regression line (significant at 99%), and determination coefficient (R^2) are shown.

thickness and retreat date in only 15% of the seasonal ice zone area. Hence, at the local scale, ice thickness anomalies appear to exert a weak control on interannual variability in ice retreat dates. This could suggest that sea ice transport anomalies, which are usually wind-driven, may have a larger contribution in setting the date of retreat at interannual timescales than in the mean state. Previous studies support this hypothesis. In the Ross Sea, sea ice retreat date anomalies have been correlated to spring zonal winds and induced ice drift by Holland et al. (2017). Moreover, model experiments indicate that interannual variability in the retreat date is significantly reduced in the absence of wind stress variability (Kusahara et al., 2019). A joint examination of interannual variability in ice retreat date, ice drift and winds could help better constrain the role of these processes. Additionally, potential issues with the fairly recent sea ice thickness product used here may increase the lack of significant correlations at the local scale. To test this hypothesis, the correlation map of Figure 4b could be replicated using alternative observational or reanalysis ice thickness datasets.

We plan to conduct the suggested analyses above before attempting to publish this chapter, in order to assess the relative role of wind-driven processes and observational errors in weakening the ice thickness-retreat date link at the interannual time scale.

In conclusion , the climatological retreat date is overall set by sea ice thickness at the beginning of the melt season. Ice dynamics alter this relationship locally, closer to Antarctica. This framework complements the previous Chapter I.1 (Himmich et al., 2023), allowing to comprehensively describe the mean state of Antarctic sea ice seasonality from simple constraints exerted by ice-ocean thermodynamics.

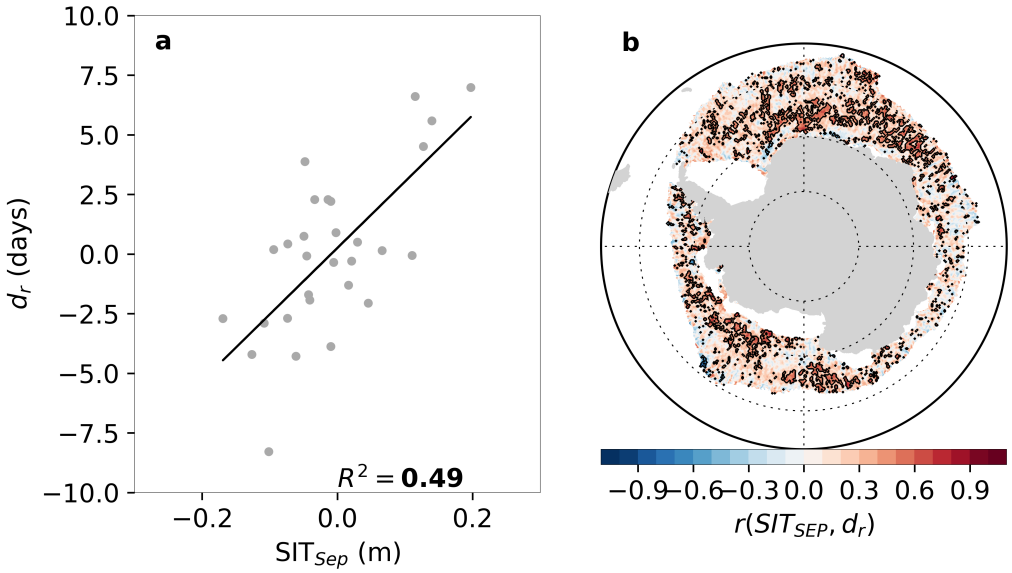

Figure I.4: **Links between interannual variability in ice retreat date and thickness.** Retreat dates (d_r) versus previous September sea ice thickness (SIT_{Sep}) **a**, detrended anomalies and **b**, correlation coefficient (r) between detrended time series at each grid-point. A least Square linear regression was performed for **a**; the corresponding regression line (significant at 99%), and corresponding coefficients of determination (R^2) are shown. In **b**, the black contour indicates where correlations are statistically significant at the 95% level while white patches indicate regions out of the seasonal ice zone.

CHAPTER

II

Drivers of Antarctic Sea Ice Seasonality: a Model Study

In Chapter I, we established an analytical framework explaining the spatial distribution of climatological sea ice advance and retreat dates. We highlighted that these dates are predominantly set by freezing and melting, whereas ice dynamics contribute and can even dominate in some limited areas. In addition, we found strong preconditioning by the seasonal maximum of mixed layer heat content on the timing of advance, and by the sea ice thickness at the melt onset on the timing of retreat. These constraints manifest as robust linear links between sea ice thickness and retreat date, retreat date and mixed layer heat content, and mixed layer heat content and advance date, albeit with a notably large scatter.

Physical considerations from Chapter I support a thermodynamic origin for these links. They also suggest that the spread around linearity could be caused, first, by the spatial variability in the net heat fluxes (from oceanic and atmospheric origins) required to melt sea ice or cool down the mixed layer to the freezing temperature. Second, sea ice import and export could also contribute to the spread around linearity by hastening or delaying retreat, and also by modifying air-ice-sea fluxes (Nihashi & Cavalieri, 2006; Tamura et al., 2011). However, these arguments based on the sole observational analyses such as presented in Chapter I remain somehow speculative, and could be reinforced by performing similar analyses with a model. Indeed, ice-ocean models have proven instrumental to overcome observational limitations and improve understanding of the sea ice seasonal cycle (e.g. Goosse et al., 2023; Kusahara et al., 2019; Lebrun et al., 2019; Roach et al., 2022); this could also apply in the present context.

Another incentive to reproduce the analyses from Chapter I in a model, is that this could inform on model behavior and progress to understand the issues they suffer from. This might prove particularly useful in the context of the substantial uncertainties in the representation of Antarctic sea ice processes in Earth System Models highlighted in the General introduction (Beadling et al., 2020; Casagrande et al., 2023; Roach et al., 2020).

In this chapter, I present work in progress where the analytical framework from Chapter I is applied within simulations with the NEMO ice-ocean model, either forced by atmospheric

reanalyses or run in coupled mode. Our objectives are (i) to confirm the thermodynamic origin of linearity and progress on understanding the spread around it in the relationships, (ii) to identify what can be learned on model behavior and biases based on such analyses. To achieve this, we present an analysis of the thickness-retreat-heat-content-advance relationships in the model simulations. We investigate the impacts of varying heat fluxes and sea ice dynamics through heat and sea ice concentration budget analyses. We also analyze experiments where sea ice dynamics are deactivated.

Impacts of Heat Fluxes and Sea Ice Dynamics on Antarctic Sea Ice Seasonality

Kenza Himmich, Martin Vancoppenolle, Gurvan Madec, Casimir de Lavergne, Hugues Goosse

The timings of seasonal Antarctic sea ice retreat and advance are strongly constrained by ice-ocean thermodynamics. Linear links emerge between observed spatial distributions of climatological September ice thickness, ice retreat date, seasonal maximum mixed layer heat content, and ice advance date, although with substantial dispersion around linearity. Yet, the causes of such behavior are not entirely understood. In this work in progress, we investigate the drivers of Antarctic sea ice advance and retreat using simulations performed with the NEMO ice-ocean model, in forced-atmosphere and fully-coupled mode. We find linear relationships in all simulations, albeit with more dispersion around linearity than in observations. Linearity survives when ice dynamics are switched off, which confirms a thermodynamic origin. Regarding the dispersion around linearity, we attribute it to two contributing factors. A first source of dispersion is the spatial variability in vertical air-ice-sea fluxes, especially during the open water season, as highlighted by a heat budget analysis. Sea ice drift provides an extra source of dispersion during the melt season, as sea ice drift can either hasten or delay sea ice retreat. We also suspect that climatological averaging reduces dispersion around linearity, raising possible limitations in the comparison with observations when running simulations with climatological forcing. Our findings offer potential implications for the roles of heat fluxes and sea ice dynamics in the real world. They also inform on ice-ocean processes as simulated by NEMO, in particular on the origin of some of its seasonal biases.

1 Introduction

In contrast to the Arctic, the Antarctic sea ice cover is mainly seasonal. On average, 15 million square kilometers, or three quarters of maximum extent, grow and decay within the year (Parkinson, 2019, 2014). Seasonal variations in Antarctic sea ice are in large part driven by thermodynamic processes (Chapter I; Holland & Kimura, 2016). Seawater freezing (Talley et al., 2011; Thompson et al., 2020) predominantly sets the onset of the ice season, except in an outer band a few degrees wide where advance is due to the import of drifting ice into warmer waters (Himmich et al., 2023). From then on, sea ice thickens, with September typically marking the onset of the melt season. Antarctic sea ice primarily melts from its base (Andreas & Ackley, 1982; Vancoppenolle et al., 2009), primarily under solar heating of the upper ocean layer through open water (Maykut & McPhee, 1995; Ohshima et al., 1998; Vivier et al., 2016). Basal

melt implies the loss of thinnest ice, increasing the open water fraction at a rate depending on mean thickness (Häkkinen & Mellor, 1990; Holland et al., 2006; Massonnet et al., 2018). This chain of mechanisms leads to a strong amplifying mechanism between open water fraction, solar absorption and basal melt (Maykut & Perovich, 1987), commonly referred to as the sea ice albedo feedback (Goosse et al., 2018). Once the seasonal ice zone becomes ice free, the ocean mixed layer absorbs heat (mostly in solar form) throughout the warm season (Perovich et al., 2007), and subsequently cools down in autumn (Pellichero et al., 2017), until it reaches the freezing temperature and restarts a new cycle (Himmich et al., 2023), enabling sea ice expansion through sea water freezing.

Thermodynamics impose strong local constraints on the dates of ice retreat and advance (Chapter I; Himmich et al., 2023; Holland et al., 2017; Lebrun et al., 2019; Smith et al., 2020; Stammerjohn et al., 2012, 2008), respectively defined as the first day in the year when sea ice concentration falls below or exceeds 15% (Massom et al., 2008; Stammerjohn et al., 2008). Notably, in Chapter I, linear links were highlighted between spatial distributions of climatological September ice thickness, ice retreat date, seasonal maximum of mixed layer heat content, and ice advance date, subsequently referred to as TRHA links.

Are these links purely thermodynamic? How are they affected by heat fluxes and sea ice transport? This remains uncertain as disentangling the role of these processes is not easy with observations. Simple sea ice and ocean mixed layer heat budget models indicate that the dispersion around linear TRHA relationships relates to the spatial distribution of mean net heat fluxes into sea ice over the melt season and into the mixed layer over the open water season (Chapter I; Himmich et al., 2023). In addition, sea ice transport and air-ice-sea heat fluxes could be linked. Indeed, during the melt season, the horizontal sea ice velocity field is often divergent (Eayrs et al., 2019; Holland & Kimura, 2016) which locally forms open water, and increases ocean solar heat uptake (Maykut & Perovich, 1987; Nihashi & Cavalieri, 2006; Vivier et al., 2016). During the advance season, sea ice is exported from most of the inner seasonal ice zone to an outer circular band near the winter ice edge, where it melts (Himmich et al., 2023; Holland & Kimura, 2016), potentially affecting the mixed layer heat budget there. Improving our understanding of TRHA relationships thus involves analyzing heat fluxes, sea ice transport, and their interactions. However, such an analysis is hindered by observational limitations, in particular the lack of reliable heat flux observations in the seasonal ice zone (Swart et al., 2019).

Sea ice-ocean models could be used to progress, as they simulate heat fluxes and allow to experiment with ice drift. However, the large disparity between global climate models and observations regarding the seasonal cycle of Antarctic sea ice (Casagrande et al., 2023; Roach et al., 2020) suggests that underlying processes may not be well represented. What

insights do TRHA relationships offer on how models represent key drivers of sea ice seasonality?

In this exploratory study, we use simulations from a sea ice-ocean model to answer the above questions. Specifically, we use the NEMO (Nucleus for European Modelling of the Ocean) model, in which the respective influence of initial ice thickness and ocean conditions on the timings of sea ice retreat and advance seems to hold (Goosse et al., 2023). In section 3, we assess the strength of the TRHA relationships in different configurations of the NEMO model, differing mostly in terms of atmospheric representation and tuning. This assessment relies on two pre-existing simulations conducted by Goosse et al. (2023) and one additional simulation conducted for the purpose of this study. We subsequently examine, in section 4.1, the influence of heat fluxes on the strength of these links through heat budget diagnostics. We also assess, in section 4.2, the role of sea ice dynamics based on sea ice concentration budget analyses and a sensitivity experiment in which sea ice drift is deactivated. We finally discuss how our findings provide insights into seasonal sea ice processes in both the model and real worlds (section 5).

2 Methods

2.1 Analysis framework

Ice-ocean thermodynamics link sea ice retreat and advance dates to preceding seasonal maxima of sea ice thickness and mixed layer heat content, respectively, through TRHA relationships (Chapter I; Himmich et al., 2023). Ice dynamics also affect the timing of sea ice retreat, but independently of this framework, and are not considered here.

THRA relationships stem from heat conservation in the ocean mixed layer-sea ice system (Dong et al., 2007; Lebrun et al., 2019; Semtner, 1976). Neglecting snow, sensible heat and salt storage in the snow-sea ice system, one gets:

$$\rho L \frac{\partial SIT}{\partial t}(t,x,y) = Q_{ice}(t,x,y), \tag{II.1}$$

$$\frac{\partial MLH}{\partial t}(t,x,y) = Q_{ML}(t,x,y). \tag{II.2}$$

ρ is the ice density, L is the ice latent heat of fusion, SIT is the sea ice thickness, and MLH is the mixed layer heat content. $Q_{ice} = Q_{atm} + Q_w$ is the net heat flux to the sea ice, with Q_{atm} the net surface heat flux (including shortwave, longwave, latent and sensible heat contributions) and

Q_w the ocean-to-ice heat flux. Q_{ML} is the net heat flux into the mixed layer, including surface heat fluxes, as well as entrainment, diffusion and advection at the base of the mixed layer. The mixed layer heat content is defined as:

$$MLH = \rho_w c_p MLD\left(T - T_{ref}\right), \tag{II.3}$$

where ρ_w is the reference density of seawater, c_p, the specific heat of seawater, MLD the mixed layer depth, T the mixed layer temperature, and T_{ref} a reference temperature.

Integrating equation (1) over the melt season, i.e. from the date of the seasonal ice thickness at the melt onset (d_{SIT}) to the date of sea ice retreat (d_r), we get:

$$d_r(x,y) - d_{SIT}(x,y) = \left\langle m(x,y)\right\rangle \cdot SIT_{mo}(x,y), \tag{II.4}$$

where SIT_{mo} is the ice thickness at the melt onset, $< . >$ refers here as an average over the melt season and the melt rate is defined as

$$\langle m\rangle = \frac{\rho L}{\left\langle Q_{ice}(x,y)\right\rangle} \tag{II.5}$$

Now, integrating (2) over the open water warming (from d_r to d_{MLH}) and cooling (from d_{MLH} to d_a) periods we get:

$$\begin{cases} d_{MLH}(x,y) - d_r(x,y) = -\left(MLH_{max}(x,y) - MLH_{dr}(x,y)\right)\cdot\left\langle Q^+_{ML}(x,y)\right\rangle^{-1}. \\ d_a(x,y) - d_{MLH}(x,y) = -\left(MLH_{max}(x,y) - MLH_{da}(x,y)\right)\cdot\left\langle Q^-_{ML}(x,y)\right\rangle^{-1} \end{cases} \tag{II.6}$$

where d_{MLH} is the date of maximum MLH. $< Q^+_{ML} >$ and $< Q^-_{ML} >$ refer to the net heat flux into the mixed layer, averaged over the warming and the cooling periods, respectively.

Equations (4) and (6) show linear relationships between anomalies of (i) d_r and SIT_{mo}, (ii) MLHmax and d_r and (iii) d_a and MLH_{max}. Hence, linear relationships for those quantities would hold in the spatial climatologies, provided $< Q_{ice} >$, $< Q^+_{ML} >$ and $< Q^-_{ML} >$ are spatially uniform in the climatology.

2.2 Model overview

2.2.1 Model description

Methodological caveat: it should be noted that the selection of the following simulations

was opportunistic, and as such, the simulation protocol was not specifically designed for the purposes of this study. Protocol limitations and issues are identified and discussed throughout the study.

This study is based on two sets of simulations using different but physically close versions of the NEMO ocean modelling system, including a sea ice model (see Table 1). The first set of simulations (referred to as N1) was conducted using the configuration of Rathore et al. (*in prep.*). This configuration is based on NEMO version 4.2 (Madec et al., 2023), which includes the SI^3 (Sea Ice modelling Integrated Initiative) model (Vancoppenolle et al., 2023) as a sea ice component. The second set of simulations (referred to as N025) comprises simulations conducted by Goosse et al. (2023) using NEMO 3.6 (Madec et al., 2017) including LIM3.6 as a sea ice model (Rousset et al., 2015). In both versions, the ocean component is a three-dimensional, free-surface, hydrostatic, primitive-equation global ocean general circulation model. SI^3 and LIM3 can be considered as successive and close versions of the same continuum sea ice model, based on an energy- and salt-conserving approach (Bitz & Lipscomb, 1999; Vancoppenolle et al., 2009), a five-category ice thickness distribution (Bitz et al., 2001; Lipscomb, 2001), a second-order-moment-conserving scheme for horizontal advection (Prather, 1986) and an viscous–plastic rheology. LIM3.6 uses the elastic-viscous-plastic numerical solver (Bouillon et al., 2013) whereas the adaptive-EVP method is used in SIĺ3, which improves numerical convergence (Kimmritz et al., 2016).

N1 simulations use the global ORCA1 grid, with a nominal horizontal resolution of 1° at the Equator and a reduction in meridional grid spacing towards higher latitudes to match the accompanying reduction of the zonal dimension of the grid cells. Contrastingly, N025 simulations use a regional circum-Antarctic configuration on the ePERANT025 grid (Mathiot et al., 2017). This grid has a nominal horizontal resolution of 1/4° with an isotropic spacing, meaning that the resolution is ∼24 km at 30° S but increases up to 3.8 km over the Antarctic continental shelf. In the vertical, N1 and N025 both have 75 levels, with thickness increasing from 1 m at the surface to 200 m at depth (Storkey et al., 2018).

The physical representation of ocean and sea ice is fundamentally similar in the two model versions. However, both set of simulations are tuned differently. Notably, N1 incorporates a comprehensive tidal mixing parametrization (de Lavergne et al., 2020; Rathore et al., *in prep.*) whereas N025 does not.

2.2.2 Forcing and spin-up

The model forcing and spin-up strategies also differ between the two sets of simulations

Table II.1: **Overview of the simulations considered in the study.**

Simulations set name	N1	N025
NEMO Version	4.2	3.6
Resolution	1°	1/4°
Spin-up time	1000 years	10 years
Experiments		
Forced-atmosphere	N1_For (CORE2 - *Normal Year* 1984-2006)	N025_For (ERA5 1990-1991)
Fully-coupled	-	N1_Atm (COSMO_CLM2 1995-1996)
No ice dynamics	N1_NoDy_Feb N1_NoDy_Sep	-

and are summarized in Table 1. All forced simulations convert atmospheric state forcing fields into heat, mass and momentum fluxes using CORE bulk formulas (Large & Yeager, 2009).

N1 simulations were conducted only in forced-atmosphere mode, using the CORE normal year forcing data version 2 (Large & Yeager, 2009). The normal-year type consists of single annual cycles of all data needed to force an ice-ocean model. The normal-year is representative of climatological conditions at the end of the 20th century (practically 1984-2006; see (Large & Yeager, 2009) and include weather patterns of a single year (1995), as normal as possible (Large & Yeager, 2004). COREv2 forcing data set includes 6-hourly data fields of zonal and meridional wind, air temperature and humidity at 10 m.

N025 simulations were conducted in both forced- and coupled-atmosphere modes. Forced-atmosphere simulations use 3-hourly fields from the ERA5 reanalysis (Hersbach et al., 2020). The same forcing is applied to each year of simulation, based on the period between 1 May 1990 and 30 April 1991, which is considered a normal period regarding the major modes of climate variability. Coupled N025 simulations use the COSMO-CLM2 atmospheric model, which includes version 5.0 of the Consortium for Small-scale Modeling (COSMO) regional atmospheric model (Rockel et al., 2008) and the Community Land Model (CLM) version 4.5 (Oleson et al., 2013). A more extensive description of COSMO-CLM2 and N025 simulations can be found in Goosse et al. (2023).

N1 simulations are run 1000 year in order to stabilize the deep deep ocean thermohaline structure while N025 simulations follow a 10-year spin-up, which is sufficient to attain a quasi-equilibrium for surface variables (Verfaillie et al., 2022).

2.2.3 Experiments

Our analysis is based on three unperturbed simulations and one sensitivity experiment where sea ice dynamics are disabled (Table 1).

Unperturbed simulations consist of two forced-atmosphere (N1_For and N025_For) and one coupled-atmosphere (N025_Atm) simulations. Following spin-up, a 2-year period starting on March 1st is analyzed for each simulation, allowing to extract a complete sea ice seasonal cycle starting on September 15th of the first year, around the time of the first sea ice extent maximum.

The sensitivity experiment was conducted using the N1 configuration in which sea ice velocity is set to zero (N1_NoDy). Under such a strong perturbation, the model can drift toward an unrealistic mean state after a few months. Consequently, we conducted two distinct simulations, shutting down ice dynamics on either September 15th (N1_NoDy_Sep) or February 15th (N1_NoDy_Feb), in order to investigate the impact on sea ice dynamics respectively during the ice retreat and advance periods.

2.3 Analysis of model output

2.3.1 TRHA relationships

In order to test the linearity of the TRHA relationships in N1_For, N025_For and N025_Atm, we diagnosed the seasonal ice thickness maximum, the sea ice retreat date, the maximum mixed layer heat content and the sea ice advance date, from the same seasonal cycle, assumed to start on September 15th. We also evaluated the mixed layer heat content at the date of retreat and advance. For the N1_NoDy experiments, only half a seasonal cycle was analyzed in each simulation. Ice thickness at the melt onset and retreat date were diagnosed from N1_NoDy_Sep, whereas mixed heat content diagnostics and advance dates were diagnosed from N1_NoDy_Feb.

Diagnostic methods for retreat and advance dates take advantage of experience developed over previous studies (Himmich et al., 2023; Lebrun et al., 2019; Parkinson, 1994; Simpkins et al., 2013; Stammerjohn et al., 2012). Retreat and advance dates are derived using sea ice

concentration time series, on which a 15-day temporal filter was applied to avoid retaining any date reflecting short events. The retreat (advance) date was identified as the first day filtered sea ice concentration drops below (exceeds) 15%. As a representative value of the sea ice thickness at the melt onset, we take the September 15th value. This choice is convenient, first for consistency with previous work (Chapter I; Chapter III). Second, this choice allows to have a fixed initial thickness when experimenting with sensitivity to sea ice dynamics. The mixed layer heat content was calculated as defined in (3), with $T_{ref} = -1°C$. The rationale for the chosen reference temperature is explained in section 2.5.

To assess the linearity of TRHA relationships, optimal least-square linear regressions were computed between spatial distributions of ice thickness and retreat date (hereafter referred to as TR), retreat date and mixed layer heat content (RH), and between mixed layer heat content and advance date (HA). Outliers out of the 1-99% confidence range were not taken into account when computing the regressions.

2.3.2 Heat budget

Methodological caveat: The following budget aims to identify the different heat flux contributions to the seasonal evolution of the mixed layer heat content. However, we initially implemented the calculation of a mixed layer temperature budget in our model configuration and did not have time to rewrite this budget in terms of heat content, then rerun our simulations. Consequently, in this chapter, we use the mixed layer temperature budget as an approximation of the heat budget. Implications of such an approximation will be investigated in the near future and may lead to rewrite the budget in terms of mixed layer heat content.

In N1_For, we approximate the contributions of bottom, lateral and surface heat fluxes to $< Q^{+}_{ML} >$ and $< Q^{-}_{ML} >$, using a mixed layer temperature budget as a proxy of the mixed layer heat budget. The temperature budget is based on a three-dimensional temperature equation integrated over the entire mixed layer by Vialard and Delecluse (1998):

$$\partial_t \overline{T} = \overbrace{-\left(\overline{u\partial_x T} + \overline{v\partial_y T}\right)}^{\text{HADV}} \overbrace{-\overline{w\partial_z T}}^{\text{VADV}} + \overbrace{\overline{D_L(T)}}^{\text{HMIX}} + \overbrace{\frac{Q_{s,z=-h}}{\rho C_p h}}^{\text{FOR}} \underbrace{- \frac{k_z \partial_z T_{z=-h} - \partial_t h[\overline{T} - T_{z=-h}]}{h}}_{\text{VMIX}}, \qquad \text{(II.7)}$$

where $\overline{T} = \int_{-h}^{0} T\,dt$, is the mixed layer temperature and h, the mixed layer depth. (u, v, w) are the velocity components of local ocean currents, D_L is the lateral diffusion operator, k_z the vertical diffusion coefficient and Q_s, the total surface heat flux term. Following the notations of

Jullien et al. (2012), HADV represents horizontal advection; VADV represents vertical advection; HMIX, represents lateral diffusion; FORC represents the heat input by surface solar and non-solar fluxes in the mixed layer; and VMIX represents the heat input through the mixed layer base by vertical mixing (including entrainment, detrainment and local vertical diffusion at the mixed layer base).

Each contribution to the total mixed layer temperature tendency was ultimately averaged over the open water warming and cooling periods, to respectively approximate heat flux contributions to $< Q_{ML}^{+} >$ and $< Q_{ML}^{-} >$. In addition, we estimated $< Q_{ice} >$ by averaging, over the melt season, the sea ice mass loss rate (diagnosed from model output as a sum of all loss terms) and dividing by the latent heat of fusion L= 335 kJ/kg.

2.3.3 Sea ice concentration budget

In N1_For, we also assess the respective roles of ice dynamics and thermodynamics in setting the dates of sea ice retreat and advance, using similar sea ice concentration (SIC) budget analyses as in Chapter I. These analyses include diagnosing the dynamic (including effect of advection and divergence; Dy) and thermodynamic (including freezing and melting; Th) contributions to the sea ice concentration tendency over the melt (from September 15th to the retreat date) and open water-cooling (from the date of maximum mixed layer heat content to the date of advance) seasons:

$$\begin{aligned} \Delta\mathrm{SIC} &= \int \frac{\partial \mathrm{SIC}}{\partial t} dt, \\ Dy &= \frac{1}{\Delta\mathrm{SIC}} \int \nabla \cdot (\boldsymbol{u}\mathrm{SIC})\, dt, \\ Th &= \frac{1}{\Delta\mathrm{SIC}} \int f\, dt, \end{aligned} \tag{II.8}$$

where **u** represents the sea ice velocity and f, the contribution thermodynamic processes. These diagnostics were computed for the N1_For simulation, using model outputs of $\nabla \cdot (\boldsymbol{u}\mathrm{SIC})$ and f.

2.4 Comparison to observations

Methodological caveat: to evaluate the representation of the key processes driving sea ice seasonality in NEMO, we compared our simulations outputs to climatological observations. This choice was motivated by the lack of interannual mixed layer depth data required to calculate the mixed layer heat content. The consistency of such a comparison relies on the assumption that our simulations outputs closely match the model's climatology, which is likely not the

case. In particular, N025_Atm represents the model behaviour during a specific year (1995) which may differ from the climatology. Additionally, individual-year simulations with climatological forcing (N1_For, N025_For) may also differ from a multi-year climatology, as the ocean's response to atmospheric forcing is not necessarily linear. However, we did not have time to assess the exact impact of this inconsistency on the model-observations comparisons in this study.

To assess the realism of considered NEMO simulations, we replicate the key observational analyses of Chapter I using model outputs.

We compare model-based TRHA relationships to observations. The climatological seasonal cycle of mixed layer heat content was derived based on the method of (Himmich et al., 2023), which we slightly modified for consistency with the model-based results. We estimated the observational mixed layer heat content for any date, t, during the open water season, as:

$$MLH \approx \rho_w c_p MLD_t \left(T - T_{ref}\right), \tag{II.9}$$

where $T_{ref} = -1°C$ (see section 2.4). MLD_t is the monthly mixed layer depth evaluated on the month of the given date, from the 1970-2018 monthly climatology of Sallée et al. (2021). SST is the climatological (1982-2018) sea surface temperature evaluated on relevant dates, based on thermal infra-red radiance measurements, from the European Space Agency (ESA) SST Climate Change Initiative (CCI) analysis (Merchant et al., 2019). We use observed diagnostics of maximum sea ice thickness, sea ice retreat and advance dates from Chapter I. The seasonal maximum ice thickness was approximated as the mean September thickness, from a monthly satellite-based sea ice thickness climatology over 1994-2022 (Bocquet, 2023). Climatological retreat and advance dates were derived using passive microwave sea ice concentration from OSI-SAF over 1982-2018, for RH and HA relationships and over 1994-2022, for the TR relationship.

We also compare model- and observation-based sea ice concentration budgets, using the dynamic (Dy) and thermodynamic (Th) contributions to the sea ice concentration tendency over the melt and open water-cooling seasons as in (9). Observation-based diagnostics were calculated based on the method of Holland and Kwok (2012), and using sea ice concentration (Lavergne et al., 2019) and drift (Lavergne & Down, 2023) data from the EUMETSAT Ocean and Sea Ice Satellite Application Facility (OSI-SAF). For the retreat date, the integration period for observational Th and Dy is the same as for the model-based diagnostics, as in Chapter I. In contrast, observed contributions could not be integrated before the date of advance, as in the model, due to data quality issues with sea ice concentration below 15%. Instead, we integrated each contribution over the 30 days following the date of advance, following the methodology

of Himmich et al. (2023). This choice is the consequence of large observational errors in the low-concentration ice near the ice edge, making it difficult to evaluate the sea ice concentration budget prior to the advance date.

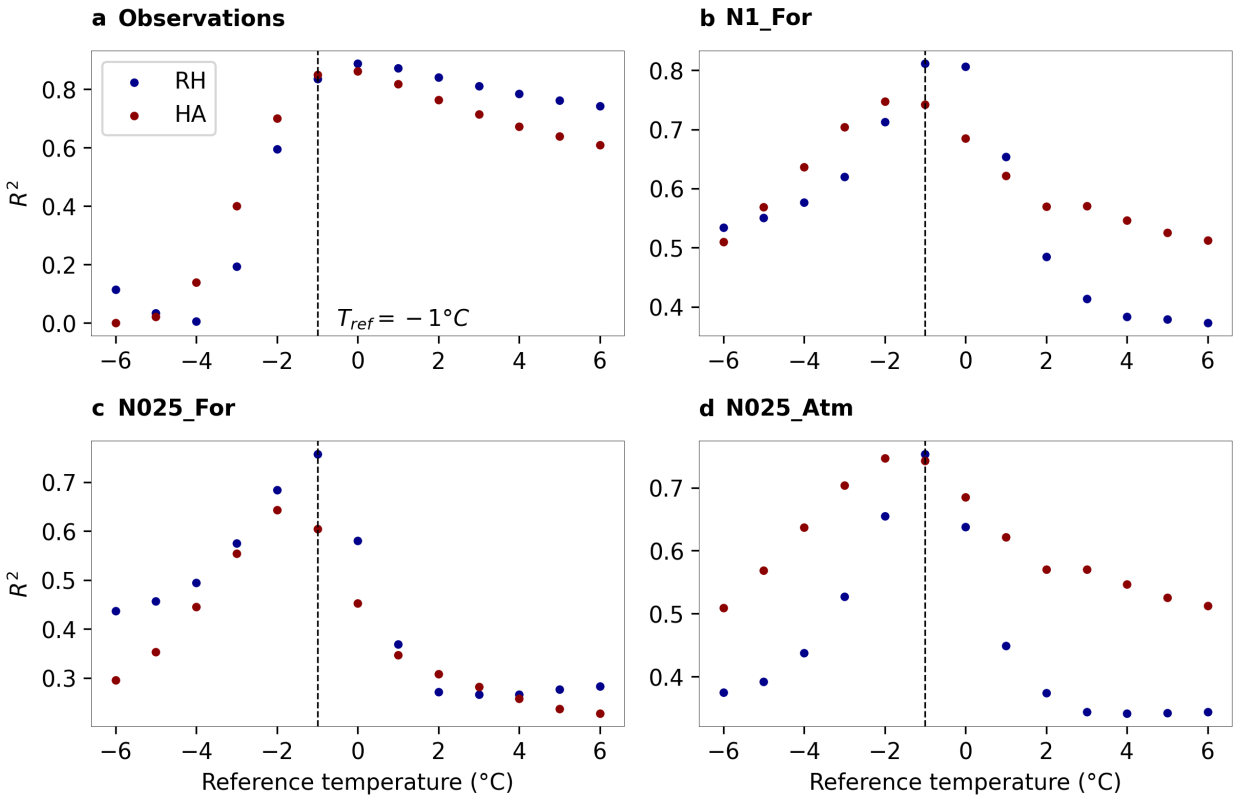

Figure II.1: **Sensitivity of relevant linear relationships to the reference temperature (T_{ref}) used to compute the mixed layer heat content.** Least-Square linear regressions were computed for ice retreat date-seasonal maximum of mixed layer heat content (RH) and maximum heat content-ice advance date (HA) relationships for different T_{ref}, using **a**, observations and outputs from **b**, N1_For, **c**, N025_For and **d**, N025_Atm simulations. Corresponding determination coefficients (R^2) are shown. Stippled lines mark $T_{ref} = -1°C$ which was used in this study.

2.5 Reference temperature for mixed layer heat content calculation

Methodological caveat: the reference temperature for mixed layer heat content calculation proves unexpectedly impactful on the main results of this study, in particular on the TRHA relationships. This finding emerged late in the writing process; thus, we did not have time to really investigate reasons or implications for it.

The linearity of observed and simulated retreat-heat content (RH) and heat content-advance (HA) relationships is sensitive to T_{ref}, which is illustrated in Figure 1, where analyses are

repeated for different thresholds. In all simulations, the determination coefficient associated corresponding to a least square linear fit reaches a maximum at $T_{ref} = -1°C$ for the TR relationship, and at $T_{ref} = -2°C$ for the HA relationship. Contrastingly, the maximum determination coefficient, based on observations, is reached at $T_{ref} = 0°C$, which corresponds to the reference temperature used in Himmich et al. (2023). This issue will be further investigated in the near future. Meanwhile, we choose $T_{ref} = -1°C$ for this study, as an optimal compromise that maximizes the strength of linear RH and HA relationships in both models and observations (see Figure 1).

3 Testing the TRHA relationships in different configurations of NEMO

3.1 Mean state

We analyze the mean state of the ocean and sea ice in N1_For, N025_For and N025_Atm, in comparison to observations (Figure 2). These three simulations share similar representations of sea ice and ocean but differ mostly in terms of atmospheric representation, resolution and tuning.

All three simulations skillfully reproduce the generic seasonal evolution of sea ice extent and sea surface temperature, with consistent timings of extent and temperature extrema among models and observations (Figures 2a, c). In addition, spatial distributions of simulated September thickness, maximum mixed layer heat content, sea ice advance and retreat dates reproduce many observed features (Figure 3). This suggests that certain key simulated seasonal processes are in reasonably realistic. However, in some respects, the simulations largely differ from observations.

The three simulations exhibit same-sign seasonal biases regarding sea ice. Simulated sea ice extent is larger than observed in winter and spring and smaller than observed in summer and autumn (Figure 2a). Simulated sea ice also typically drifts faster than observed (Figure 2d). In contrast, integrated oceanic variables exhibit varying-sign biases among simulations. In all seasons but summer, the mixed layer depth, averaged over the seasonal ice zone (Figure 2b), is deeper than observed in N1_For and N025_Atm and shallower in N025_For. In summer, the mixed layer is shallower than observed in all simulations. In addition, the mean sea surface temperature over the seasonal ice zone is warmer than observed in N025_For and N1_For and colder in N025_Atm (Figure 2c). However, these biases are small and likely attributable to differences in the seasonal ice zone in location and size among simulations and observations (see Figure 3).

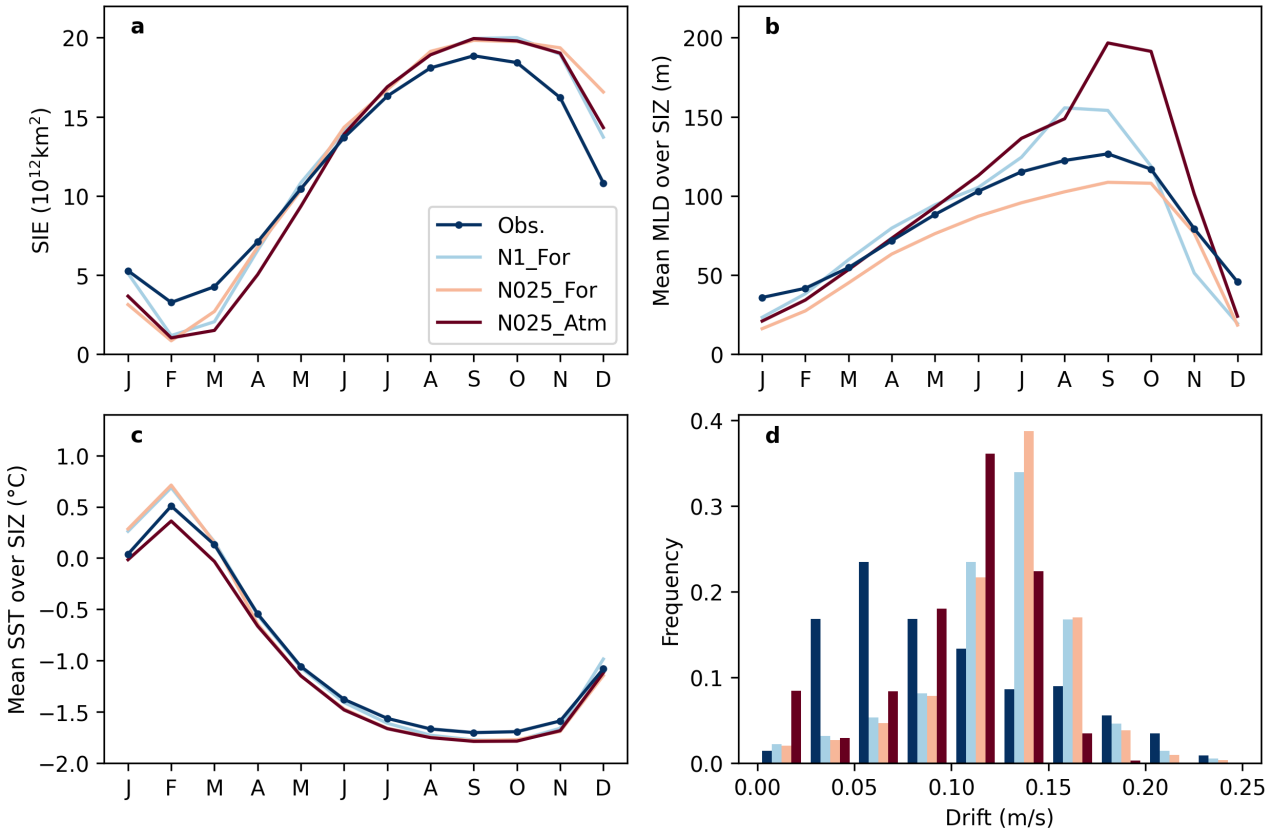

Figure II.2: **Comparison of simulated ocean and sea ice mean state to observations.** Seasonal cycles of **a**, sea ice extent (SIE), **b**, mean mixed layer depth (MLD) and **c**, sea surface temperature (SST) over the seasonal ice zone (SIZ) and **d**, annual mean sea ice drift histogram. The seasonal ice zone varies among simulations and observations (see Figure 3). For observational reference, we use a number of climatologies. We use passive microwave SIE (derived from sea ice concentration) (Lavergne et al., 2019) (1982-2018) and drift (Lavergne & Down, 2023) (1992-2020) from OSISAF; infrared SST from CCI (Merchant et al., 2019) (1982-2018); in situ MLD from Sallée et al. (2021) (1970-2018).

Spatial patterns in the four variables of interest also differ across models and observations, to different degrees (Figure 3). Notably, the retreat date (Figures 3e-h) shows greater deviations from observations and more variability among simulations than the advance date (Figures m-p). Also, sea ice thickness (Figures 3a-d) and seasonal maximum mixed layer heat content (Figures 3i-l) exhibit pronounced differences across models and observations. Sea ice is thinner in the simulations than in observations, in particular east of the Antarctic Peninsula. This negative bias has already been noted by Bocquet (2023); Kacimi and Kwok (2020), in comparisons of altimetry-based sea ice thickness data to ice-ocean model simulations. Thicker than observed simulated sea ice is only found in the Weddell Sea, and to a lesser extent in the Ross Sea. These biases could reflect varying drift patterns and heat supply across models and the real world and also possible issues in the observations. In contrast, the mixed layer heat content overall resembles observations except near the maximum ice edge. There, we observe a regional maximum across models and observations; however, this maximum is significantly larger in N1_For, and smaller in N025_For and N1_Atm.

In summary, simulations reproduce some of the observed seasonal behavior of the ocean and sea ice, but they also exhibit significant biases and variations among them. Such biases are likely to affect the main ice-ocean processes driving sea ice seasonality in NEMO.

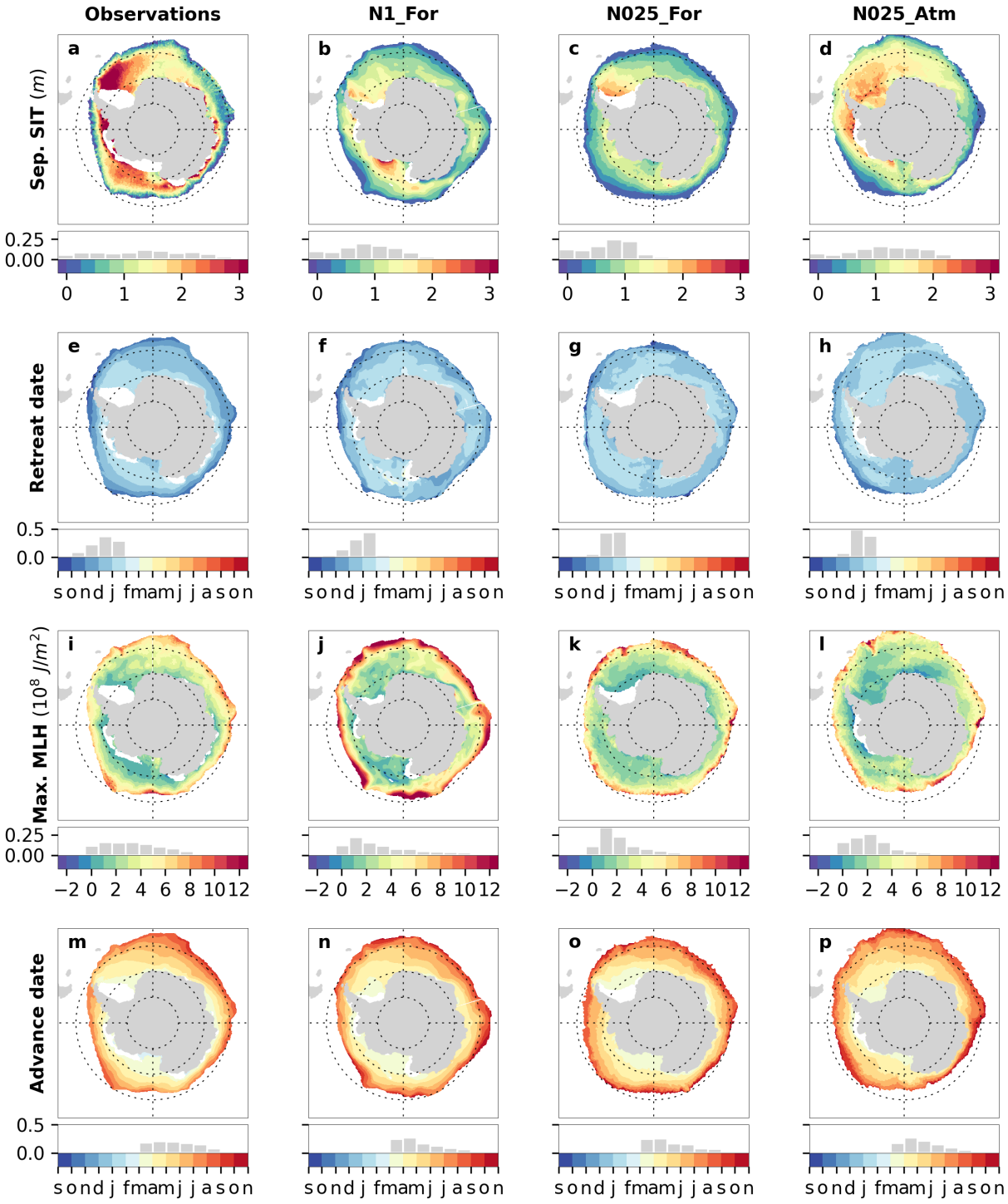

Figure II.3: **Maps of key variables derived from climatological observations and N1_For, N025_For and N025_Atm simulations. a-d**, September sea ice thickness (SIT); **e-h**, date of sea ice retreat; **i-l**, seasonal maximum of mixed layer heat content (MLH); **m-p**, date of sea ice advance. Corresponding frequency histograms are shown under each map. White patches indicate regions out of the seasonal ice zone. For observational reference, climatologies. We use retreat and advance dates derived from OSISAF passive microwave sea ice concentration (Lavergne et al., 2019) (1982-2018 and 1994-2022); altimetry SIT from Bocquet (2023) (1994-2022); maximum MLH from in situ mixed layer depth (Sallée et al., 2021) (1970-2018) and CCI infrared sea surface temperature (Merchant et al., 2019) (1982-2018).

3.2 TRHA relationships

Next, we specifically examine ice-ocean thermodynamic processes, and assess if they align with climatological observations in N1_Ref, N025_Ref and N025_Atm simulations. Specifically, we investigate how ice thickness and mixed layer heat content constrain the dates of sea ice retreat and advance, as described by the TRHA relationships framework (see Methods). Following the methodology of Himmich et al. (2023), we conduct pair-wise linear regressions of spatial distributions of September ice thickness, retreat date, mixed layer heat content and advance date, as shown in Figure 3. We find that TRHA relationships are statistically linear in all considered simulations ($p < 0.05$), albeit with varying strength and slopes among them and compared to observations (Figure 4).

First, relationships are overall weaker in the simulations than in our observational analysis, with the most pronounced weakening observed for the thickness-retreat (TR) relationship (Figure 4). Based on averaged determination coefficients (R^2) over the three simulations, we find that September ice thickness explains 36% of the spatial variance in retreat date whereas the retreat date explains 77% of the spatial variance in maximum mixed layer heat content. In turn, heat content explains 70% of the spatial variance in advance date. Larger fractions were obtained based on observations (Figures 4a, e, i). Observed fractions of explained variance are larger than simulated ones, increasing by 10-15% for the retreat date-mixed layer heat content (RH) and mixed layer heat content-advance date (HA) and by almost 100% for the TR relationship. Model-observation differences could reflect an inconsistency in their comparison, as the observations we use are climatological and simulations are not (see section 2.4), or issues in the model mean state. In particular, the largest model-observations and inter-model differences are observed for thickness, retreat dates (Figure 3) and the TR relationship (Figure 4), suggesting potential issues regarding the processes controlling sea ice decay during the melt season.

Second, determination and slope coefficients of model-based TRHA relationships vary among simulations (Figure 4). Comparing N025_For and N025_Atm simulations, we find that the fraction of explained variance varies while slopes are similar. This suggests that the linear

relationships strength is sensitive to atmospheric coupling while slopes are not. In contrast, both determination and slope coefficients vary between N025_For and N01_For, indicating they are both sensitive to the applied atmospheric forcing dataset (here ERA5 against CORE2), or the model resolution or tuning.

Ultimately, all considered NEMO configurations appear to reasonably capture the key thermodynamic processes governing sea ice seasonality, as described by the linear TRHA relationships. However, these relationships are likely weakened by specific model configuration choices (atmospheric representation and forcing) and issues with the model mean state. Despite these issues, the consistent linearity of TRHA relationships in NEMO allows us to further examine their underlying processes. In the next section, we explore how heat fluxes and sea ice dynamics affect the linearity of these links, using the N1_For simulation.

4 Towards a better understanding of the role of heat fluxes and sea ice drift

4.1 On the role of heat fluxes

In the histograms of Figures 4b, f and j, a significant spread around linear TRHA relationships is evident for N1_For, particularly for the TR relationship. In this section, we assess whether this spread can be attributed to the spatial variability of mean net heat fluxes into the ice (TR relationship) or into the mixed layer (RH and HA relationships), as the conceptual model developed in section 2.1 suggests. Specifically, we assess if regionally larger (smaller) heat fluxes induce deviations in predicted values towards larger (smaller) than predicted maximum mixed layer heat content; earlier (later) sea ice retreat and advance.

We first compare the spatial distribution of deviations from the linear TR relation (Figure 5a) with that of $< Q_{ice} >$ (Figure 5d). These deviations indicate later retreat in large parts of the inner seasonal ice zone and earlier retreat elsewhere. Spatial patterns in $< Q_{ice} >$ differ and thus cannot explain the deviations from linear predictions of retreat date. For instance, most of the later than predicted retreat correspond to regions of increased warming during the melt season, which could not have caused such deviation. Hence, deviations from predicted retreat by the linear TR relation cannot be attributed to the spatial variability of $< Q_{ice} >$.

Next, we turn to RH and HA relationships. We compare deviations from linear predictions (Figures 5b and 5c) to mean mixed-layer temperature tendencies over the heating ($< \partial_t T^+ >$; Figure 5e) and cooling ($< \partial_t T^- >$; Figure 5f) periods, which approximate$< Q^+_{ML} >$ and $< Q^-_{ML} >$, respectively. The reasons and implications of this approximation are given in section 2.3.2. We find larger (smaller) than predicted maximum mixed layer heat content

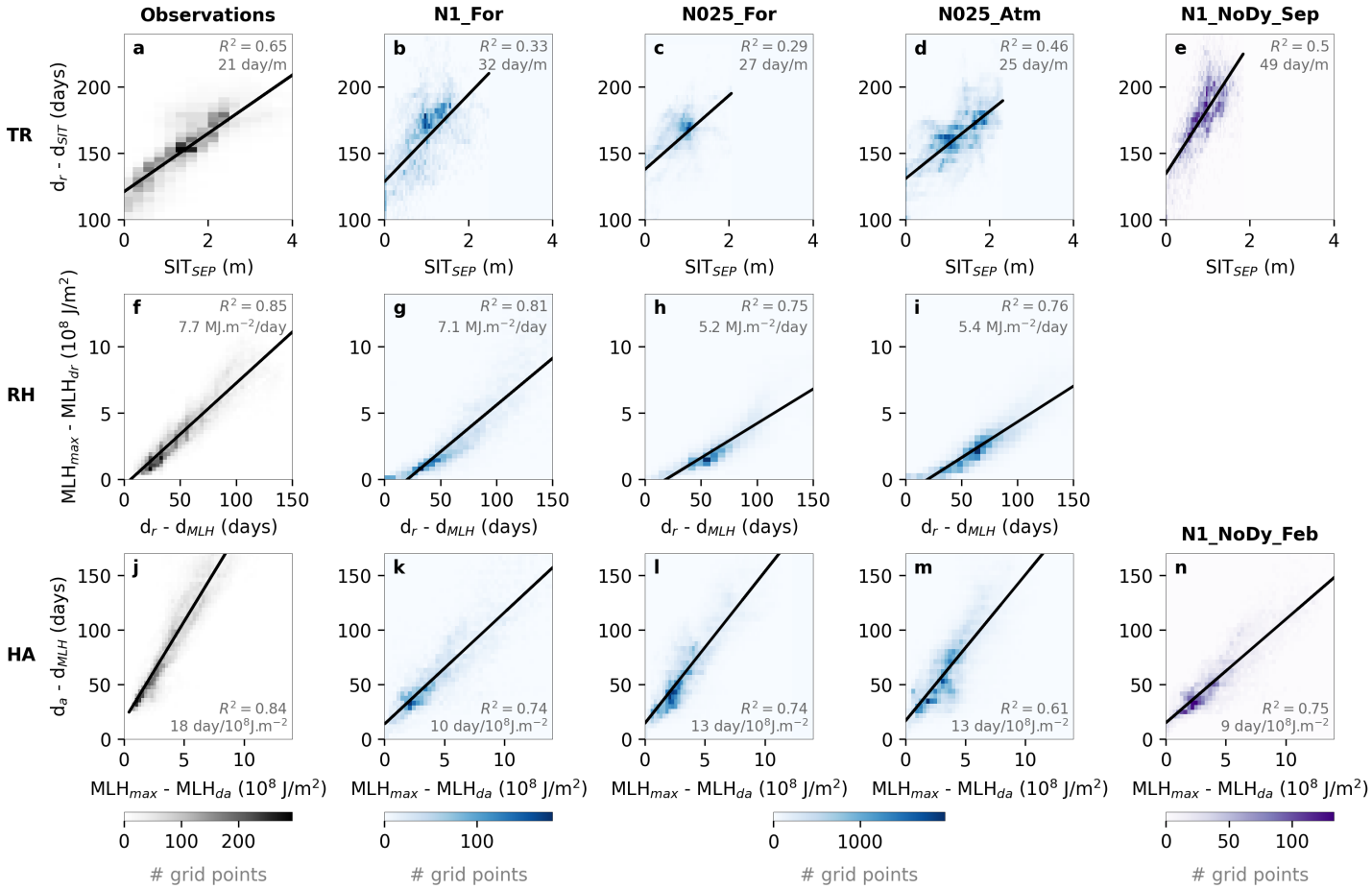

Figure II.4: **Selected spatial relationships between the key variables displayed in Figure 3.** Relationships are plotted as 2D histograms of **a-e**, sea ice thickness evaluated on September 15th (SIT_{SEP}) vs retreat dates (d_r), **f-i**, retreat dates vs seasonal maximum of mixed layer heat content (MLH_{max}), **j-n**, MLH_{max} vs advance dates (d_a). Anomalies are used, tailored to best showcase the relevant relationships (see Methods). d_a and d_r anomalies refer to the date of maximum mixed layer heat content (d_{MLH}) or to September 15th (d_{SIT}) such that positive anomalies indicate later advance (retreat). MLH_{max} anomalies refer to the mixed layer heat content value at sea ice advance (retreat) date. Color gives the number of points in each pixel of the 2D histogram space. A Least Square linear regression was performed for each plot; the corresponding regression line (significant at 99%), slope and determination (R^2) coefficients are shown. Observational sources are mentioned in the Figure 3 caption

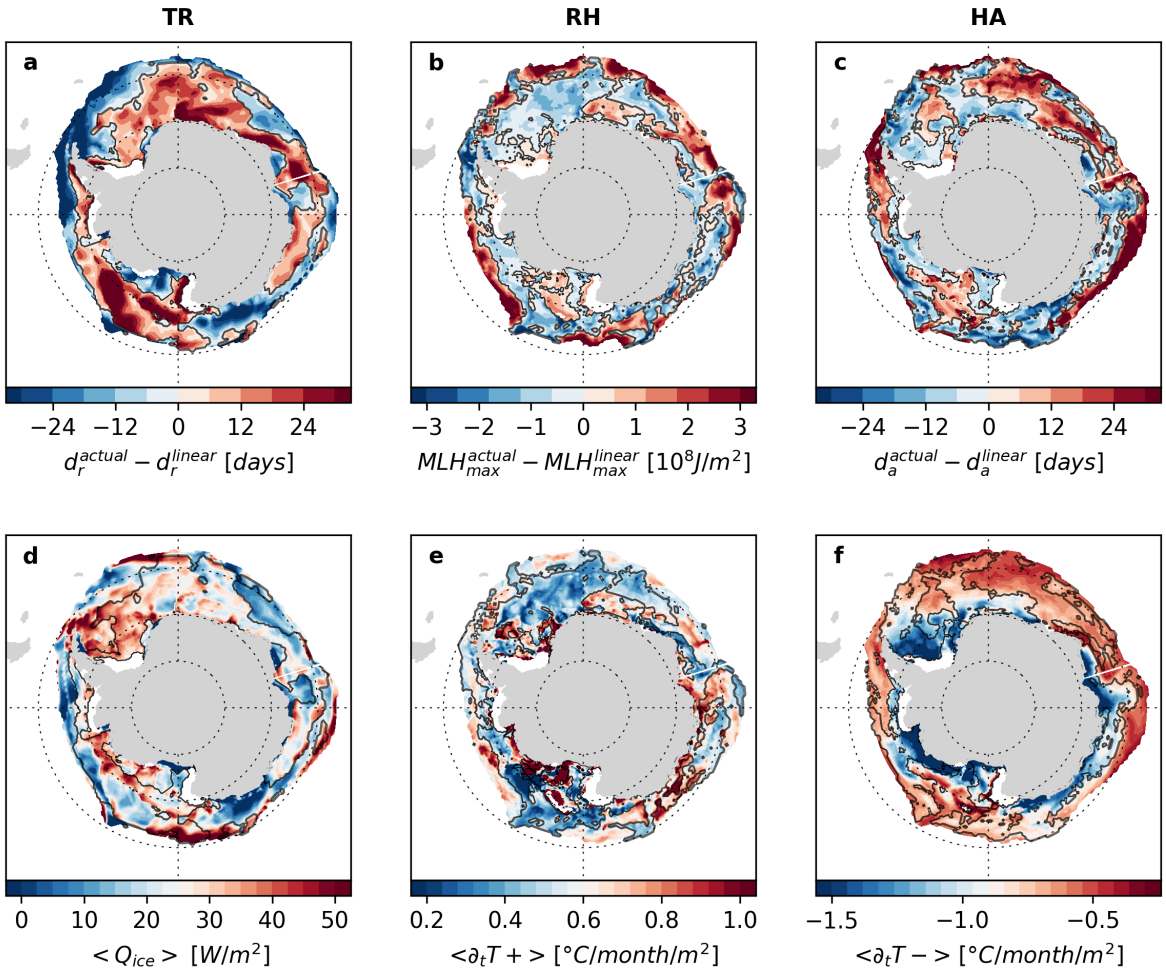

Figure II.5: **Deviations from linear relationships, as displayed in Figure 4 for N1_For, and their relation to selected heat fluxes.** Differences from linear predictions of **a**, retreat dates (d_r), **b**, maximum mixed layer heat content (MLH_{max}) and **c**, advance dates (d_a); **d**, heat flux required to melt ice ($< Q_{ice} >$) and total mixed layer temperature tendency over **e**, the heating ($< \partial_t T^+ >$) and **f**, the cooling period ($< \partial_t T^- >$) of the open water season. Deviations are derived as the difference between the actual values, as displayed in Figures 3b, f, j, n, and the predicted values by the linear models of Figure 4b, g, k. The black contours mark the 0-deviation for differences from linear d_r in **a** and **d**, MLH_{max} in **b** and **e**, d_a in **d** and **f**. White patches indicate regions out of the seasonal ice zone.

correspond to larger (smaller) than average $< \partial_t T^+ >$. Similarly, later (earlier) than predicted advance date correspond to largest (smallest) $< \partial_t T^- >$. This indicates that deviations from predicted maximum mixed layer heat content and advance dates strongly correspond to the spatial variability of $< Q_{ML}^+ >$ and $< Q_{ML}^- >$.

To specify the origin of the spatial variability in $< Q_{ML}^+ >$ and $< Q_{ML}^- >$, we examine, in Figure 6, the relative contributions of oceanic heat inputs and surface forcing to $< \partial_t T^+ >$ and $< \partial_t T^- >$ using mixed layer temperature budget diagnostics described in section 2.3.2. We find that during the heating period, vertical surface heating and bottom oceanic cooling

comparably contribute to $< \partial_t T^+ >$ in regions of both larger and smaller than predicted maximum mixed layer heat content (Figure 6a). The contribution of horizontal heat fluxes is, by comparison, negligible. In contrast, during the cooling period, we find that surface forcing largely dominates $< \partial_t T^- >$ anomalies in regions of both earlier and later than predicted sea ice advance (Figure 6b). This suggests that surface heat fluxes variations dominate the spatial variability in $< Q_{ML}^- >$, while both surface and bottom heat fluxes contribute to the spatial variability in $< Q_{ML}^+ >$.

Therefore, the deviations the linear RH relationship arise from the variable balance between vertical surface warming and bottom cooling, while deviations from the linear HA relationship are mostly caused by variability in surface cooling. Contrastingly, deviations from the TR relationship cannot be caused by the sole spatial variability of heat fluxes during the melt season, which may suggest a strong impact of sea ice dynamics on the timing of sea ice retreat.

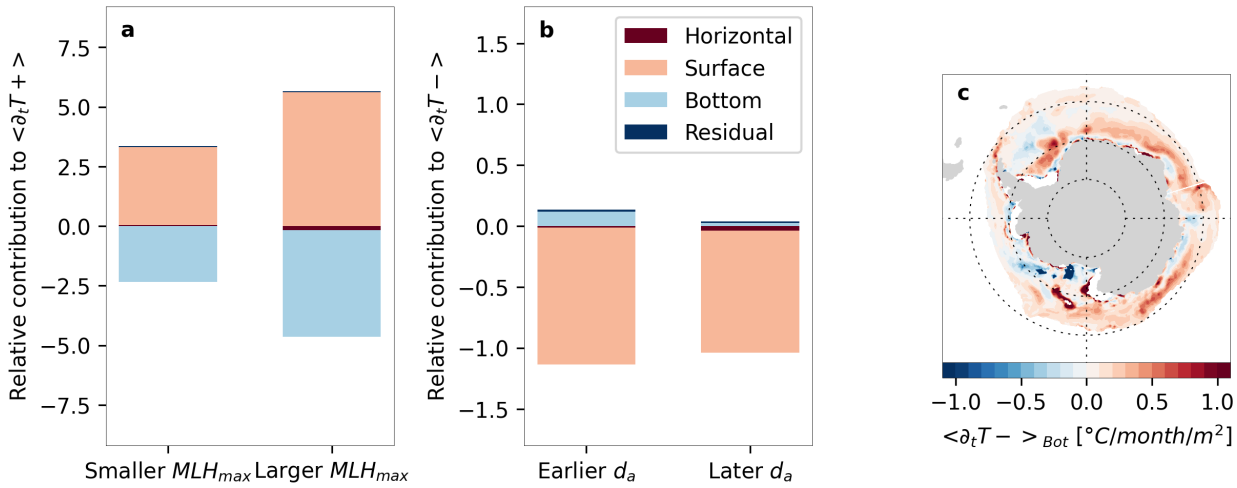

Figure II.6: **Heat flux contributions to the total mixed layer temperature tendency over the open water season in N1_For.** Ratio of heat flux contribution to the total mixed layer temperature tendency over **a**, the heating period ($< \partial_t T^+ >$) and **b**, the cooling period ($< \partial_t T^- >$) of the open water season. Relative contributions are given as unitless ratios evaluated in regions of negative and positive deviations from linear predictions of maximum mixed layer heat content (MLH_{max}) and advance dates (d_a), as displayed in Figures 5b and c. A map of the bottom heat fluxes contribution during the cooling period is displayed in **c**.

4.2 On the role of sea ice dynamics

In this section, we explore how sea ice drift processes affect the TR and HA relationships in the N1_For simulation.

We first assess the realism of simulated ice concentration budget terms before sea ice re-

treat and advance. Using the same approach as in Chapter I (see section 2.4), we integrated the thermodynamic (Th) and dynamic (Dy) contributions to the sea ice concentration budget during both melting (Figure 7) and cooling (Figure 8) periods.

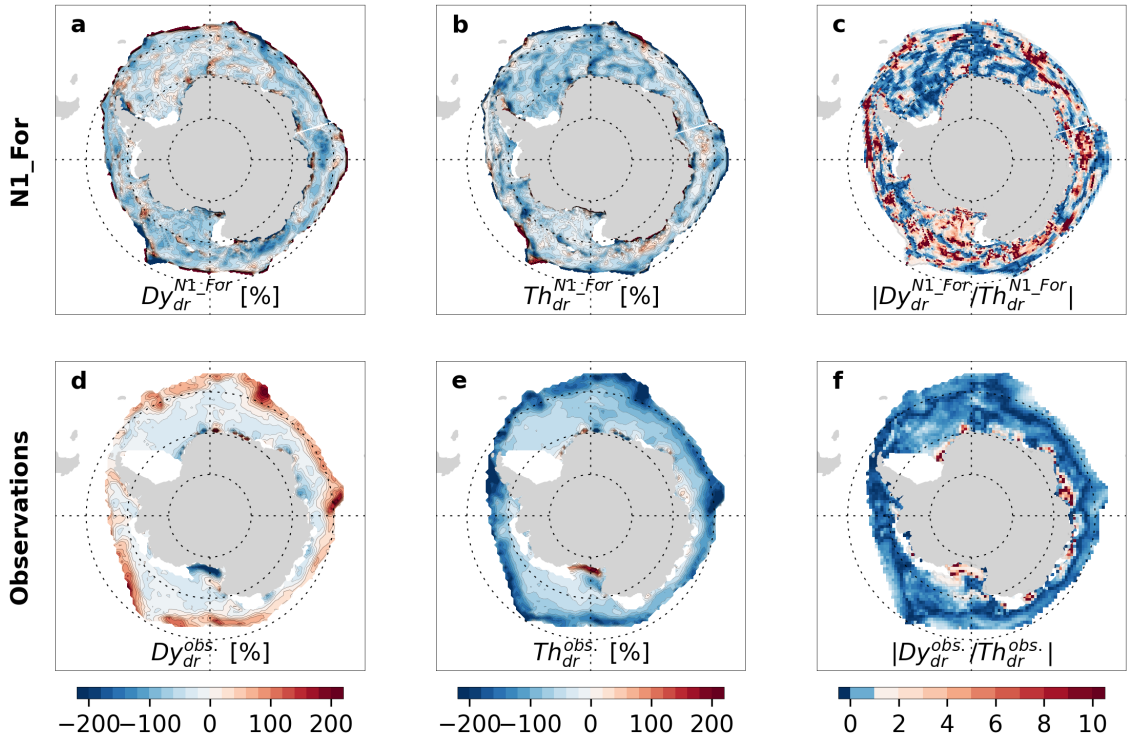

Figure II.7: **Sea ice concentration budget terms leading to sea ice retreat.** The dynamic (Dy_{dr}, **a, d**) and thermodynamic (Th_{dr}, **b, e**) contribution to the total sea ice concentration tendency over the melt season, as well as their absolute ratio ($|Dy_{dr}/Th_{dr}|$, **c, f**). White patches indicate regions out of the seasonal ice zone. **a**, **b** and **c** are based on N1_For outputs whereas **d**, **e** and **f** are observation-based (see section 2.4).

In the model, we find that prior to sea ice retreat, ice export and melting occur in most of the seasonal ice zone ($Th < 0$ and $Dy < 0$; Figures 7a, b), aligning with observations (Figures 7d, e). However, substantial disparities in the spatial patterns of Th, Dy and their ratio are also apparent when comparing model outputs and observations. First, the model lacks a marked zone, near the winter ice edge, where ice import ($Dy > 0$; Figure 7a) occurs as in observations (Figure 7d). Instead, in the model, small zones of positive Dy appear to flow into the overall negative Dy. This could be caused by issues with the representation of sea ice dynamics, which is common among sea-ice models (Hutter et al., 2022) and supported by a mean-state velocity in N1_For differing from observations (Figure 2d). Second, these import zones correspond to local maxima in the contribution of melting ($Th < 0$; Figure 7b). These maxima are not present

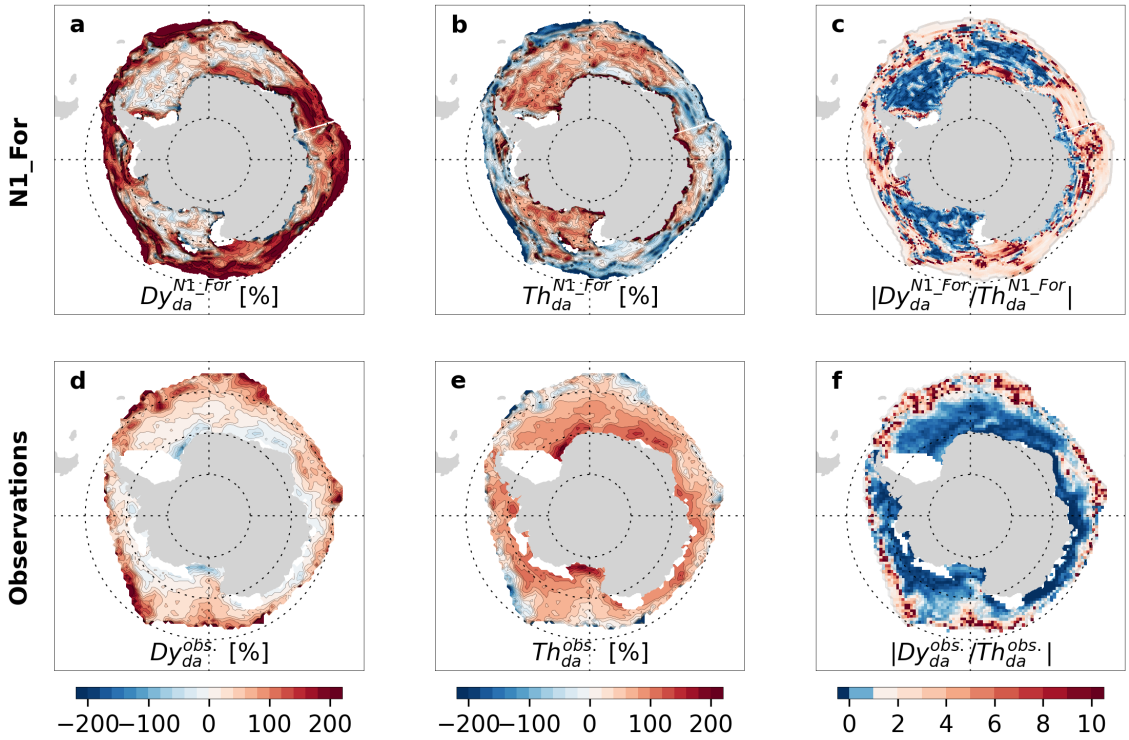

Figure II.8: **Sea ice concentration budget terms leading to sea ice advance.** The dynamic (Dy_{da}, **a, d**) and thermodynamic (Th_{da}, **b, e**) contribution to the total sea ice concentration tendency over the open water season (**a-c**) or the 30 days following the date of advance (**d-g**), as well as their absolute ratio ($|Dy_{da}/Th_{da}|$, **c, f**). White patches indicate regions out of the seasonal ice zone. **a**, **b** and **c** are based on N1_For outputs whereas **d**, **e** and **f** are observation-based (see section 2.4).

in observations (Figure 7e), suggesting that the contribution of melting may be overestimated by the model. The thin-ice bias exhibited by the N1_For simulation (Figures 3a, b), especially in the Weddell Sea, could explain this discrepancy, as ice area removal caused by melting increases with decreasing thickness in models (Massonnet et al., 2018). Ultimately, differences in the spatial distributions of Dy and Th result in distinct model-observation relative contributions of sea ice dynamics and thermodynamics to ice removal ($|Dy/Th|$; Figures 7c, f). In the model, melting dominates ice removal ($|Dy/Th| < 1$) in about 50% of the seasonal ice zone while export dominates in the other half ($|Dy/Th| > 1$). By contrast, in observations, melting only dominates in small regions near the coast, representing less 7% of the seasonal ice zone area.

Prior to ice advance, patterns are closer to observations (Figure 8). We identify the same two sea ice advance regimes as highlighted by Himmich et al. (2023). In the inner seasonal ice zone, sea ice is exported northward (Dy < 0; Figure 8a) and freezing dominates the sea ice concentration increase ($Th > 0$ and $|Dy/Th| < 1$; Figures 8b, c). By contrast, in a large outer band reaching the winter ice edge, and referred to as the outer zone, ice import ($Dy > 0$) and melting occur ($Th < 0$) with dynamics dominating the ice concentration increase ($|Dy/Th| > 1$).

However, the size of the outer zone (Figures 8a, c) is larger in the model than in observations (Figure 8d, f). The difference in the definitions of observational- and model-based sea ice concentration diagnostics (see section 2.4) could contribute to this disparity. Alternatively, faster-than-observed ice drift or biases in ocean stratification properties (Figure 2a, b) could also be a plausible contributor of the larger-than-observed outer zone.

Our findings thus indicate that the simulation better replicates the sea ice concentration budget leading to sea ice advance than the one leading to sea ice retreat. They also suggest that differences with observations may be caused by issues with the representation of a number of ice-ocean processes.

Next, we examine how the date of ice retreat (advance) is modified when removing ice drift processes, for similar initial September sea ice thickness, using N1_NoDy_Sep (maximum mixed layer heat content, using N1_NoDy_Feb) as in the reference N1_For simulation. In both N1_NoDy experiments, the size of the seasonal ice zone is significantly reduced, due to a larger extent in summer and smaller extent in winter (Figures 9a, b). This can be understood in light of the previous sea ice concentration budget analyses (see Figures 7, 8). During the melt season, the absence of ice export prevents dynamical ice removal, allowing more sea ice to persist into summer. During the advance season, no ice transport induces a decrease in the winter extent by preventing sea ice advance through ice import where freezing is not thermodynamically sustainable.

Alterations in sea ice seasonality are larger during the retreat season (N1_NoDy_Sep), than during the advance season (N1_NoDy_Feb) (Figure 9), consistently with the findings of Goosse et al. (2023). We attribute this to the fact that advance is largely set by thermodynamic processes (Figure 8c), which is common among the experiment and the control, whereas retreat is influenced by sea ice dynamics (Figure 7c), which differs among them. In particular, during the retreat season, sea ice extent decreases more slowly in N1_NoDy_Sep than in the control simulation (Figures 9a). Consequently, dates of retreat are delayed by 19 days, on average (Figure 9c). The TR relationship is also modified in N1_NoDy_Sep, compared to N1_For, showing stronger linearity, yet with a large remaining scatter (R^2 = 0.5 vs. R^2 = 0.32; Figure 4). This scatter, in contrast to N1_For (see Figure 5d), is explained by $< Q_{ice} >$, with later (earlier) than predicted retreat corresponding to decreased (increased) $< Q_{ice} >$ (Figure 10a). Turning to the advance season, we find that the dates of advance are only delayed by 4 days on average (Figure 9d). The HA relationship is also unaltered in N1_NoDy_Feb (Figure 4n) compared to N1_For (Figure 4j), likely due to unchanged spatial distributions of $< Q_{ML}^{-} >$ among these two simulations (Figures 5f and 10b).

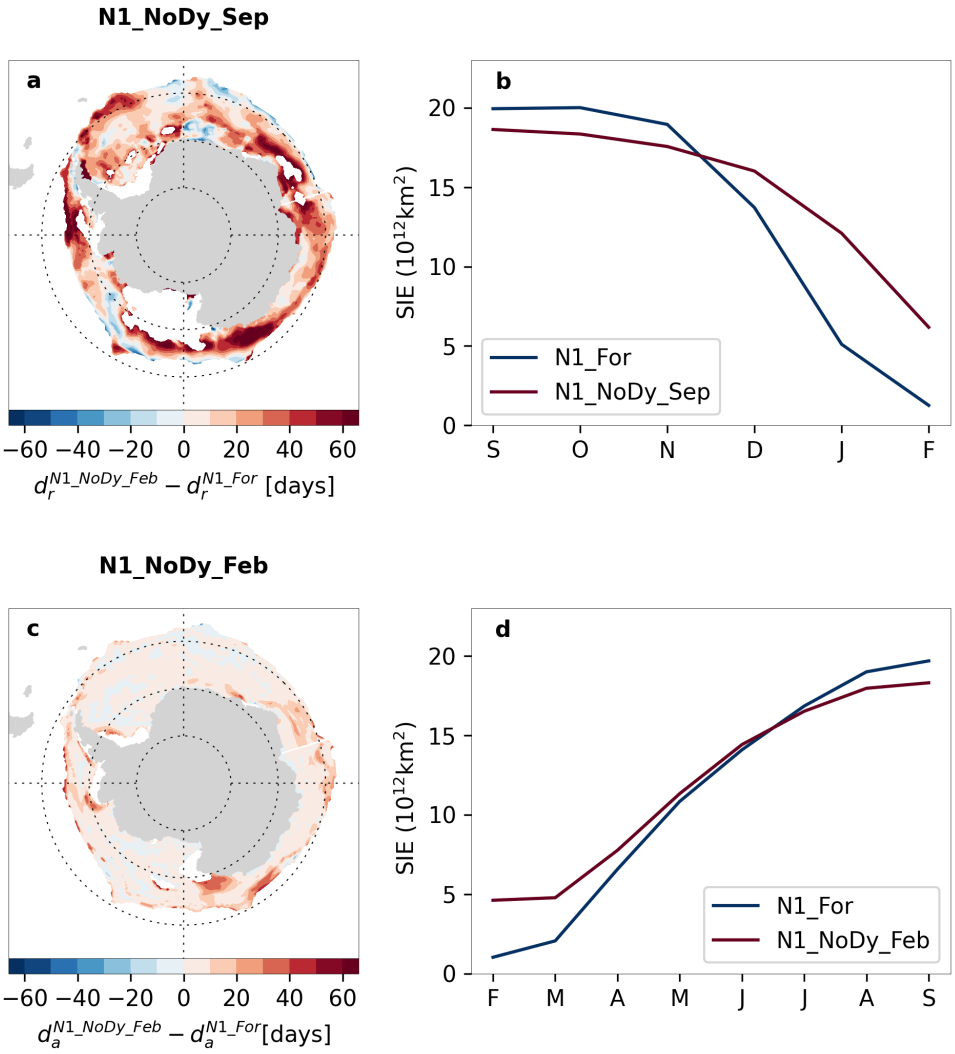

Figure II.9: **Impact of turning off ice drift on the sea ice seasonal cycle.** Seasonal cycles of sea ice extent (SIE) in **a**, N1_NoDy_Sep and **b**, N1_NoDy_Feb experiments; anomalies of **c**, retreat date in N1_NoDy_Sep and **d**, advance date in N1_NoDy_Feb relative to N1_For. White patches in **c** and **d** indicate regions out of the seasonal ice zone.

In summary, the HA relationship is weakly affected by sea ice dynamics. In contrast, sea ice drift processes significantly weaken the TR relationship, increasing deviations from linearity. Nonetheless, heat fluxes seem to be a significant contributor to these deviations, given that in the absence of sea ice dynamics, the persisting large scatter around the linear TR relationship is overall explained by the spatial variability in $< Q_{ice} >$.

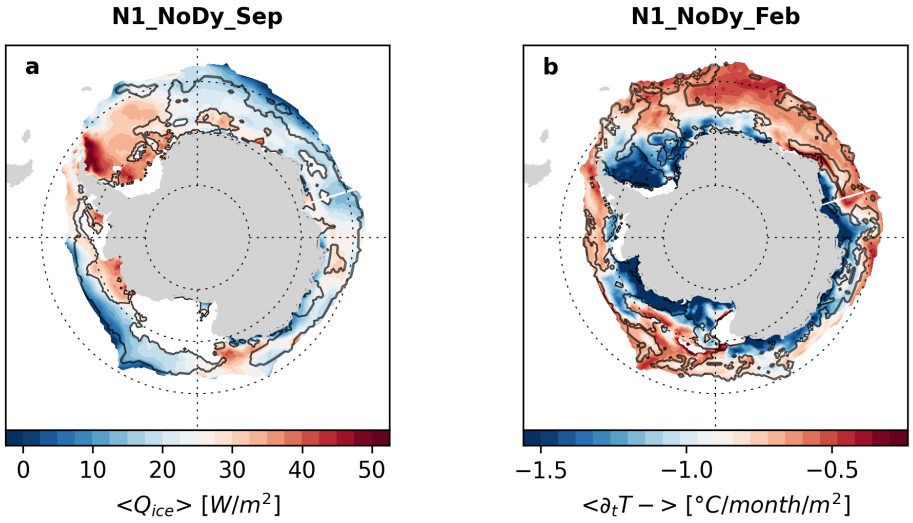

Figure II.10: **Impact of deactivating ice drift on relevant heat fluxes.** a, Required heat flux to melt the ice (< Q_{ice} >) in N1_NoDy_Sep and b, total mixed layer temperature tendency over the cooling period (< $\partial_t T^-$ >) of the open water season N1_NoDy_Feb. Black contours mark the 0-contour of deviations from linear predictions of retreat dates (a) and advance dates (b). Deviations are derived as the difference between the actual values and the predicted values by the linear models of Figure 9. White patches indicate regions out of the seasonal ice zone.

5 Discussion

This study assesses the representation of TRHA (Thickness-Retreat-Heat content-Advance) relationships in NEMO, and explores the processes shaping them. We analyse various simulations with varying atmospheric coupling strategy, model resolution and tuning protocol. We find close-to-linear TRHA relationships in all simulations. These relationships seem influenced by the simulated ice-ocean processes (e.g. sea ice dynamics, ocean thermohaline structure). However, they also seem influenced by model configuration and protocol issues, including differences in climatological averaging. The linearity persists in the absence of sea ice dynamics, supporting theoretical (section 2.1) and observational (Chapter I) evidence of a thermodynamic origin. Air-sea-ice heat fluxes largely affect each of these relationships, explaining the deviations from linearity. In contrast, sea ice dynamics affect these relationships only during the melt season. We next discuss the insights these findings provide on reality and on the model.

The model appears to be sufficiently realistic to improve our understanding of real-world drivers of sea ice seasonality. Indeed, the consistent linearity of TRHA relationships across various configurations suggest that the model captures the key thermodynamic constraints on sea ice retreat and advance. In addition, several findings on heat fluxes and sea ice dynamics seem consistent with observations. On the role of sea ice dynamics, the weak influence of ice transport processes on the date of advance corroborates the finding of Himmich et al. (2023),

indicating that ice dynamics only affect advance in the outermost band of the sea ice zone. On the role of heat fluxes, we find that deviations from the HA relationship are mainly caused by surface heat fluxes, while deviations in the RH relationship arise from both surface and bottom heat fluxes into the mixed layer. The variable contribution of heat fluxes at both the surface and the base of the mixed layer during the open water season aligns with observational estimates of seasonal heat entrainment from the subsurface by Pellichero et al. (2017). Consequently, our simulations can offer valuable insights into how sea ice dynamics and heat fluxes may impact observational TRHA relationships. Notably, our findings support the theoretical arguments (see Methods) indicating that deviations from linear relationships are mainly caused by the spatial variability in heat fluxes. During the open water season, when the effects of sea ice dynamics are weak, these deviations may inform on the spatial variability air-sea heat fluxes over the seasonal ice zone, which lack reliable measurements (Swart et al., 2019).

Our analysis also highlights that sea ice seasonality is influenced by several model configuration choices, that we could not fully disentangle with the simulations we had at hand. First, TRHA relationships are sensitive to model tuning, resolution and also possibly to atmospheric representation (coupled or forced, forcing field used). However, the relative importance of each of these configuration choices differs according to the retained criteria (slope or determination coefficient). Second, the model presents some biases that may affect our conclusions. In particular, the biases in the simulated thermohaline structure could affect the contribution of bottom heat fluxes to the mixed layer heat budget. These issues might explain the low contribution of entrainment to the mixed layer heat budget in the outer seasonal ice zone during cooling (Figure 6c), which contradicts previous suggestions of significant oceanic heat supply likely occurring there (Himmich et al., 2023; Su, 2017). Also, we find that some dynamic and thermodynamic sea ice processes may not be optimally represented during the melt season. Indeed, simulated sea ice is faster and thinner than observed. This could explain the weaker linearity of the TR relationship compared to the other relationships and the disparities in patterns of ice concentration budget between the model and observations.

Several methodological and protocol-related caveats were identified in section 2, possibly limiting the strength of our conclusions. These mainly arise from the simulations being selected opportunistically and not specifically designed for our purposes. To address these caveats, additional work will be undertaken before attempting to publish this chapter. This includes an investigation into the reasons behind the sensitivity of RH and HA relationships to the reference temperature used to compute the mixed layer heat content (Figure 1). We also plan to rerun our simulations considering a few protocol adjustments to better align with observations. Interannual forcing is more appropriate for a sensible comparison to observations, as the latter is based on a climatological averaging of yearly data. In addition,

modifying the current on-line mixed layer budget diagnostics in terms of mixed layer heat content instead of temperature could add precision to the evaluation of heat flux contributions.

Another stream of work could be to use the TRHA framework to evaluate the representation of key drivers of sea ice seasonality in any ocean model. It could also be used to highlight changes in model realism when testing the improvement brought by new model developments. This framework, therefore, holds the potential to reduce uncertainties surrounding Antarctic sea ice in global climate models (Beadling et al., 2020; Casagrande et al., 2023; Roach et al., 2020).

CHAPTER

III

Recent Changes in Antarctic Sea Ice Seasonality

In chapters I and II, we highlight robust drivers of mean-state Antarctic sea ice seasonality using climatological observations and model simulations. These drivers include a strong thermodynamic control by the seasonal maximum mixed layer heat content and the sea ice thickness at melt onset on the dates of sea ice advance and retreat, respectively. However, this control is likely weakened by variability in air-ice-sea heat fluxes and sea ice transport, as indicated by model simulations presented in Chapter II. Furthermore, in Chapter I, we found that thermodynamics explain, to a certain extent, interannual anomalies in the dates of advance and retreat. However, these links are weaker than in the mean state. This weaker association could be attributed to potential measurement errors or to a stronger influence of ice transport and air-sea-ice heat fluxes on interannual variability compared to mean state.

Here, I focus on the large recent changes in Antarctic sea ice following 2016, culminating in 2023. The choice of 2016 is motivated by a shift identified in Antarctic sea ice around this particular year (Purich 2023; Parkinson 2019). Indeed, after a gradual increase over 1979-2016, Antarctic sea ice extent has abruptly shifted towards lower coverage, over 2016-2023 (see Figure 2 of General Introduction). This reduction has been attributed to changes in atmospheric circulation (e.g. Meehl et al., 2019; Schroeter et al., 2023; Turner et al., 2022) and to oceanic warming (Meehl et al., 2019; Purich & Doddridge, 2023; Zhang et al., 2022), with no clear consensus. Large changes in the sea ice seasonal cycle are therefore expected after 2016, but remain undocumented. Long-term changes in sea ice retreat and advance dates have been documented until 2013, and attributed to changes in Southern Ocean winds and to the ice-albedo feedback (Holland et al., 2017; Simpkins et al., 2013; Stammerjohn et al., 2012, 2008). However, these previous documentations require an update by including the most recent years.

In this final chapter, in revision in *JGR Oceans*, we study the post-2016 changes in sea ice seasonality and their drivers, based on the analytical framework from Chapter I. This framework could provide useful insights to explain these changes. Analyzing anomalies in retreat and advance dates, sea ice thickness and sea surface temperature following 2016, we explore

potential links between them to assess the role of the thermodynamic constraints highlighted in chapters I and II. We also conduct a sea ice concentration budget analysis to assess the role of sea ice transport. We ultimately discuss new insights into the mechanisms causing the recent Antarctic sea ice shift.

Thermodynamics Drive Changes in the Antarctic Sea Ice Seasonal Cycle Following 2016

Kenza Himmich, Martin Vancoppenolle, Sharon Stammerjohn, Marion Bocquet, Gurvan Madec, Jean-Baptiste Sallée, Sara Fleury

Antarctic sea ice extent has been persistently low since late 2016, possibly owing to changes in atmospheric and oceanic conditions. However, the relative contributions of the ocean, the atmosphere and the underlying mechanisms by which they have affected sea ice remain uncertain. To investigate possible causes for this sea-ice decrease, we establish a seasonal timeline of sea ice changes following 2016, using remote sensing observations. Anomalies in the timing of sea ice retreat and advance are examined along with their spatial and interannual relations with various indicators of seasonal sea ice and oceanic changes. They include anomalies in winter ice thickness, spring ice removal rate due to ice melt and transport, and summer sea surface temperature. We find that the ice season has shortened at an unprecedented rate and magnitude, due to earlier retreat and later advance. We attribute this shortening to a winter ice thinning, in line with the ice-albedo feedback, with ice transport playing a more minor role. Reduced ice thickness has accelerated spring ice area removal as thinner sea ice requires less time to melt. The consequent earlier sea ice retreat has in turn increased ocean solar heat uptake in summer, ultimately delaying sea ice advance. We speculate that the observed winter sea ice thinning is consistent with previous evidence of subsurface warming of the Southern Ocean.

Key Points:

- The Antarctic sea ice season duration has undergone an unprecedented shortening since 2016;
- The changes include thinner ice, faster melt, earlier retreat, larger ocean heat uptake, later advance, in line with ice-albedo feedback;
- The near-circumpolar ice thinning is consistent with a possible increase in sensible heat supply by the ocean.

1 Introduction

Antarctic sea ice has been subject to puzzling changes since the start of remote sensing observations. Over more than three decades, there was a striking contrast between the substantial decrease in Arctic sea ice (Cavalieri & Parkinson, 2012) and the overall weak but clear increase in Antarctic sea ice (Comiso, 2017; Parkinson & Cavalieri, 2012). In late 2016, however, Antarctic sea ice extent underwent an abrupt decline, sustained in the following years by several record lows (Parkinson, 2019; Raphael & Handcock, 2022).

The initial decrease in late 2016 has been mainly attributed to atmospheric processes. Anomalous winds produced by tropical teleconnections (Meehl et al., 2019) and a negative phase of the Southern Annular Mode (SAM; Schlosser et al., 2018; Turner et al., 2017) have warmed the surface ocean (Meehl et al., 2019) and limited the northward expansion of sea ice (Stuecker et al., 2017; Turner et al., 2017). By contrast, the sustained low sea ice state following 2016 has been attributed to both oceanic and atmospheric changes. Atmospheric changes include strengthened southward winds (Schroeter et al., 2023) and increased storm frequency (Turner et al., 2022). However, simulations using a coupled climate model suggest that the sole contribution of the atmosphere is insufficient to explain observed sea ice changes (Zhang et al., 2022). Instead, several studies point to a warming of the Southern Ocean subsurface as a key potential cause of the low sea ice state (Meehl et al., 2019; Purich & Doddridge, 2023; Zhang et al., 2022). Notably, the post-2016 shift in the seasonal persistence of sea ice anomalies (Purich & Doddridge, 2023), which is linked to the vertical structure of oceanic properties (Holland et al., 2013; Libera et al., 2022), suggests that recent subsurface ocean and sea ice changes could be connected. Subsurface warming has been identified as a long-term response to a phase of negative Interdecadal Pacific Oscillation (IPO) and positive SAM, with resulting Ekman suction of warm subsurface waters (Ferreira et al., 2015; Kostov et al., 2017; Meehl et al., 2016). Northward sea ice transport induced by a positive SAM may have also contributed to this warming by increasing stratification and reducing subsurface ventilation (Haumann et al., 2020). Yet, how changes in atmospheric and oceanic conditions have affected sea ice remain unclear. Moreover, further evidence is required to establish the predominant role of subsurface warming over atmospheric processes in driving the recent sea ice changes.

Next to ice extent, useful markers of sea ice changes include the dates of advance and retreat, which represent two key transitions in the seasonal cycle of sea ice. Sea ice advance or retreat dates respectively mark the start and end of the sea ice season, defined as the first day in the year when sea ice concentration exceeds or falls below 15% (Massom et al., 2008; Stammerjohn et al., 2008). These two metrics allow for spatial analysis across the entire seasonal ice zone, and highlight which regions are changing, and which are not.

Changes in the timing of sea ice retreat and advance can be respectively traced back to prior ice thickness (Smith et al., 2020) and mixed layer heat content(Himmich et al., 2023). On the grid-point scale, a reduction in ice thickness implies a larger prevalence of thin ice that is removed more efficiently upon melting (Holland et al., 2006), and thus retreats earlier. Thinner ice promotes solar radiation uptake, basal melting (Maykut & McPhee, 1995; Maykut & Perovich, 1987; Vivier et al., 2016) and accelerates sea ice concentration decreases. Also, earlier retreat increases solar radiation uptake (Perovich et al., 2007) and the mixed layer heat content during the open water season, delaying sea ice advance (Himmich et al., 2023; Holland et al., 2017; Stammerjohn et al., 2012). Both processes are linked to ice-albedo feedbacks. Ice transport also contributes to changes in sea ice seasonality by modifying sea ice concentration (Holland et al., 2017; Holland & Kwok, 2012) or, more indirectly, by increasing the open water fraction and triggering the ice-albedo feedback (Holland et al., 2017; Massom et al., 2008; Stammerjohn et al., 2008). Examining changes in sea ice seasonality alongside changes in ice thickness, ocean heat content and ice concentration budget can therefore provide valuable insights into the drivers of the sea ice shift following 2016. However, changes in sea ice seasonality have only been documented until 2012, with large regional trends towards later retreat and earlier advance in the Amundsen and Bellingshausen Seas and, earlier retreat and later advance in the Ross Sea (e.g. Simpkins et al., 2013). Possible shifts in sea ice seasonality following 2016 have yet to be investigated.

In this study, we evaluate the changes in sea ice seasonality following 2016, based on passive microwave sea ice concentration records. We analyze possible drivers of these changes using satellite observations of sea ice thickness, sea surface temperature and ice concentration budget diagnostics, including ice-albedo feedback processes and ice transport. Finally, we discuss whether those changes point to the atmosphere or the ocean as the key driver of the recent sea-ice shift.

2 Data

This study is based on satellite observations of sea ice concentration, drift, thickness and sea surface temperature. We use daily passive microwave sea ice concentration over 1979-2022 (Lavergne et al., 2019) and sea ice drift over 1991-2020 (Lavergne & Down, 2023) from the EUMETSAT Ocean and Sea Ice Satellite Application Facility (OSI SAF), with respective resolutions of 25 and 75 km. Fields of sea ice drift are retrieved using different methods according to the season. In winter, from April to September, ice drift is retrieved using a maximum cross correlation algorithm applied to brightness temperature from a number of sensors (SSM/I, SSMIS, AMSR-E and AMSR2). In summer, from November to February, a free-drift model based

on the ERA5 wind fields is used (Hersbach et al., 2020). In October and March, the fields are derived from both model and satellite-based outputs.

For sea ice thickness, we utilized altimetry-based ice thickness retrievals from 1994 to 2022, as provided by Bocquet (2023). This dataset integrates year-round 12.5 km gridded radar freeboard time series from ERS-1, ERS-2, Envisat, and CryoSat-2 missions. Different missions are inter-calibrated, leveraging mission overlap. Ku-band radar echoes are corrected for the varying speed of light in snow (Mallett et al., 2020) and converted to radar freeboards following the methodology outlined by Laxon et al. (2003). The density of ice (875-920 kg/m³) and snow (320-350 kg/m³) includes specified seasonal variations(Kurtz & Markus, 2012; Maksym & Markus, 2008). Snow depth is taken from a climatology of radiometer-based estimation developed for SI-CCI (Paul et al., 2021). Finally the ice thickness is deduced from the radar freeboard and the snow using the equilibrium equation of the snow covered ice in the sea water. The resulting ice thickness dataset was evaluated against the ASPeCt dataset (Worby et al., 2008), AWI moorings in the Weddell Sea (Behrendt et al., 2013), and Operation Ice Bridge (Kurtz et al., 2013), resulting in reasonable agreement despite potential biases.

Finally, we use a daily satellite product of sea surface temperature available over 1982-2022, based on thermal infra-red radiance measurements, and taken from the global L4 (gap-free, gridded) European Space Agency (ESA) SST Climate Change Initiative (CCI) analysis with a resolution of 0.05 ° (Merchant et al., 2019). All data are either interpolated on the OSI-SAF Equal-Area Scalable Earth 2 (EASE2) 25 km or 75 km grid.

3 Materials and Methods

3.1 Sea ice concentration budget

To unravel the thermodynamic and dynamic nature of the processes contributing to the recent sea ice changes, we use a sea ice concentration budget decomposition based on the governing equation for sea ice concentration (C; e.g. Holland & Kwok, 2012):

$$\frac{\partial \mathrm{SIC}}{\partial t} = \nabla.(\boldsymbol{u}\ \mathrm{SIC}\ ) + \mathrm{residual}, \tag{III.1}$$

$$\nabla.(uC) = \mathbf{u}.\nabla C + C\nabla.\mathbf{u}, \tag{III.2}$$

where $\mathbf{u}$ is the sea ice drift field. The dynamic term ($\nabla.(\boldsymbol{u}\ \mathrm{SIC}\ )$) represents advection ($\mathbf{u}.\nabla C$) and divergence ($C\nabla.\mathbf{u}$) of sea ice caused by ice drift whereas the residual term includes both thermodynamic processes (melting / freezing) and mechanical redistribution (ridging/rafting).

We apply the exact methodology of Holland and Kimura (2016) on OSI SAF sea ice concentration and drift data to compute the dynamic and residual contributions to the budget. Sea ice concentration fields are interpolated on the 75-km grid of ice drift. A 7x7 cell square-window smoothing filter is then applied to the ice drift fields in order to avoid noise in the dynamic term. The time derivative in ice concentration is calculated as a central difference in time of sea ice concentration fields at a daily frequency. Advection and divergence terms are calculated as central differences in space then averaged over 3-days periods to synchronize with time derivatives.

3.2 Diagnostics of sea ice and sea surface changes

In this study, we consider that each year starts and ends in September, during the ice season. For example, 1980 starts on September 15th 1979 and ends in September 14th 1980. To diagnose the changes in sea ice seasonality, we derived the dates of sea ice retreat and advance from the OSI-SAF sea ice concentration, on which we applied a 15-day temporal filter to avoid retaining any date reflecting short events (Lebrun et al., 2019). The date of retreat is defined as the first day filtered sea ice concentration drops below 15% while the date of advance is the first day filtered sea ice concentration exceeds 15%, similar to previous studies (Lebrun et al., 2019; Parkinson, 1994; Simpkins et al., 2013; Stammerjohn et al., 2012). To ensure retreat dates and subsequent advance dates of the same yearly seasonal cycle are retained, we looked for advance (retreat) dates starting on a month where no sea ice advance (retreat) occurs, on average over 1980-2022. We selected January 1st of the current year as the start date for advance, and May 1st of the previous year for retreat, since most of advance and retreat dates occurs after those dates. Ultimately, for each year, only the dates between September 15th of the previous year and September 14th of the current year are retained.

To diagnose possible changes during the ice and open water seasons, we respectively use mean September sea ice thickness, representing the end-of-winter thickness, and seasonal maxima of sea surface temperature. Each yearly sea surface temperature maximum was selected between the retreat date and the following advance date of the corresponding year. To investigate the changes in spring ice removal processes possibly leading to changes in the retreat dates, we define the spring (over October, November and December) sea ice removal rate (IRR) as:

$$IRR = -\int_{OND} \left.\frac{\partial C}{\partial t}\right|_{<0} dt. \tag{III.3}$$

The IRR filters the positive derivatives to ensure focus on removal processes. Using the sea ice concentration budget decomposition, we also calculate the dynamic and residual contributions to the IRR for each year over 1992-2020. Climatological fields of IRR and contributions show that the dynamic term is positive in the inner sea ice zone due to ice export out of that

inner zone and negative in the outer sea ice zone due to ice import into that outer zone. This dynamic contribution is, however, small compared to the residual, which dominates the removal rate over all the seasonal ice zone (see Supplementary Figure 1). Based on these considerations, positive (negative) anomalies in IRR can be interpreted as an increase (decrease) in ice removal. Positive (negative) anomalies in dynamic contribution would suggest increased (decreased) ice export in the inner pack and decreased (increased) ice import in the outer pack. Interpreting the sign of anomalies in residuals is not as straightforward because it accounts for both melt and mechanical redistribution processes.

For any statistical calculations conducted in this study involving the previously mentioned diagnostics, a missing value is assigned where the number of years with undefined retreat or advance dates (corresponding to year-round ice-free or ice-covered grid points) is less than one third of the total number of years in the considered period, following Lebrun et al. (2019). This procedure ensures that meaningful and consistent averages, trends or correlations are obtained.

4 Unprecedented shortening of the sea ice season following 2016

We examine the changes in ice season duration and ice retreat and advance date over 1980-2022 (Figure 1), based on mean anomalies over the seasonal ice zone (see Figure 2).

Over 1980-2016, the sea ice season duration exhibits a clear increase of 3.6 days per decade (Figure 1a; Table 1) due to trends towards 1 day later retreat and 2.6 days earlier advance per decade (Figures 1b and c). Over 2016-2017, however, an abrupt shortening occurs, followed by large negative anomalies maintaining the ice season duration at low values until 2022 (Figures 1a-c). As a result of this reversal in behavior after 2016, the ice duration trend over 1980-2022 is small and not statistically significant (Table 1). The weakening of circumpolar trends results from regional pattern changes, evident when comparing regional trends over 1980-2022 and 1980-2016 (see Supplementary Figure 2). The largest regional trends towards a longer ice season prior to 2017, located in the Ross and Weddell Seas, have weakened over 1980-2022. Additionally, significant trends towards a shorter ice season have emerged in the Bellingshausen Sea and the Indian sector over 1980-2022. Spatial patterns of ice season length anomalies following 2016 align consistently with the evolution of regional trends (Figures 2a-c). Based on the 6-year averaged anomalies over 2017-2022, we find that the ice season shortening is overall circumpolar, but largest in the Ross, Bellingshausen, Weddell and Indian sectors. On average over the seasonal ice zone, the ice season is 8.9 days shorter in 2017-2022 compared to 1980-2016, due to 3.7 days earlier retreat and 5.2 days later advance.

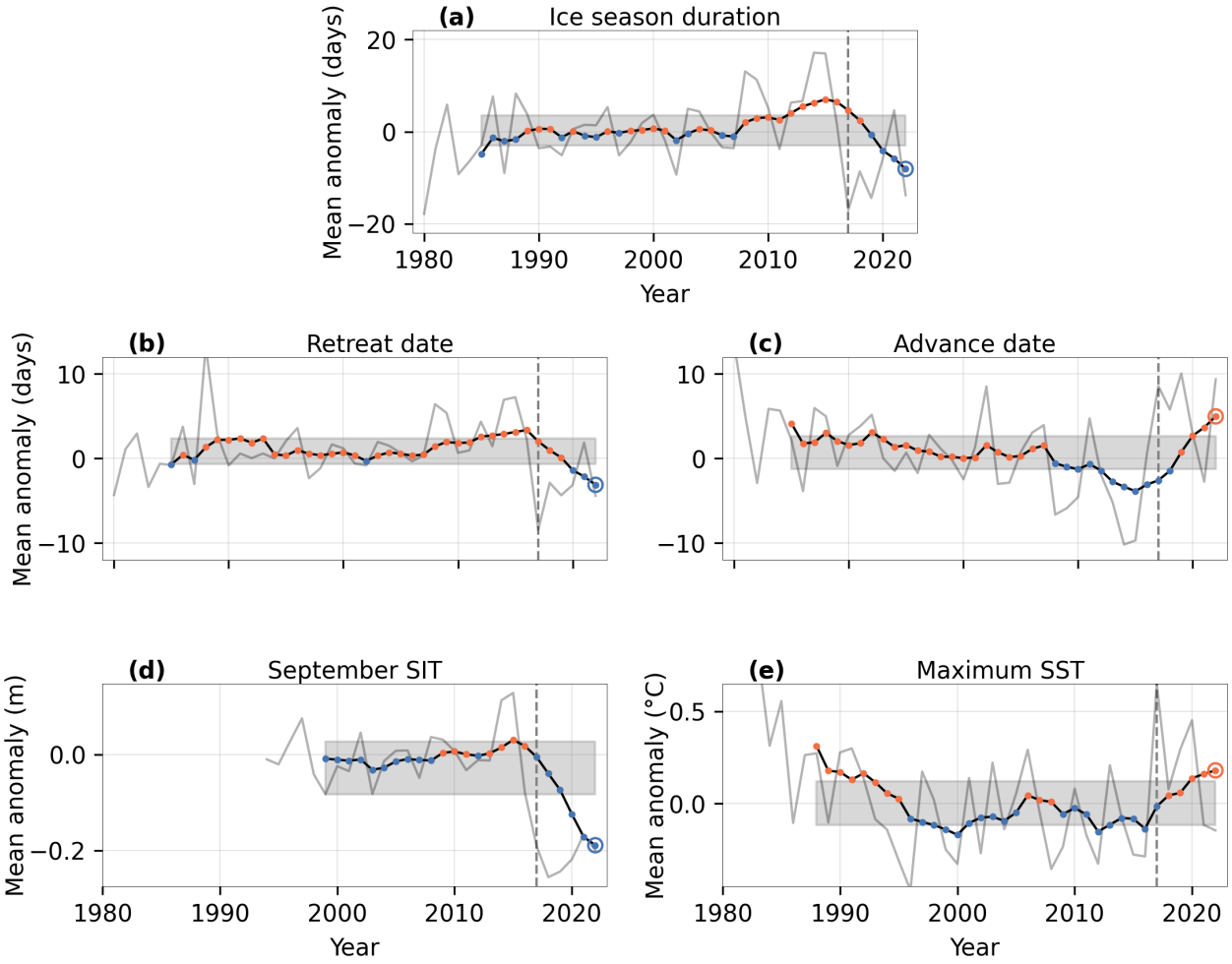

Figure III.1: **Time series of selected sea ice and ocean diagnostics.** Grey solid lines show yearly anomalies averaged over the seasonal ice zone in **a**, ice season duration, **b**, retreat dates, **c**, advance dates, in **d**, September sea ice thickness (SIT) and **e**, maximum sea surface temperature (SST). Black lines with colored dots show 6-year moving averages such that the last point represents the 2017-2022 mean anomalies depicted in Figure 2. Anomalies are relative to 1980-2016 in **a**, **b** and **c**, to 1983-2016 in d and to 1994-2016 in **e**. Red dots mark positive values whereas blue dots mark negative values. Stippled grey lines mark the 2017 yearly anomalies. The grey areas delimit the mean +/- the standard deviation of 6-year moving averages over the whole time series.

We next assess the magnitude and rate of the recent ice season shortening. We find that the mean anomalies in ice season length, retreat and advance dates for 2017-2022 with respect to 1980-2016 (Figures 1a-c) are larger than any previous 6-year mean anomalies. Specifically, the 2017-2022 anomaly in ice season duration is the lowest on record, being 2 days shorter than the previous shortest ice season anomaly (2016-2021) and exceeding three times the standard deviation (Figures 1a). The 2017-2022 anomaly is also record breaking for both retreat and advance dates by approximately 1 day (Figures 1b, c). This indicates that the earlier retreat, later advance and consequent shorter sea ice season following 2016 are unprecedented. The interannual changes in sea ice seasonality are also unusually rapid when comparing 7-year periods ending after 2017, exceeding the standard deviation in mean rates of change (Figures

Table III.1: **Long-term trends in selected sea ice and ocean diagnostics.** Trends are defined as the linear least square fit slopes for the yearly anomalies, averaged over the seasonal ice zone, over time periods ending either in 2016 or in 2022. Time periods are chosen according to underlying data availability and are indicated in the first column of the table. Slopes standard errors are given as uncertainties. Bold numbers indicate statistically significant trends at the 95% level.

	Trends ending in 2016	Trends ending in 2022
Ice season duration (days/dec.) 1980-2022	**3.6 +/- 1.0**	0.6 +/- 1.0
Retreat date (days/dec.) 1980-2022	**1.0 +/- 0.5**	-0.2 +/- 0.5
Advance date (days/dec.) 1980-2022	**-2.6 +/- 0.6**	-0.8 +/- 0.6
September SIT (cm/dec.) 1994-2022	1.8 +/- 1.8	**-6.0 +/- 2.0**
Maximum SST (°C/dec.) 1983-2022	**-0.15 +/- 0.04**	-0.06 +/- 0.04

3a-c). The fastest 7-year changes in retreat and advance dates over the entire time series occur over the 2013-2019 and 2014-2020 periods, respectively (i.e., ending in 2019 and 2020, as shown in Figures 3b, c), reaching respectively more than 3 times and 2 times the standard deviation.

Due to a near-circumpolar shortening following 2016, the evolution of sea ice season duration over 1980-2022 closely parallels the changes observed in ice extent, with a long-term increase followed by an unprecedentedly large and rapid decrease in 2017, as shown by Parkinson (2019).

5 Drivers of the recent sea ice season shortening

5.1 Shorter ice season: response to ice thinning?

We hypothesize that the recent ice season shortening might be tied to changes in ice thickness and upper ocean heat content. Accordingly, in this section, we examine the changes in the September sea ice thickness over 1994-2022 and in the seasonal maximum of sea surface temperature, used as a proxy of the summer mixed layer heat content (Himmich et al., 2023), over 1983-2022.

Similar to retreat and advance dates, September ice thickness and maximum sea surface temperature have undergone an unprecedented shift since 2016. This finding is based on mean anomalies over the seasonal ice zone (Figures 1d, e). Over 1994-2016, sea ice thickness anomalies exhibit no statistically significant trend, while over the 6-year thickness time series

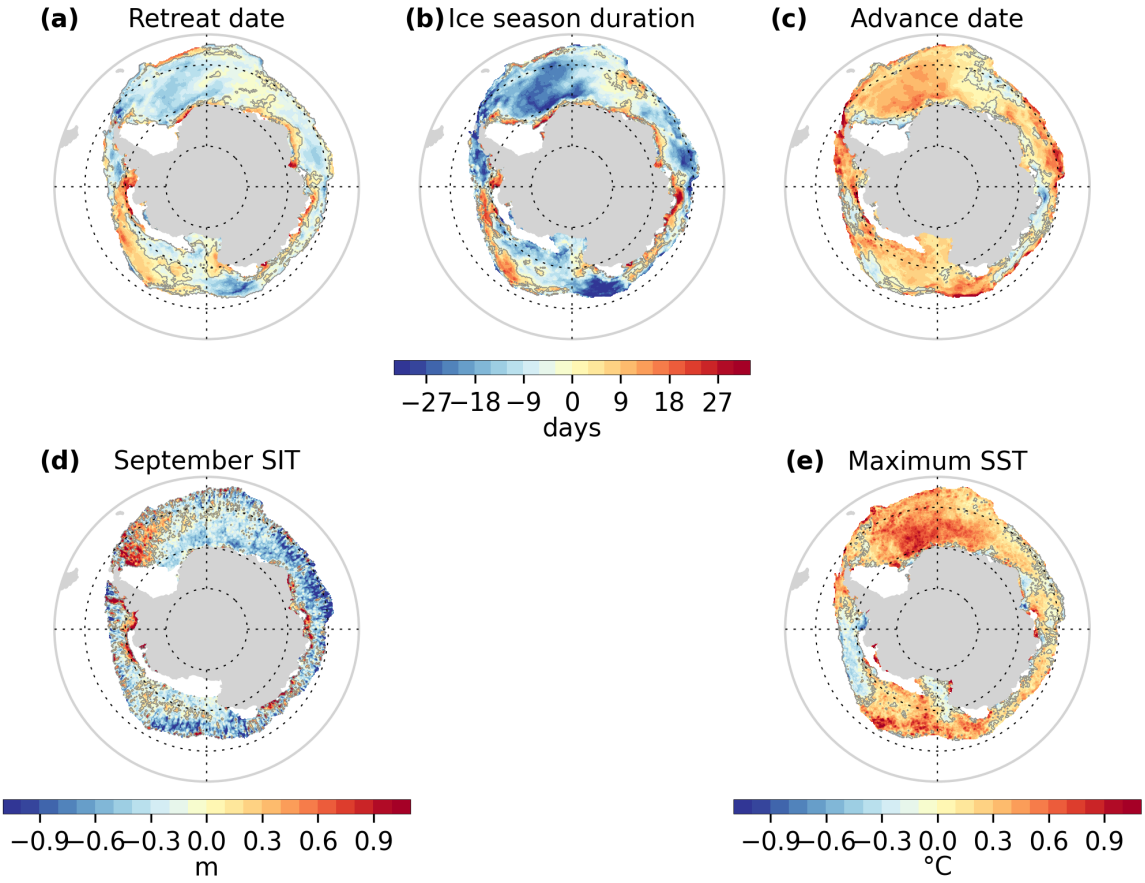

Figure III.2: **Mean anomalies in selected sea ice and ocean diagnostics over 2017-2022.** **a**, Ice season duration, **b**, retreat dates, **c**, advance dates, **d**, September sea ice thickness (SIT), **e**, maximum sea surface temperature (SST). Anomalies are relative to 1980-2016 in **a**, **b** and **c**, to 1983-2016 in **d** and to 1994-2016 in **e**. White patches indicate regions out of the seasonal ice zone.

ending in 2022, a statistically significant trend emerges, showing at decrease of 6 cm per decade. A shift is also observed for sea surface temperature in 2016. Over 1983-2016, maximum sea surface temperature anomalies exhibit a statistically significant trend toward colder sea surface temperatures by 0.15°C per decade. However, over 1983-2022, the trend becomes almost nil (Table 1). This shift in long-term trends stems from widespread thinner sea ice and warmer sea surface following 2016 (Figure 2d, e), occurring at an unprecedented magnitude and rate. Notably, the average anomaly over 2017-2022 is the lowest on record for thickness and the second highest on record for temperature, among 6-year average anomalies (Figures 1d, e). Moreover, the top 3 7-year periods with fastest sea ice thinning and sea surface warming end after 2017 (Figures 3d, e).

The coinciding earlier retreat, later advance, thinner sea ice and warmer sea surface temperatures suggest that these variables could be linked and driven by a common underlying mechanism. That the post-2016 ice thinning and sea surface warming (Figures 2d, e) occur

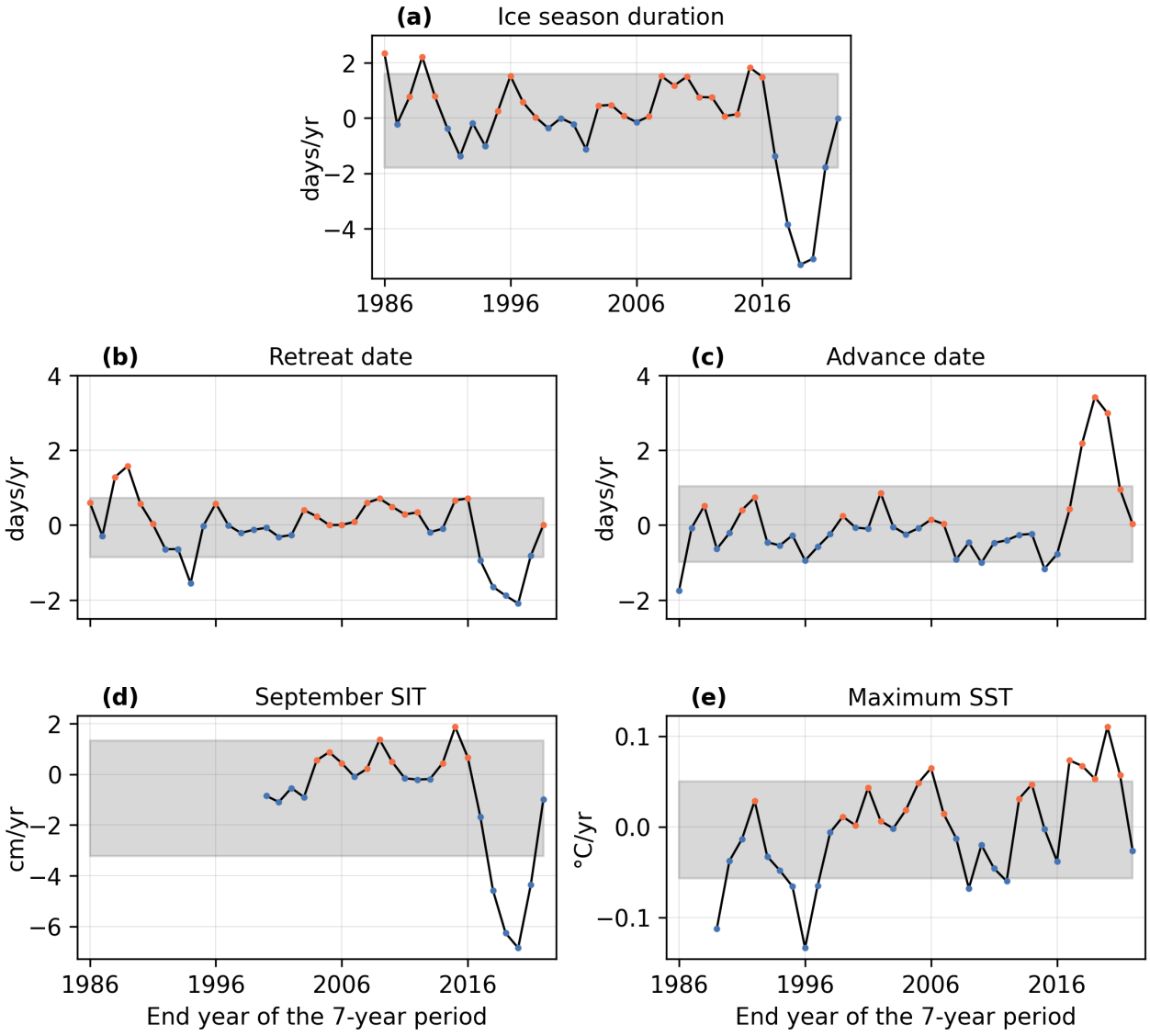

Figure III.3: **Rate of seven-year changes in selected sea ice and ocean diagnostics.** Rates are calculated as least-square slopes over 7 years of mean anomalies over the seasonal ice zone in **a**, Ice season duration, **b**, retreat date, **c**, advance date **d**, September sea ice thickness (SIT), and **e**, maximum of sea surface temperature (SST). Blue dots mark negative values whereas red dots mark positive values. The grey areas delimit the mean +/- the standard deviation over the whole time series.

mainly where the changes in retreat and advance date are the largest (see Supplementary Figure 3) further supports this hypothesis. Remarkably, we find that 74% of seasonal ice zone grid points with earlier retreat spatially correspond to thinner September sea ice. Earlier retreat due to thinning reflects either a thermodynamic response, with increased melt rate, or a dynamic response, with increased sensitivity to transport, as suggested by Holland et al. (2006). This point will be further investigated in the next section. In addition, we find that 85% of the grid points with higher maximum sea surface temperature also show an early retreat. In turn, 92% of grid points with later advance have a higher sea surface temperature. The correspondence between earlier retreat, warmer sea surface temperature and later advance is consistent with

ice-albedo feedback processes during the open water season (Himmich et al., 2023; Holland et al., 2017; Stammerjohn et al., 2012): earlier retreat increases solar heat uptake into the mixed layer; the extra heat needs more time to be released, which delays sea ice advance. Accordingly, 77% of the grid points with later sea ice advance also have earlier ice retreat.

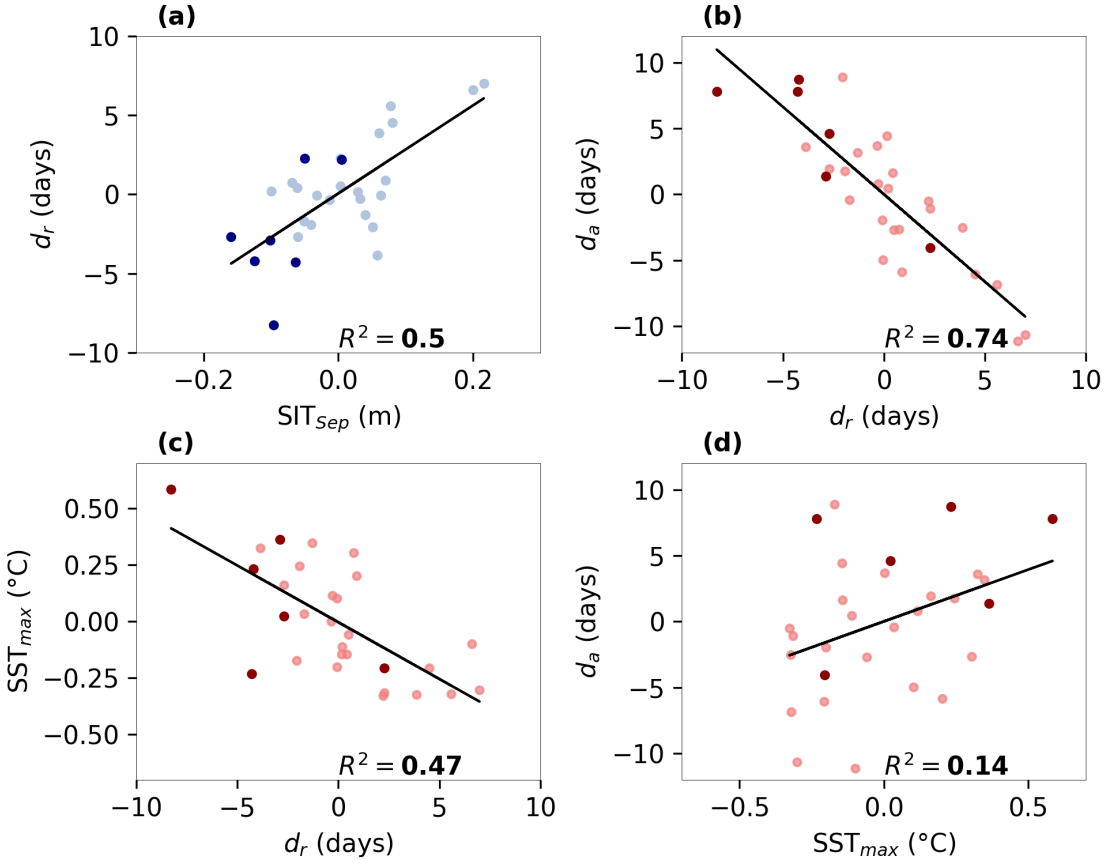

Figure III.4: **Interannual relationships between selected sea ice and ocean diagnostics, over 1994-2022.** Detrended anomalies of **a**, retreat dates (d_r) versus September sea ice thickness (SIT_{Sep}), **b**, advance dates (d_a) versus d_r, **c**, maximum sea surface temperature (SST_max) versus d_r, **d**, d_a versus SST_{max}. Blue tones indicate ice season relations whereas red tones indicate open water season, as illustrated in Figure 5. 2017-2022 anomalies are marked in dark colours. A Least Square linear regression was performed for each plot; the corresponding regression line (significant at 99%), and corresponding coefficients of determination (R^2) are shown. The 1994-2022 period was selected to ensure consistency of the analysis, as all relevant diagnostics are available over this timeframe.

Yearly anomalies follow a consistent sequence of processes: low winter thickness results in early retreat, increased summer ocean heat content, and late advance. For instance, in 2016/17, the anomalously low September sea ice thickness comes first in order, followed by the earlier retreat, warmer maximum sea surface temperature and ultimately, later advance (Figure 1). Correlations between 1994-2022 time series of mean detrended anomalies averaged over the seasonal ice zone support this analysis, with this specific period selected due to

the availability of relevant diagnostics. We observe a statistically significant link ($R^2 = 0.49$, $p < 0.01$) between the mean September sea ice thickness and the subsequent mean retreat date (Figure 4a). This relationship indicates that for each centimeter of ice thinning, the retreat occurs 0.28 days earlier. We also observe a statistically significant link between retreat and subsequent advance date anomalies ($R^2 = 0.74$, $p < 0.01$), indicating a delay in advance of 1.3 day per day of early retreat (Figure 4b). The link between anomalies in retreat date and subsequent maximum sea surface temperature appears relatively strong ($R^2 = 0.47$, $p < 0.01$; Figure 4c), when compared with the link between maximum sea surface temperature and subsequent advance date ($R^2 = 0.14$, $p < 0.01$; Figure 4d). We argue this reflects the importance of accounting for mixed layer depth to accurately evaluate the mixed layer heat content when the ocean is cooling down during open water season (Himmich et al., 2023). The maximum sea surface temperature is potentially a better proxy of the mixed layer heat content during the warming period, due to shallower mixed layers, explaining why the temperature is more strongly linked to retreat dates than to advance dates.

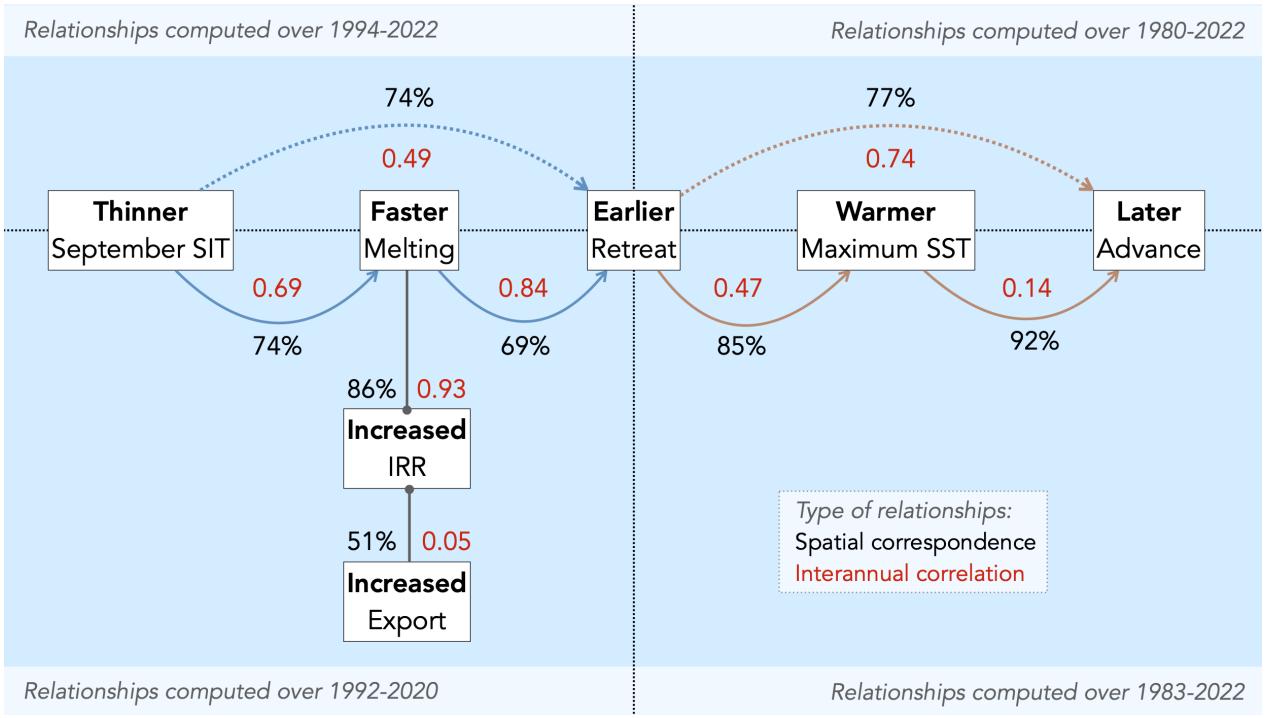

Figure III.5: **Schematic of the thermodynamic response of sea ice and sea surface to the ice thickness reduction following 2016.** Colored lines represent ice-albedo feedback processes occurring within the sea-ice season (blue) versus open water season (red). Grey lines represent the dynamic and thermodynamic contributions to the IRR. Red numbers refer to the coefficient of determination of interannual correlations between the considered variables, as shown in Figures 4 and 7. Percentages quantify the spatial correspondence between specified variable changes following 2016, based on mean anomalies (see Figures 2, 6 and Supplementary Figure 3). The time period considered for each spatial relationship, which depends on underlying data availability, is specified on the schematic.

Based on these spatial and interannual linkages (see Figure 5), we surmise that the decrease

in the September ice thickness has contributed to the earlier sea ice retreat following 2016. This has, in turn, lead to a warming of the upper ocean and delayed sea ice advance through the ice-ocean feedback. However, whether the ice thinning is a result of thermodynamic or dynamic changes remains to be established.

5.2 Earlier retreat: a dynamic or thermodynamic response of ice thinning?

To unravel the thermodynamic or dynamic nature of the relationship between ice thinning and early retreat, we examine melt season processes based on a sea ice concentration budget derived from passive-microwave concentration and drift. We evaluate the average sea ice area removal rate (IRR) over spring (October, November, December) as well as the dynamic and residual contributions to the IRR, over 1992-2020. The dynamic contribution to the IRR is mostly due to the northward export of sea ice (see Supplementary Figure 1) whereas residuals include both melting and, also, to some extent, mechanical redistribution through ridging and rafting (Holland & Kimura, 2016).

We find that the post-2016 shift is also seen in the spring ice removal processes. Mean IRR anomalies decrease to lower than average values over 1992-2016, then undergo an unprecedentedly rapid rise (see Supplementary Figure 4) starting in the spring before the early ice retreat of 2017 (Figure 6a). Anomalies in the residual contribution to the IRR evolve similarly (Figure 6c) and account for 93% of the interannual variance in total IRR (Figure 7a). Conversely, anomalies in the dynamic contribution show comparatively small variations (Figure 6e) and only explain 5% of the variance in total IRR (Figure 7b).

Residuals thus appear to be the major contributor to the recent increase in IRR compared to sea ice export. This is also highlighted by similar spatial patterns of mean anomalies over 2017-2020 in IRR and residual contribution (Figure 6b and d). Notably, 86% of the seasonal ice zone grid points with increased IRR correspond to increased residual contribution. By contrast, substantial discrepancies are observed between the spatial mean anomalies of the IRR and of the dynamic contribution (Figure 6b and f). Furthermore, the absence of ice thickening in spring (see Supplementary Figure 5) in regions of increased residual contribution (Figure 6d) suggests that ridging and rafting weakly contribute to the IRR, and that thermodynamics must dominate the increase. Hence, the recent IRR increase is likely caused by a more rapid melt-back.

We next investigate how the recent changes in residual IRR would relate to changes in September sea ice thickness and retreat date. We find that 74% of grid points showing an increase in residual IRR (Figure 6d) correspond to thinner sea ice (Figure 2d). Additionally, 69%

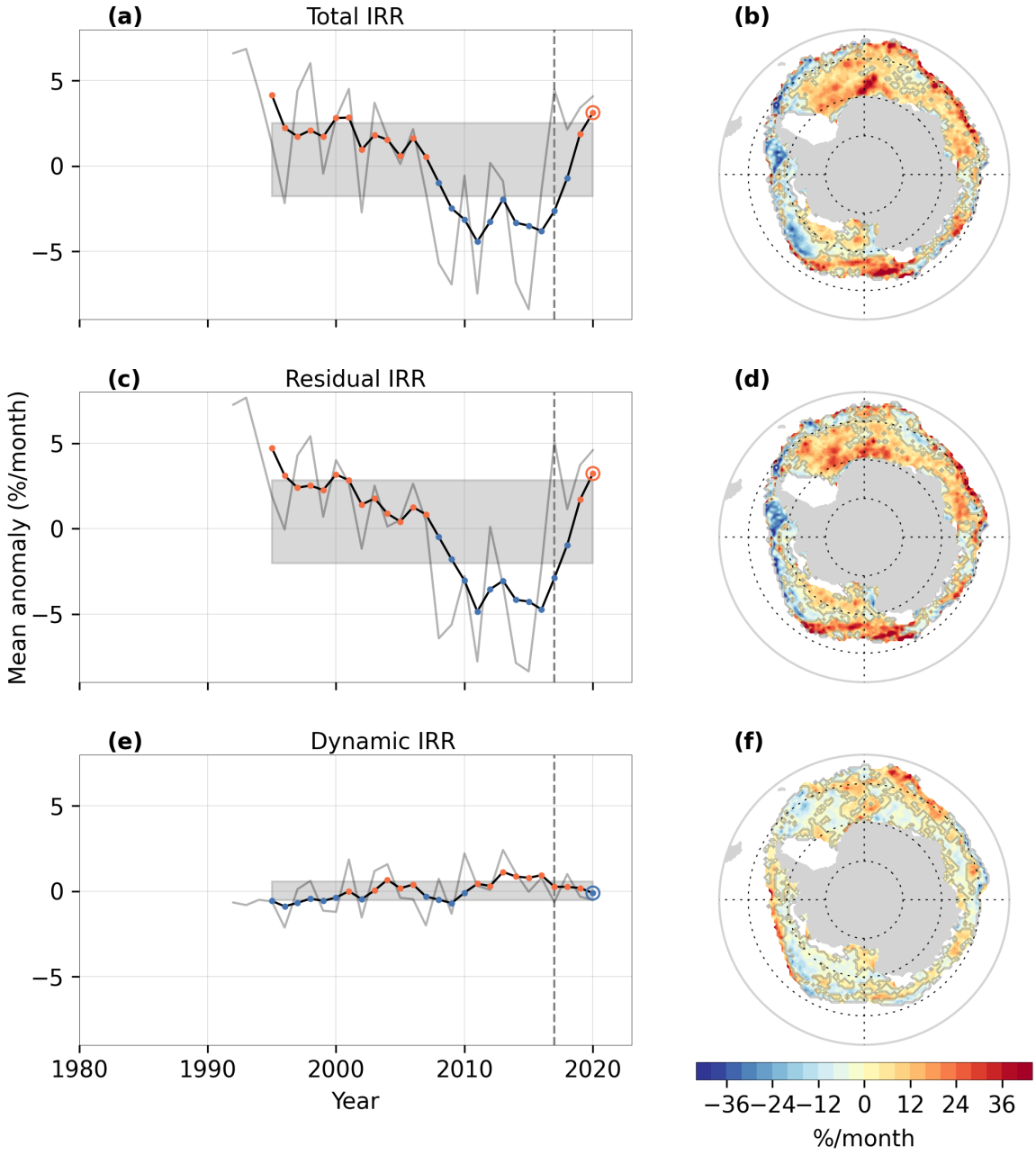

Figure III.6: **Changes in the spring sea ice removal rate (IRR) and its contributions over 1992-2020.** Grey solid lines show yearly anomalies averaged over the seasonal ice zone in **a**, total IRR, **c**, residual IRR, **e**, dynamic IRR (grey lines). Black lines in **a**, **c** and **e** show 4-year moving averages such that the last point represent the 2017-2020 mean anomalies depicted in **b**, for total IRR, **d**, for residual IRR and **f**, for dynamic IRR. Anomalies are relative to the 1992-2016 average. Red dots mark positive values whereas blue dots mark negative values. Stippled grey lines mark the 2017 yearly anomalies. The grey areas delimit the mean +/- the standard deviation of 4-year moving averages over the whole time series.

of grid points with early retreat (Supplementary Figure 3) correspond to increased residual contribution (Figure 6d). The same links are also evident at interannual time scales. Mean detrended anomalies in September sea ice thickness over the seasonal ice zone sectors explain 69% of the interannual variance in residual IRR in the following spring (Figure 7c). In turn, mean detrended anomalies in residual IRR explain 84% of the variance in the following retreat

dates (Figure 7d). Spatial and interannual linkages between thinner sea ice, increased residual IRR due to sea ice melt and earlier retreat (see Figure 5) are therefore compatible with a thermodynamic response to sea ice thinning (Holland et al., 2006). Idealized simulations of the sea ice melt period shown in Appendix A feature similar links and highlight that the ice-albedo feedback processes contribute to such response.

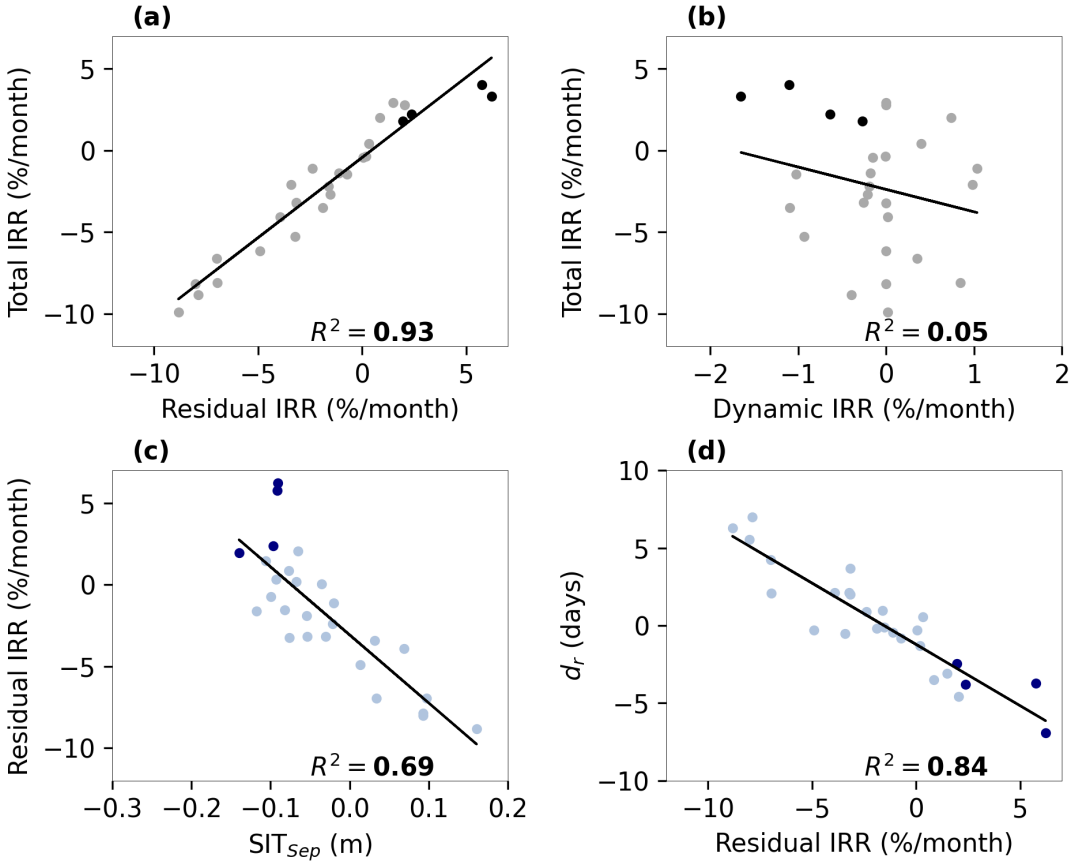

Figure III.7: **Interannual relationships between the spring sea ice removal rate (IRR) and relevant sea ice diagnostics, over 1992-2020.** Detrended anomalies of **a**, total ice removal rate (IRR) versus residual IRR, **b**, total IRR versus dynamic IRR, **c**, residual IRR versus September sea ice thickness (SIT_{Sep}) **b**, retreat dates (d_r) versus residual IRR. The 2017-2020 anomalies are marked in dark colors. A Least Square linear regression was performed for each plot; the corresponding regression line (significant at 99%), and corresponding determination coefficient (R^2) are shown. The 1992-2020 period was selected to ensure consistency of the analysis, as all relevant diagnostics are available over this timeframe.

6 Discussion and conclusion

The sea ice season duration has undergone an unprecedented shortening since 2016 due to earlier ice retreat and later advance. These anomalies in the timing of sea ice retreat and advance are strongly linked to anomalies in winter sea ice thickness, summer sea surface temperature

and spring ice removal rate related to sea ice melt (Figure 5). The correspondence between thickness and other markers of sea ice and sea surface changes is particularly remarkable considering the large uncertainties associated with satellite observations of sea ice thickness (Kurtz & Markus, 2012). Our findings indicate that the ice season shortening following 2016 is consistent with an ice thinning and the seasonal progression of thermodynamic processes inherent to the ice-albedo feedback (in the sense of Holland et al. (2006)), in response to an initial ice thinning. According to our analysis, sea ice transport plays a comparatively minor role, consistent with previous studies highlighting that sea ice changes are primarily driven by thermodynamics (Guo et al., 2023; Kimura et al., 2023).

However, some local exceptions are also visible, where ice-albedo feedback processes do not explain the changes in sea ice seasonality following 2016. First, in the northwest Weddell Sea off the eastern Antarctic Peninsula, we find that the mostly earlier retreat (Figure 2b) spatially corresponds to thicker sea ice (Figure 2d) and decreased ice removal rate (Figure 6b). In this region, winter sea ice is thicker but less concentrated, possibly due to increased sea ice divergence (see Supplementary Figure 5). We therefore hypothesize that during spring, the thicker ice might get removed more slowly, and still retreat earlier due to the lower concentration at the start of the melt season. Another possible cause is that there would be a regional high bias in the satellite ice thickness retrieval. Indeed, model and altimetry-based thickness retrievals are particularly inconsistent in that region (Liao et al., 2022). Additionally, in situ sources (Worby et al., 2008), albeit sparse, do not feature a thickness maximum there.

Second, in the Amundsen Sea and in portions of the eastern Ross Sea and along the East Antarctic coastal regions, a lengthening of the sea ice season is observed (Figures 1b, c). In the Amundsen and eastern Ross Seas, this lengthening mainly corresponds to a later retreat, possibly driven by southerly wind anomalies pushing sea ice (Schroeter et al., 2023) or by increased thickness (Figure 2d), but not necessarily to an earlier advance. There, changes are more likely to be driven by sea ice advection than by thermodynamic processes, as suggested by Kimura et al. (2023), which might explain this spatial mismatch. Off East Antarctica, landfast ice and polynya dynamics may contribute to the sea ice season lengthening. Therefore, for some specific regions, sea ice transport might dominate over ice-albedo feedback processes in driving the changes in sea ice seasonality following 2016.

We next discuss potential atmospheric and oceanic changes contributing to the reduction in sea ice thickness. Enhanced southward winds as evidenced by previous studies (e.g. Nihashi & Ohshima, 2015)could increase ice divergence, thereby favoring the presence of thin newly formed ice. However, in regions of thinner sea ice (Figure 2c), the apparent increase in winter import of ice area suggests otherwise (see Supplementary 5). It is therefore more

likely that the reduced ice thickness results from less growth, which can be due to changes in heat exchanges with the atmosphere and the ocean. Intensified northerly winds may increase warm air intrusions over the Southern Ocean (Schlosser et al., 2018), potentially altering the conductive flux through sea ice and reducing growth. However, increased intrusions of warm air would involve the action of several modes of atmospheric variability (e.g. Clem & Fogt, 2015)), which would result in regional reductions in ice thickness rather than in the observed almost circumpolar thinning. By contrast, a near-circumpolar warming of the subsurface ocean, as documented by several studies (Meehl et al., 2019; Purich & Doddridge, 2023; Zhang et al., 2022), could produce the observed reduction in ice thickness.

Warmer subsurface waters could potentially be entrained into the surface layer during winter, when the mixed layer reaches sufficient depth, limiting sea ice growth (Gordon, 1981; Martinson & Iannuzzi, 1998; Saenz et al., 2023; Wilson et al., 2019). Hence, a warmer subsurface ocean serves as a plausible driver of the observed reduction in sea ice thickness, more so than atmospheric changes. Nonetheless, ice-atmosphere feedbacks might amplify the effect of an ocean heat input. Thinner winter sea ice has a lower insulating power, enabling the warm underlying ocean to increase the surface air temperature, in turn leading to further sea ice thinning (Burt et al., 2016).

The cause for the subsurface warming, likely initiated around 2011 (Meehl et al., 2019; Purich & Doddridge, 2023), reaching the surface only after 2016 remains unclear. Models suggest that the persistently warm subsurface may have destabilized the mixed layer, inducing the entrainment of these warm waters into the surface (Zhang et al., 2022). However, observational evidence of this destabilization is still lacking. Ultimately, mapping hydrographic changes in the seasonal ice zone, which is beyond the scope of this work, would be required to evaluate the spatial extent of this subsurface warming and better constrain the role of the ocean in driving the recent changes in Antarctic sea ice.

Appendix A: Are the links between observations during the melt period consistent with theory?

What do the links between observed maximum thickness, removal rate and retreat date tell us about the underlying processes? Are they consistent with what we know of the Antarctic sea ice melting process?

To address this, we performed idealized model simulations of the spring sea ice decay and diagnose the same relationships as from observations. Our model encapsulates physics of sea ice melting in the Antarctic, in particular the effect of the ice-albedo feedback (IAF) on basal melting. The IAF is here viewed in the sense of Holland et al. (2006) and describes how solar radiation uptake amplifies a small change in ice concentration by promoting basal melt of thin ice, further reducing ice coverage.

Model description

We consider a given ice-covered region of the ocean (e.g., a satellite pixel), characterized by ice concentration A(t) and mean thickness h(t), and a surface ocean layer of constant thickness h_w = 20 m (Figure 8). External heat inputs to the surface ocean-sea ice system are net solar radiation uptake and sensible ocean heat flux. The surface ocean layer temperature is fixed at the freezing point, so that any heat absorbed in the surface layer is converted into basal melt.

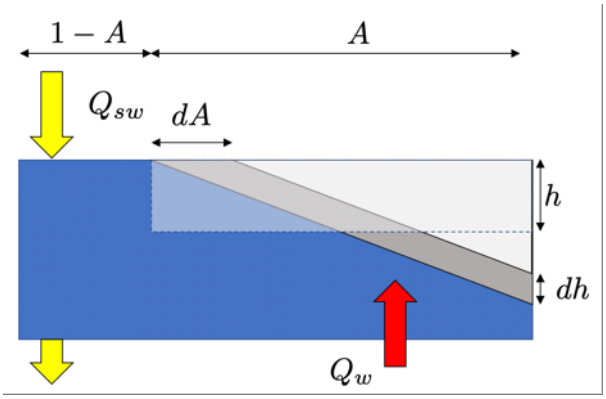

Figure III.8: Schematic view of the melting process as viewed in the model.

Net solar radiation uptake in the ocean surface layer (W/m^2) results from the balance of incident, absorbed and transmitted solar radiation, assuming absorption of most solar radiation in a thin surface layer and exponential attenuation with depth (Lengaigne et al., 2007):

$$Q_{sw} = Q_{sw}^{\downarrow}(1-\alpha_w)\cdot[1-(1-R)\cdot\exp(-\kappa h_w)]. \quad \text{(III.4)}$$

$Q_{sw}^{\downarrow}$ is the incident solar radiation (W/m^2), α_w = 0.06 is the ocean albedo, R = 0.58 is the fraction of solar radiation absorbed in a small (≈10 cm) surface layer and κ = 1/23 m$^-$1 is the bulk solar attenuation coefficient.

Ice thickness h decreases due to a prescribed sensible heat flux Q_w and net solar radiation uptake in the surface layer:

$$-\rho L \cdot \frac{dh}{dt} = Q_w + p_1 . Q_{sw} \cdot \left(\frac{1-A}{A} \right), \tag{III.5}$$

where ρ = 917 kg/m^3 is the ice density and L=335000 J/kg is the latent heat of fusion. The $(1-A)/A$ factor reflects heat conservation: solar radiation penetrates through the open water fraction $(1-A)$ and is attributed over the ice-covered fraction A of the grid cell.

The ice concentration loss rate depends on the subgrid scale ice thickness distribution, and is in particular controlled by the melt rate of thin ice (Holland et al., 2006). Here we assume that the ice thickness is homogeneously distributed between zero and twice the mean. In this context, a decrease in mean thickness implies a loss of thin ice, and the ice concentration decreases as follows:

$$\frac{dA}{dt} = p_2 \cdot \frac{A}{2h} \cdot \frac{dh}{dt}. \tag{III.6}$$

We also introduce two parameters p_1 and p_2 ($[0,1]$) that tune solar radiation uptake and the loss of concentration per unit ice thickness.

This approach was introduced in large-scale sea ice models by Fichefet and Maqueda (1997) and Häkkinen and Mellor (1990) and is known to provide a sensible first-order emulation of the ice thickness distribution.

Simulation protocol

We run three ensembles of 150-day sea ice melting simulations, starting with maximum thickness h_{max} and initial ice concentration A_{max} = 0.99. The sensible heat flux Q_w is assumed constant, with a representative value of 30 W/m^2. Solar radiation linearly increases from 50 to 250 W/m^2 from day 1 to day 150, which is representative of the Antarctic sea ice zone from September to December (Vancoppenolle et al., 2011).

We run ensembles of simulations with varying h_{max} from 0.5 to 2.5 m. Three ensembles are run. In the control ensemble, both shortwave enhancement and ice concentration loss are active ($p_1 = p_2 = 1$). They are switched off separately in the two other ensembles.

The simulations feature a rapid ice concentration and thickness loss, and achieve complete ice decay within a few weeks. From each simulation, we diagnose the average removal rate as the mean of $\frac{dA}{dt}$ over the whole simulation period, and the retreat date as the last day of simulation with $A > 15\%$.

A few insights from simulations

Figure 9 shows the simulations outputs. We find that, first, simulated relationship between d_r and h_{max} is linear, whereas the relationship between IRR and the two other variables is non-linear. The relationships are not largely responding to sensible oceanic heat flux.

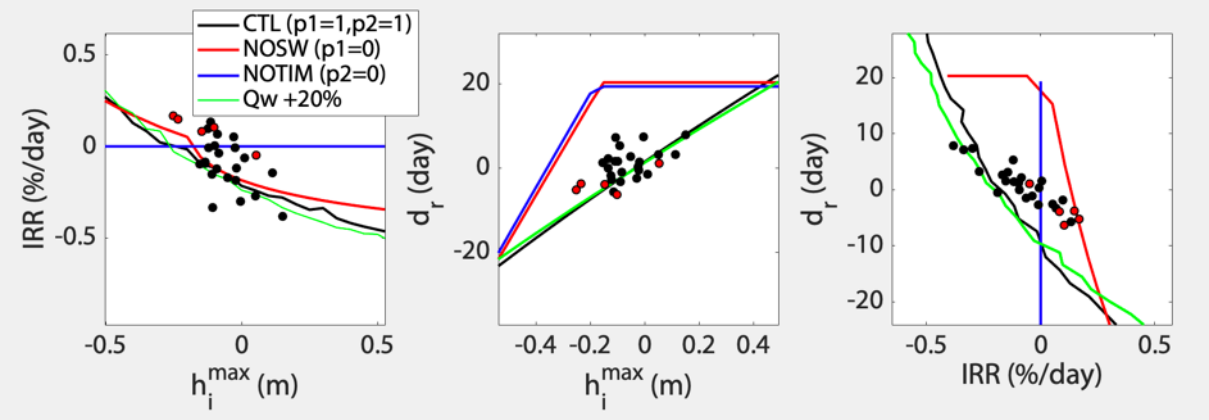

Figure III.9: Model (lines) versus observed (symbols) relationships between h_{max}; IRR and d_r. The CTL model ensemble (black) has all processes included as described above. The red ensemble assumes SW absorption is fixed at initial value ($p_1 = 0$, corresponding to $A = 0.99$). The blue ensemble assumes concentration does not decrease upon thickness decrease ($p_2 = 0$). The green ensemble has 20% larger ocean sensible heat flux. The last five years of observations are highlighted in red.

Second, relationships between observed anomalies (same data as in Figure 4 and 7) and the control ensemble (black) are compatible. Indeed, we get roughly linear relationships over the observed range of variations and slopes are compatible with observations. However, observations differ from the model in two ways. There is spread in the observations, which reflects the presence of non-ideal, non-thermodynamic drivers. Additionally, the retreat date is less sensitive to removal rate in observations than in model.

Third, the IAF is key to establish the relationships between h_{max}, IRR and d_r, sensitivity ensembles show. Indeed, with no loss of concentration upon basal melt (blue), the removal rate does not vary. Also, with prescribed solar absorption efficiency (red), the IRR vs h_{max} relationship is preserved and the latter is set by concentration loss rate (see equation 5). Retreat occurs later, but the rate of change in retreat date per unit of thickness or IRR is large.

Conclusions

The observed behavior with linearly co-evolving h_{max}, IRR and d_r are compatible with a thermodynamic response to sea ice thinning. The ice albedo feedback seems a key driver of the observed changes. In particular, observed changes in IRR are characteristic of the ice-albedo-feedback as conceptualized by Holland et al. (2006), connecting solar radiation absorption through open water, basal melt of thin ice and concentration loss.

Supplementary Figures

Figure S1 shows the mean state of this ice removal rate and its contributions. Figure S2 compares the trends in ice season duration over 1980-2016 and 1980-2022. Figure S3 investigates the sensitivity of mean anomalies in retreat and advance dates according to various relevant averaging time periods. Figure S4 shows the rate of changes in ice removal rate and its contributions. Figure S5 shows the changes in spring and winter ice thickness, winter ice concentration and winter ice divergence.

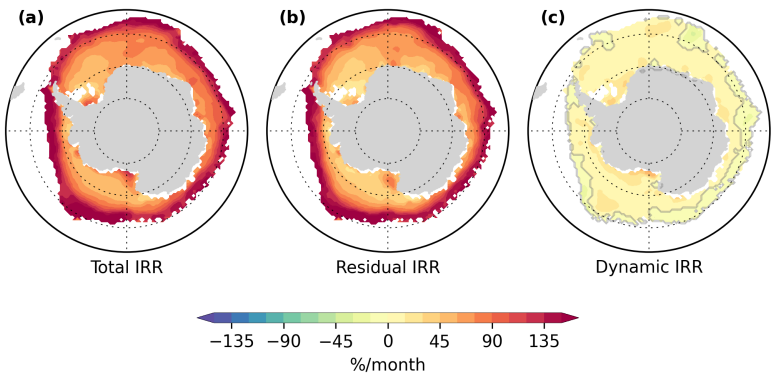

Figure III.10: Climatological spring sea ice removal rate (a; IRR) and its residual (b) and dynamic (c) contributions over 1992-2020.

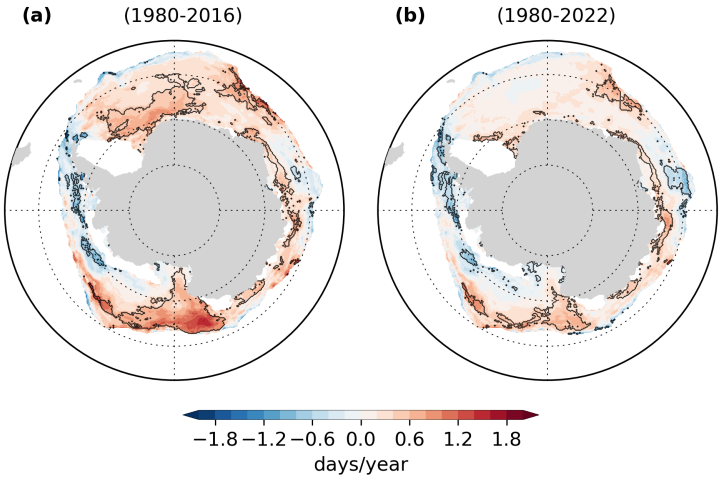

Figure III.11: Trends in the sea ice season duration over 1980-2016 (a) and 1980-2022 (b). Trends are calculated using a linear Least-Square method. The black contour delimits where trends are statistically significant to the 95% level. White patches indicate regions out of the seasonal ice zone.

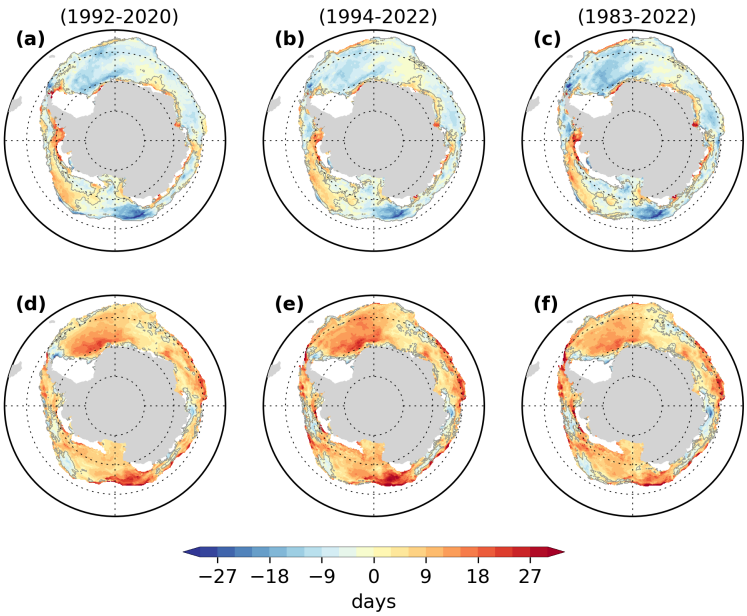

Figure III.12: Mean anomalies in retreat (a, b, c) and advance (d, e, f) dates calculated over relevant time periods. Each period is chosen according to the availability of the data used to determine diagnostics of ice thickness (1994-2022), sea surface temperature (1983-2022) and ice removal rate (1992-2020). Mean anomalies are defined as the difference between the 2017-2020 and the 1992-2016 averages in a and d; between the 2017-2022 and the 1994-2016 averages in b and e; between the 2017-2022 and the 1983-2016 averages in c and f. White patches indicate regions out of the seasonal ice zone.

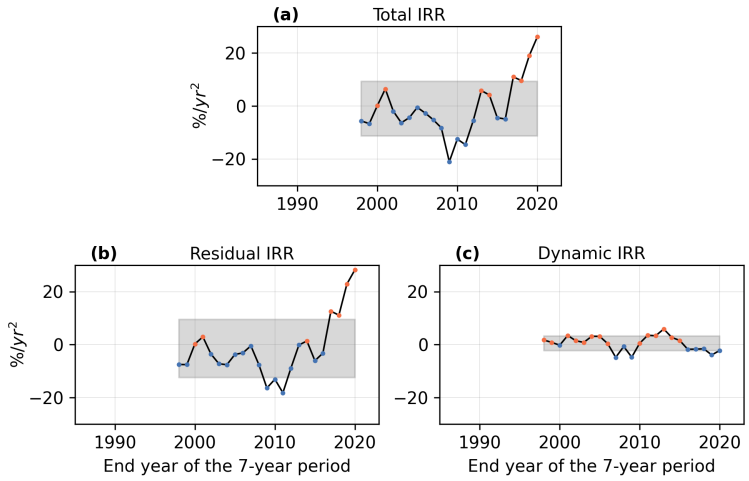

Figure III.13: Seven-year least-square slopes of mean anomalies over the seasonal ice zone in a, total ice removal rate (IRR), b, residual ice removal rate, c, dynamic ice removal rate. Slopes are obtained using a linear Least-Square regression. Blue dots mark negative values whereas red dots mark positive values. The grey areas delimit the mean +/- the standard deviation over the whole time series.

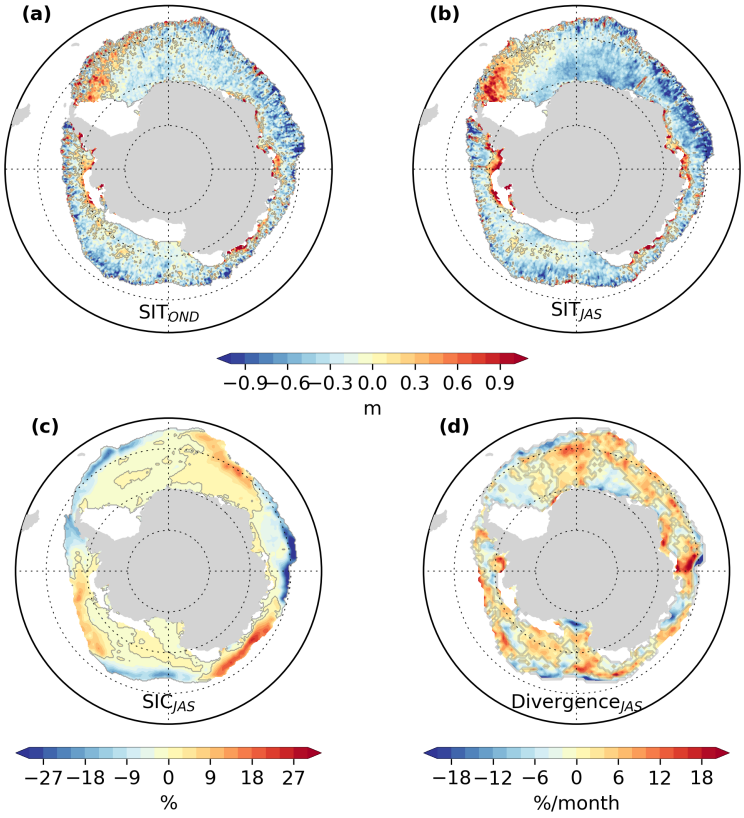

Figure III.14: Mean anomalies over 2017-2022 of a, spring sea ice thickness averaged over October, November and December (SIT_{OND}), b, winter sea ice thickness (SIT_{JAS}) and c, winter sea ice concentration (SIC_{JAS}), averaged over July, August and September. Due to ice drift data availability, mean anomalies in the contribution of divergence to the sea ice concentration budget over July, August and September in d, are averaged over 2017-2020. Anomalies are referenced 1994-2016 for sea ice concentration and thickness, and over 1992-2016 for divergence for the same reason.

Concluding Remarks

1 Conclusion

Antarctic sea ice is of major climatic importance, yet large uncertainties persist regarding its past and future responses to rising atmospheric CO2 levels. One key to reducing these uncertainties lies in improving our understanding of Antarctic sea ice processes. To this aim, the present thesis explores fundamental processes shaping the Antarctic sea ice seasonal cycle, with a particular focus on two key seasonal transitions: sea ice retreat and advance.

Three questions motivated this thesis. Here, I revisit these questions, summarize how this thesis contributes to answering them, and present the research perspectives they have raised.

What drives the timing of Antarctic sea ice advance and retreat in the mean state?

In chapters I and II, we progressed understanding of the role of the state of the ice-ocean system (ice thickness and ocean heat content), air-ice-sea heat fluxes and sea ice transport in setting the dates of sea ice advance and retreat, in the mean state. Using a simplified thermodynamic model, along with observational (Chapter I) and model analyses (Chapter II), we were able to generalize at the local scale findings previously obtained at the scale of the ice pack (e.g. Eayrs et al., 2019; Goosse et al., 2023; Roach et al., 2022). Figure 1 summarizes some our key findings.

We showed that thermodynamics exert the strongest control on sea ice advance and retreat. This control leads to linear relationships between spatial distributions of ice thickness at melt onset, retreat date, maximum mixed layer heat content and advance date, indicating that where sea ice is thinner, retreat is earlier, mixed layer heat content is larger and sea ice advance, later. These linear relationships were predicted by a simple thermodynamic ice-ocean model, and strongly hold in climatological observations and model simulations, albeit with a large scatter. We could attribute the scatter around linearity to effects of heat fluxes and sea ice

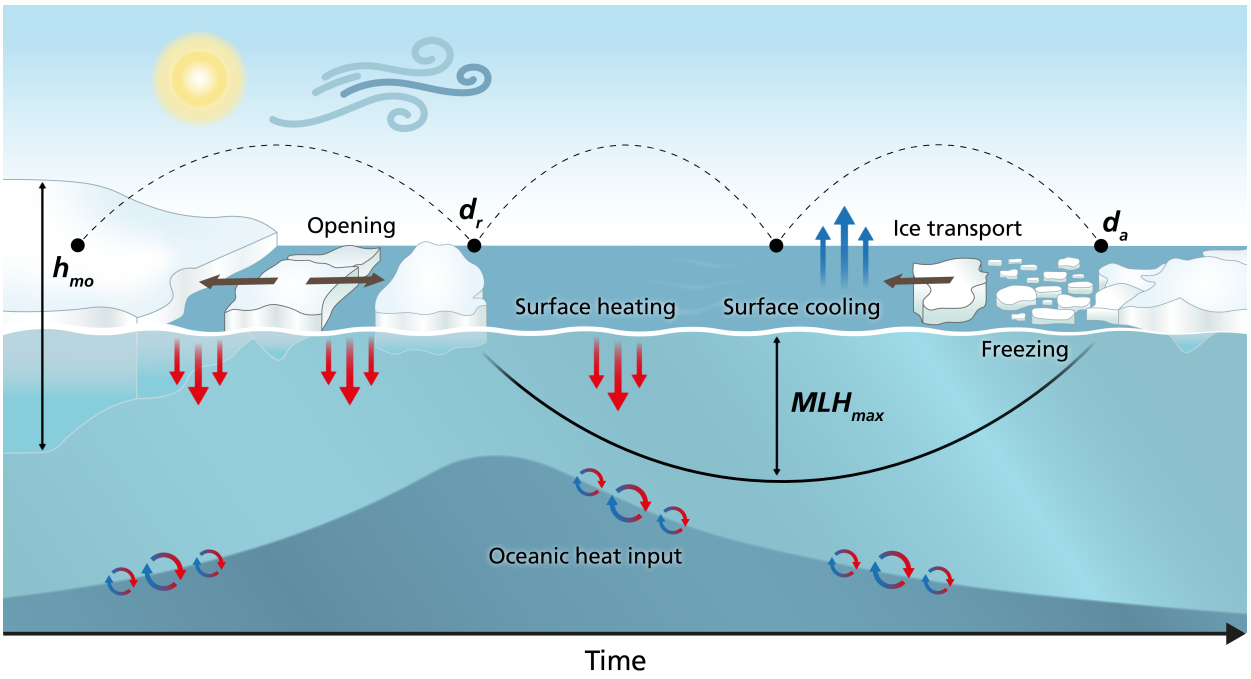

Figure III.15: **A schematic of the main drivers of Antarctic sea ice retreat and advance.** Drivers include: (i) thermodynamic constraints (dotted lines) exerted by the ice thickness at the melt onset (h_{mo}) on the date of retreat (d_r), and by the seasonal maximum of mixed layer heat content (MLH_{max}) on the date of advance (d_a); (ii) variable net heat gains (red arrows) and losses (blue arrows) by the surface, and oceanic heat inputs to the mixed layer (round arrows); (iii) sea ice transport (grey arrow) and consequent opening or ice edge advance and consequence hastening or delay effects of advance and retreat. The mixed layer is depicted in light blue while the underlying deep ocean is in darker blue. The black solid curve shows the seasonal evolution of mixed layer heat content.

dynamics.

On heat fluxes, our thermodynamic model indicated their spatial variability as the primary source of dispersion around linear relationships. Consistently, model simulations revealed that deviations from linear predictions in advance date are mainly explained by the spatial variability in the ocean heat losses during the ice-free period. Deviations from linear retreat date predictions have slightly contrasting causes. They are partly explained by spatial variability in the heat gain required to melt the ice and also by sea ice transport processes.

Sea ice dynamics hasten or delay retreat and advance depending on the direction of the ice flow at the ice edge. This control of dynamics can even overcome that of thermodynamics, but this only occurs in regions of limited size. We were able to locate these regions using an observational sea ice concentration budget. In a narrow outer band near the winter ice edge, advance results from drifting ice imported into warmer waters rather than from sea water freezing. In polynya regions near the coast, ice export prevails over thermodynamics in setting the date of retreat.

Several caveats may limit the scope of these conclusions. First, our model-based approach include issues with biases in the model mean state and inconsistencies in the simulation protocol. To strengthen our model-based conclusions, we will adjust our protocol choices and rerun some simulations in the near future. Additional caveats relate to low temporal frequency of climatological mixed layer properties (available monthly) and observational errors, particularly in sea ice thickness and the concentration budget near the ice edge. While the exact impact of these observational limitations is difficult to assess, the consistency of our main findings across models and observations suggests they do not affect our conclusions.

What insights can retreat and advance dates provide regarding the representation of seasonal Antarctic sea ice processes in ice-ocean models?

In Chapter II, we tested a process-based framework allowing to evaluate the drivers of sea ice retreat and advance in the NEMO ice-ocean model. Based on the key analyses conducted in Chapter I, this framework specifically (i) delineates the relative contributions of sea ice transport and thermodynamics to retreat and advance, and (ii) measures the strength of thermodynamic constraints on their timing.

We showed that drivers of sea ice advance and retreat are reasonably well represented by different NEMO simulations, regardless of configurations and despite errors in the mean state. Similar to observations, the model indicates a prevailing role of sea ice thermodynamics over dynamics in setting dates of retreat and advance. Furthermore, the model reproduces the linear relationships between spatial distributions of sea ice advance (retreat) date and seasonal maximum of mixed layer heat content (ice thickness at the melt onset).

Our evaluation framework also revealed substantial differences between simulations and observations, and proved insightful on their origin. Discrepancies are the largest during the melt season, likely reflecting model deficiencies regarding sea ice thermodynamics (ice is too thin) and dynamics (differing transport patterns from observations). During the open water season, issues with the simulated thermohaline structure, which controls ocean heat inputs into the mixed layer, likely contribute to model-observations differences. Ultimately, inter-model differences also probably depend on model resolution, tuning, and coupling strategy with the atmosphere, highlighting their importance for representing seasonal sea ice processes.

What are the recent changes in the timing of Antarctic sea ice retreat and advance, and their drivers?

After more than thirty years of an observed slow increase, the Antarctic sea ice extent has

experienced an abrupt decline since 2016 (Parkinson, 2019), the causes of which remain ambiguous (e.g. Meehl et al., 2019; Purich & Doddridge, 2023; Schroeter et al., 2023). In Chapter III, we showed that this shift coincides with an unprecedented and near-circumpolar shortening of the sea ice season duration, due to earlier retreat and later advance.

Drivers are essentially thermodynamic, according to our analysis. We were able to link the sea ice season shortening to thinner ice in winter, faster melting in spring and warmer upper ocean in summer. We showed that these seasonal changes are consistent with ice-albedo feedback processes, triggered by an initial ice thinning in winter. Based on their circumpolar footprint, we ultimately argued that these changes may be driven by an increase in sensible heat supply by the ocean, in line with previous evidence of ocean subsurface warming (Meehl et al., 2019; Purich & Doddridge, 2023; Zhang et al., 2022).

Generalizing our analysis of ice-albedo feedbacks to anomalies over the entire satellite data period (chapters I and III), we showed that ice-albedo feedback processes also explain, to a certain extent, interannual variability in retreat and advance dates. However, a significant portion of the interannual variance remains unexplained, raising unanswered questions on its origin. Does this remaining variance reflect an increased importance of unexplored processes (heat flux variability and sea ice transport) at the interannual timescale compared to the mean state? Does it also reflect observational limitations to our analysis? Limitations include large sea ice thickness errors (Bocquet, 2023), and approximating the mixed layer heat content with temperature due to the lack of interannual in situ measurements. We plan to conduct additional analyses in the near-future to investigate how unexplored processes and observational limitations affect our analysis of interannual variability in advance and retreat dates.

2 Perspectives

Beyond near-future perspectives to strengthen ongoing studies, I outline, here, three promising long-term research prospects that have emerged from my work.

First, we highlighted robust and strong thermodynamic constraints on Antarctic seasonal sea ice. Are they an inherent characteristic of Antarctic sea ice or do they also hold in the Arctic? Are they consistent in the past? In the future? To address these questions, one could assess the strength of the thickness-retreat and mixed layer heat content-advance relationships in the Arctic using satellite records. One could also explore them in future climate projections from Coupled Model Intercomparison Project (CMIP) scenario simulations. One could finally look into the past and use paleoclimate proxies (Crosta et al., 2022) or reconstructions (Dalaiden et al., 2023; Fogt et al., 2022). Such analyses could provide additional constraints on the past and future sea ice variability.

Second, we developed a framework allowing to simply and systematically evaluate key seasonal sea ice processes in ice-ocean models. This framework was only tested on one model but could be generalized to CMIP models for a multi-model assessment. CMIP models share a common protocol and give access to all variables required by our framework, which could facilitate such an analysis. This exercise, if successful could give good insights on the representation of Antarctic sea ice seasonality in climate models, which is supposedly not adequate (Casagrande et al., 2023; Roach et al., 2020).

Third, we retraced the seasonal timeline of sea ice and sea surface changes associated with the low sea ice extent anomalies following 2016. Our findings pointed to an increase in winter heat supply by the ocean, due to subsurface warming, as a likely cause of the observed ice thickness reduction. However, the link between oceanic heat input and ice thinning remains hypothetical. As a final perspective for this thesis, I propose diagnosing and mapping seasonal stratification changes following 2016, using in situ measurements. Cross-analyzing the resulting maps with those of key markers of seasonal sea ice changes could help better constrain the causes behind the recent Antarctic sea ice changes.

References

Abernathey, R. P., Cerovecki, I., Holland, P. R., Newsom, E., Mazloff, M., & Talley, L. D. (2016). Water-mass transformation by sea ice in the upper branch of the Southern Ocean overturning. *Nature Geoscience*, *9*(8), 596–601. doi: 10.1038/ngeo2749

Aiken, C. M., & England, M. H. (2008). Sensitivity of the Present-Day Climate to Freshwater Forcing Associated with Antarctic Sea Ice Loss. *Journal of Climate*, *21*(15), 3936–3946. doi: 10.1175/2007JCLI1901.1

Andreas, E. L., & Ackley, S. F. (1982). On the Differences in Ablation Seasons of Arctic and Antarctic Sea Ice. *Journal of the Atmospheric Sciences*, *39*(2), 440–447. doi: 10.1175/1520-0469(1982)039<0440:OTDIAS>2.0.CO;2

Ayres, H., & Screen, J. (2019). Multimodel Analysis of the Atmospheric Response to Antarctic Sea Ice Loss at Quadrupled CO2. *Geophysical Research Letters*, *46*(16), 9861–9869. doi: 10.1029/2019GL083653

Ayres, H. C., Screen, J. A., Blockley, E. W., & Bracegirdle, T. J. (2022). The Coupled Atmosphere–Ocean Response to Antarctic Sea Ice Loss. *Journal of Climate*, *35*(14), 4665–4685. doi: 10.1175/JCLI-D-21-0918.1

Beadling, R. L., Russell, J. L., Stouffer, R. J., Mazloff, M., Talley, L. D., Goodman, P. J., Sallée, J. B., Hewitt, H. T., Hyder, P., & Pandde, A. (2020). Representation of Southern Ocean Properties across Coupled Model Intercomparison Project Generations: CMIP3 to CMIP6. *Journal of Climate*, *33*(15), 6555–6581. doi: 10.1175/JCLI-D-19-0970.1

Behrendt, A., Dierking, W., Fahrbach, E., & Witte, H. (2013). Sea ice draft in the Weddell Sea, measured by upward looking sonars. *Earth System Science Data*, *5*(1), 209–226. doi: 10.5194/essd-5-209-2013

Bester, M. N., Bornemann, H., & McIntyre, T. (2017). Antarctic marine mammals and sea ice. In *Sea Ice* (pp. 534–555). John Wiley & Sons, Ltd. doi: 10.1002/9781118778371.ch22

Bintanja, R., van Oldenborgh, G. J., Drijfhout, S. S., Wouters, B., & Katsman, C. A. (2013). Important role for ocean warming and increased ice-shelf melt in Antarctic sea-ice expansion. *Nature Geoscience*, *6*(5), 376–379. doi: 10.1038/ngeo1767

Bitz, C. M., Holland, M. M., Weaver, A. J., & Eby, M. (2001). Simulating the ice-thickness distribution in a coupled climate model. *Journal of Geophysical Research: Oceans*, *106*(C2), 2441–2463. doi: 10.1029/1999JC000113

Bitz, C. M., & Lipscomb, W. H. (1999). An energy-conserving thermodynamic model of sea ice. *Journal of Geophysical Research: Oceans*, *104*(C7), 15669–15677. doi: 10.1029/1999JC900100

Blanchard-Wrigglesworth, E., Roach, L. A., Donohoe, A., & Ding, Q. (2021). Impact of Winds and Southern Ocean SSTs on Antarctic Sea Ice Trends and Variability. *Journal of Climate*, *34*(3), 949–965. doi: 10.1175/JCLI-D-20-0386.1

Bocquet, M. (2023). *Arctic and Antarctic sea ice volume changes estimation from satellite altimetry between 1994 ans 2023* (Unpublished doctoral dissertation).

Bocquet, M. (2024). Arctic and Antarctic sea ice thickness and volume changes from observations between 1994 and 2023 (submitted). *Journal of Geophysical Research: Oceans*.

Bouillon, S., Fichefet, T., Legat, V., & Madec, G. (2013). The elastic–viscous–plastic method revisited. *Ocean Modelling*, *71*, 2–12. doi: 10.1016/j.ocemod.2013.05.013

Burt, M. A., Randall, D. A., & Branson, M. D. (2016). Dark Warming. *Journal of Climate*, *29*(2), 705–719. doi: 10.1175/JCLI-D-15-0147.1

Casagrande, F., Stachelski, L., & de Souza, R. B. (2023). Assessment of Antarctic sea ice area and concentration in Coupled Model Intercomparison Project Phase 5 and Phase 6 models. *International Journal of Climatology*, *43*(3), 1314–1332. doi: 10.1002/joc.7916

Cavalieri, D. J., & Parkinson, C. L. (2012). Arctic sea ice variability and trends, 1979–2010. *The Cryosphere*, *6*(4), 881–889. doi: 10.5194/tc-6-881-2012

Clem, K. R., & Fogt, R. L. (2013). Varying roles of ENSO and SAM on the Antarctic Peninsula climate in austral spring. *Journal of Geophysical Research: Atmospheres*, *118*(20), 11,481–11,492. doi: 10.1002/jgrd.50860

Clem, K. R., & Fogt, R. L. (2015). South Pacific circulation changes and their connection to the tropics and regional Antarctic warming in austral spring, 1979–2012. *Journal of Geophysical Research: Atmospheres*, *120*(7), 2773–2792. doi: 10.1002/2014JD022940

Comiso, J. (2017). *Bootstrap Sea Ice Concentrations from Nimbus-7 SMMR and DMSP SSM/I-SSMIS Passive Microwave Data, Version 3* (Tech. Rep.).

Comiso, J. C., Gersten, R. A., Stock, L. V., Turner, J., Perez, G. J., & Cho, K. (2017). Positive Trend in the Antarctic Sea Ice Cover and Associated Changes in Surface Temperature. *Journal of Climate*, *30*(6), 2251–2267. doi: 10.1175/JCLI-D-16-0408.1

Crosta, X., Kohfeld, K. E., Bostock, H. C., Chadwick, M., Du Vivier, A., Esper, O., Etourneau, J., Jones, J., Leventer, A., Müller, J., Rhodes, R. H., Allen, C. S., Ghadi, P., Lamping, N., Lange, C. B., Lawler, K.-A., Lund, D., Marzocchi, A., Meissner, K. J., Menviel, L., Nair, A., Patterson, M., Pike, J., Prebble, J. G., Riesselman, C., Sadatzki, H., Sime, L. C., Shukla, S. K., Thöle, L.,

Vorrath, M.-E., Xiao, W., & Yang, J. (2022). Antarctic sea ice over the past 130 000 years – Part 1: A review of what proxy records tell us. *Climate of the Past*, *18*(8), 1729–1756. doi: 10.5194/cp-18-1729-2022

Dalaiden, Q., Rezsöhazy, J., Goosse, H., Thomas, E. R., Vladimirova, D. O., & Tetzner, D. (2023). An Unprecedented Sea Ice Retreat in the Weddell Sea Driving an Overall Decrease of the Antarctic Sea-Ice Extent Over the 20th Century. *Geophysical Research Letters*, *50*(21), e2023GL104666. doi: 10.1029/2023GL104666

de Lavergne, C., Vic, C., Madec, G., Roquet, F., Waterhouse, A. F., Whalen, C. B., Cuypers, Y., Bouruet-Aubertot, P., Ferron, B., & Hibiya, T. (2020). A Parameterization of Local and Remote Tidal Mixing. *Journal of Advances in Modeling Earth Systems*, *12*(5), e2020MS002065. doi: 10.1029/2020MS002065

Dong, S., Gille, S. T., & Sprintall, J. (2007). An Assessment of the Southern Ocean Mixed Layer Heat Budget. *Journal of Climate*, *20*(17), 4425–4442. doi: 10.1175/JCLI4259.1

Durack, P. J., & Wijffels, S. E. (2010). Fifty-Year Trends in Global Ocean Salinities and Their Relationship to Broad-Scale Warming. *Journal of Climate*, *23*(16), 4342–4362. doi: 10.1175/2010JCLI3377.1

Eayrs, C., Holland, D., Francis, D., Wagner, T., Kumar, R., & Li, X. (2019). Understanding the Seasonal Cycle of Antarctic Sea Ice Extent in the Context of Longer-Term Variability. *Reviews of Geophysics*, *57*(3), 1037–1064. doi: 10.1029/2018RG000631

Enomoto, H., & Ohmura, A. (1990). The influences of atmospheric half-yearly cycle on the sea ice extent in the Antarctic. *Journal of Geophysical Research: Oceans*, *95*(C6), 9497–9511. doi: 10.1029/JC095iC06p09497

Fan, T., Deser, C., & Schneider, D. P. (2014). Recent Antarctic sea ice trends in the context of Southern Ocean surface climate variations since 1950. *Geophysical Research Letters*, *41*(7), 2419–2426. doi: 10.1002/2014GL059239

Ferreira, D., Marshall, J., Bitz, C. M., Solomon, S., & Plumb, A. (2015). Antarctic Ocean and Sea Ice Response to Ozone Depletion: A Two-Time-Scale Problem. *Journal of Climate*, *28*(3), 1206–1226. doi: 10.1175/JCLI-D-14-00313.1

Fichefet, T., & Maqueda, M. A. M. (1997). Sensitivity of a global sea ice model to the treatment of ice thermodynamics and dynamics. *Journal of Geophysical Research: Oceans*, *102*(C6), 12609–12646. doi: 10.1029/97JC00480

Fogt, R. L., Sleinkofer, A. M., Raphael, M. N., & Handcock, M. S. (2022). A regime shift in seasonal total Antarctic sea ice extent in the twentieth century. *Nature Climate Change*, *12*(1), 54–62. doi: 10.1038/s41558-021-01254-9

Fox-Kemper, B., Hewitt, H. T., Xiao, C., Aðalgeirsdóttir, G., Drijfhout, S. S., Edwards, T. L., Golledge, N. R., Hemer, M., Kopp, R. E., Krinner, G., Mix, A., Notz, D., Nowicki, S., Nurhati, I. S., Ruiz, L., Sallée, J.-B., Slangen, A. B. A., & Yu, Y. (2021). Ocean, cryosphere and sea level change. In V. Masson-Delmotte et al. (Eds.), *Climate change 2021: The physical science ba-*

sis. contribution of working group i to the sixth assessment report of the intergovernmental panel on climate change (pp. 1211–1362). Cambridge, United Kingdom and New York, NY, USA: Cambridge University Press. doi: 10.1017/9781009157896.011

Fretwell, P. T., Boutet, A., & Ratcliffe, N. (2023). Record low 2022 Antarctic sea ice led to catastrophic breeding failure of emperor penguins. *Communications Earth & Environment*, *4*(1), 1–6. doi: 10.1038/s43247-023-00927-x

Frölicher, T. L., Sarmiento, J. L., Paynter, D. J., Dunne, J. P., Krasting, J. P., & Winton, M. (2015). Dominance of the Southern Ocean in Anthropogenic Carbon and Heat Uptake in CMIP5 Models. *Journal of Climate*, *28*(2), 862–886. doi: 10.1175/JCLI-D-14-00117.1

Giles, K. A., Laxon, S. W., & Ridout, A. L. (2008). Circumpolar thinning of Arctic sea ice following the 2007 record ice extent minimum. *Geophysical Research Letters*, *35*(22). doi: 10.1029/2008GL035710

Goosse, H., Allende Contador, S., Bitz, C. M., Blanchard-Wrigglesworth, E., Eayrs, C., Fichefet, T., Himmich, K., Huot, P.-V., Klein, F., Marchi, S., Massonnet, F., Mezzina, B., Pelletier, C., Roach, L., Vancoppenolle, M., & van Lipzig, N. P. M. (2023). Modulation of the seasonal cycle of the Antarctic sea ice extent by sea ice processes and feedbacks with the ocean and the atmosphere. *The Cryosphere*, *17*(1), 407–425. doi: 10.5194/tc-17-407-2023

Goosse, H., Kay, J. E., Armour, K. C., Bodas-Salcedo, A., Chepfer, H., Docquier, D., Jonko, A., Kushner, P. J., Lecomte, O., Massonnet, F., Park, H.-S., Pithan, F., Svensson, G., & Vancoppenolle, M. (2018). Quantifying climate feedbacks in polar regions. *Nature Communications*, *9*(1), 1919. doi: 10.1038/s41467-018-04173-0

Gordon, A. L. (1981). Seasonality of Southern Ocean sea ice. *Journal of Geophysical Research: Oceans*, *86*(C5), 4193–4197. doi: 10.1029/JC086iC05p04193

Granberg, H. B., & Leppäranta, M. (1999). Observations of sea ice ridging in the Weddell Sea. *Journal of Geophysical Research: Oceans*, *104*(C11), 25735–25745. doi: 10.1029/1999JC900160

Guo, Y., Chen, X., Huang, S., & Wen, Z. (2023). Amplified Interannual Variation of the Summer Sea Ice in the Weddell Sea, Antarctic After the Late 1990s. *Geophysical Research Letters*, *50*(17), e2023GL104924. doi: 10.1029/2023GL104924

Häkkinen, S., & Mellor, G. L. (1990). One hundred years of Arctic ice cover variations as simulated by a one-dimensional, ice-ocean model. *Journal of Geophysical Research: Oceans*, *95*(C9), 15959–15969. doi: 10.1029/JC095iC09p15959

Haumann, F. A., Gruber, N., Münnich, M., Frenger, I., & Kern, S. (2016). Sea-ice transport driving Southern Ocean salinity and its recent trends. *Nature*, *537*(7618), 89–92. doi: 10.1038/nature19101

Haumann, F. A., Moorman, R., Riser, S. C., Smedsrud, L. H., Maksym, T., Wong, A. P. S., Wilson, E. A., Drucker, R., Talley, L. D., Johnson, K. S., Key, R. M., & Sarmiento, J. L. (2020). Supercooled Southern Ocean Waters. *Geophysical Research Letters*, *47*(20), e2020GL090242. doi: 10.1029/2020GL090242

Hersbach, H., Bell, B., Berrisford, P., Hirahara, S., Horányi, A., Muñoz-Sabater, J., Nicolas, J., Peubey, C., Radu, R., Schepers, D., Simmons, A., Soci, C., Abdalla, S., Abellan, X., Balsamo, G., Bechtold, P., Biavati, G., Bidlot, J., Bonavita, M., De Chiara, G., Dahlgren, P., Dee, D., Diamantakis, M., Dragani, R., Flemming, J., Forbes, R., Fuentes, M., Geer, A., Haimberger, L., Healy, S., Hogan, R. J., Hólm, E., Janisková, M., Keeley, S., Laloyaux, P., Lopez, P., Lupu, C., Radnoti, G., de Rosnay, P., Rozum, I., Vamborg, F., Villaume, S., & Thépaut, J.-N. (2020). The ERA5 global reanalysis. *Quarterly Journal of the Royal Meteorological Society*, *146*(730), 1999–2049. doi: 10.1002/qj.3803

Himmich, K., Vancoppenolle, M., Madec, G., Sallée, J.-B., Holland, P. R., & Lebrun, M. (2023). Drivers of Antarctic sea ice advance. *Nature Communications*, *14*(1), 6219. doi: 10.1038/s41467-023-41962-8

Holland, M. M., Bitz, C. M., Hunke, E. C., Lipscomb, W. H., & Schramm, J. L. (2006). Influence of the Sea Ice Thickness Distribution on Polar Climate in CCSM3. *Journal of Climate*, *19*(11), 2398–2414. doi: 10.1175/JCLI3751.1

Holland, M. M., Blanchard-Wrigglesworth, E., Kay, J., & Vavrus, S. (2013). Initial-value predictability of Antarctic sea ice in the Community Climate System Model 3. *Geophysical Research Letters*, *40*(10), 2121–2124. doi: 10.1002/grl.50410

Holland, M. M., Landrum, L., Raphael, M., & Stammerjohn, S. (2017). Springtime winds drive Ross Sea ice variability and change in the following autumn. *Nature Communications*, *8*(1), 731. doi: 10.1038/s41467-017-00820-0

Holland, P. R., & Kimura, N. (2016). Observed Concentration Budgets of Arctic and Antarctic Sea Ice. *Journal of Climate*, *29*(14), 5241–5249. doi: 10.1175/JCLI-D-16-0121.1

Holland, P. R., & Kwok, R. (2012). Wind-driven trends in Antarctic sea-ice drift. *Nature Geoscience*, *5*(12), 872–875. doi: 10.1038/ngeo1627

Hosking, J. S., Orr, A., Marshall, G. J., Turner, J., & Phillips, T. (2013). The Influence of the Amundsen–Bellingshausen Seas Low on the Climate of West Antarctica and Its Representation in Coupled Climate Model Simulations. *Journal of Climate*, *26*(17), 6633–6648. doi: 10.1175/JCLI-D-12-00813.1

Hutter, N., Bouchat, A., Dupont, F., Dukhovskoy, D., Koldunov, N., Lee, Y. J., Lemieux, J.-F., Lique, C., Losch, M., Maslowski, W., Myers, P. G., Ólason, E., Rampal, P., Rasmussen, T., Talandier, C., Tremblay, B., & Wang, Q. (2022). Sea Ice Rheology Experiment (SIREx): 2. Evaluating Linear Kinematic Features in High-Resolution Sea Ice Simulations. *Journal of Geophysical Research: Oceans*, *127*(4), e2021JC017666. doi: 10.1029/2021JC017666

Jacobs, S. S. (2004). Bottom water production and its links with the thermohaline circulation. *Antarctic Science*, *16*(4), 427–437. doi: 10.1017/S095410200400224X

Jullien, S., Menkes, C. E., Marchesiello, P., Jourdain, N. C., Lengaigne, M., Koch-Larrouy, A., Lefèvre, J., Vincent, E. M., & Faure, V. (2012). Impact of Tropical Cyclones on the Heat Budget of the South Pacific Ocean. *Journal of Physical Oceanography*, *42*(11), 1882–1906. doi: 10.1175/JPO-D-11-0133.1

Kacimi, S., & Kwok, R. (2020). The Antarctic sea ice cover from ICESat-2 and CryoSat-2: Freeboard, snow depth, and ice thickness. *The Cryosphere*, *14*(12), 4453–4474. doi: 10.5194/tc-14-4453-2020

Kern, S., & Spreen, G. (2015). Uncertainties in Antarctic sea-ice thickness retrieval from ICESat. *Annals of Glaciology*, *56*(69), 107–119. doi: 10.3189/2015AoG69A736

Kimmritz, M., Danilov, S., & Losch, M. (2016). The adaptive EVP method for solving the sea ice momentum equation. *Ocean Modelling*, *101*, 59–67. doi: 10.1016/j.ocemod.2016.03.004

Kimura, N., Onomura, T., & Kikuchi, T. (2023). Processes governing seasonal and interannual change of the Antarctic sea-ice area. *Journal of Oceanography*, *79*(2), 109–121. doi: 10.1007/s10872-022-00669-y

Kostov, Y., Marshall, J., Hausmann, U., Armour, K. C., Ferreira, D., & Holland, M. M. (2017). Fast and slow responses of Southern Ocean sea surface temperature to SAM in coupled climate models. *Climate Dynamics*, *48*(5), 1595–1609. doi: 10.1007/s00382-016-3162-z

Kurtz, N. T., Farrell, S. L., Studinger, M., Galin, N., Harbeck, J. P., Lindsay, R., Onana, V. D., Panzer, B., & Sonntag, J. G. (2013). Sea ice thickness, freeboard, and snow depth products from Operation IceBridge airborne data. *The Cryosphere*, *7*(4), 1035–1056. doi: 10.5194/tc-7-1035-2013

Kurtz, N. T., & Markus, T. (2012). Satellite observations of Antarctic sea ice thickness and volume. *Journal of Geophysical Research: Oceans*, *117*(C8). doi: 10.1029/2012JC008141

Kusahara, K., Williams, G. D., Massom, R., Reid, P., & Hasumi, H. (2019). Spatiotemporal dependence of Antarctic sea ice variability to dynamic and thermodynamic forcing: A coupled ocean–sea ice model study. *Climate Dynamics*, *52*(7), 3791–3807. doi: 10.1007/s00382-018-4348-3

Large, G., & Yeager, S. (2004). Diurnal to decadal global forcing for ocean and sea-ice models: The data sets and flux climatologies.
doi: 10.5065/D6KK98Q6

Large, W. G., & Yeager, S. G. (2009). The global climatology of an interannually varying air–sea flux data set. *Climate Dynamics*, *33*(2), 341–364. doi: 10.1007/s00382-008-0441-3

Lavergne, T., & Down, E. (2023). A Climate Data Record of Year-Round Global Sea Ice Drift from the EUMETSAT OSI SAF. *Earth System Science Data Discussions*, 1–38. doi: 10.5194/essd-2023-40

Lavergne, T., Sørensen, A. M., Kern, S., Tonboe, R., Notz, D., Aaboe, S., Bell, L., Dybkjær, G., Eastwood, S., Gabarro, C., Heygster, G., Killie, M. A., Brandt Kreiner, M., Lavelle, J., Saldo, R., Sandven, S., & Pedersen, L. T. (2019). Version 2 of the EUMETSAT OSI SAF and ESA CCI sea-ice concentration climate data records. *The Cryosphere*, *13*(1), 49–78. doi: 10.5194/tc-13-49-2019

Laxon, S., Peacock, N., & Smith, D. (2003). High interannual variability of sea ice thickness in the Arctic region. *Nature*, *425*(6961), 947–950. doi: 10.1038/nature02050

Lebrun, M., Vancoppenolle, M., Madec, G., & Massonnet, F. (2019). Arctic sea-ice-free season projected to extend into autumn. *The Cryosphere*, *13*(1), 79–96. doi: 10.5194/tc-13-79-2019

Lengaigne, M., Menkes, C., Aumont, O., Gorgues, T., Bopp, L., André, J.-M., & Madec, G. (2007). Influence of the oceanic biology on the tropical Pacific climate in a coupled general circulation model. *Climate Dynamics*, *28*(5), 503–516. doi: 10.1007/s00382-006-0200-2

Liao, S., Luo, H., Wang, J., Shi, Q., Zhang, J., & Yang, Q. (2022). An evaluation of Antarctic sea-ice thickness from the Global Ice-Ocean Modeling and Assimilation System based on in situ and satellite observations. *The Cryosphere*, *16*(5), 1807–1819. doi: 10.5194/tc-16-1807-2022

Libera, S., Hobbs, W., Klocker, A., Meyer, A., & Matear, R. (2022). Ocean-Sea Ice Processes and Their Role in Multi-Month Predictability of Antarctic Sea Ice. *Geophysical Research Letters*, *49*(8), e2021GL097047. doi: 10.1029/2021GL097047

Lipscomb, W. H. (2001). Remapping the thickness distribution in sea ice models. *Journal of Geophysical Research: Oceans*, *106*(C7), 13989–14000. doi: 10.1029/2000JC000518

Liu, J., & Curry, J. A. (2010). Accelerated warming of the Southern Ocean and its impacts on the hydrological cycle and sea ice. *Proceedings of the National Academy of Sciences*, *107*(34), 14987–14992. doi: 10.1073/pnas.1003336107

Lizotte, M. P. (2001). The Contributions of Sea Ice Algae to Antarctic Marine Primary Production1. *American Zoologist*, *41*(1), 57–73. doi: 10.1093/icb/41.1.57

Macalady, A., & Thomas, K. (Eds.). (2017). *Antarctic Sea Ice Variability in the Southern Ocean-Climate System: Proceedings of a Workshop*. Washington, D.C.: National Academies Press. doi: 10.17226/24696

Madec, G., Bell, M., Blaker, A., Bricaud, C., Bruciaferri, D., Castrillo, M., Calvert, D., Chanut, J., Clementi, E., Coward, A., Epicoco, I., Éthé, C., Ganderton, J., Harle, J., Hutchinson, K., Iovino, D., Lea, D., Lovato, T., Martin, M., Martin, N., Mele, F., Martins, D., Masson, S., Mathiot, P., Mele, F., Mocavero, S., Müller, S., Nurser, A. J. G., Paronuzzi, S., Peltier, M., Person, R., Rousset, C., Rynders, S., Samson, G., Téchené, S., Vancoppenolle, M., & Wilson, C. (2023). NEMO Ocean Engine Reference Manual. doi: 10.5281/zenodo.8167700

Madec, G., Bourdallé-Badie, R., Bouttier, P.-A., Bricaud, C., Bruciaferri, D., Calvert, D., Chanut, J., Clementi, E., Coward, A., Delrosso, D., Ethé, C., Flavoni, S., Graham, T., Harle, J., Iovino, D., Lea, D., Lévy, C., Lovato, T., Martin, N., Masson, S., Mocavero, S., Paul, J., Rousset, C., Storkey, D., Storto, A., & Vancoppenolle, M. (2017). *NEMO ocean engine* (Report). doi: 10.5281/zenodo.3248739

Maksym, T., & Markus, T. (2008). Antarctic Sea Ice Thickness and Snow-to-Ice Conversion from Atmospheric Reanalysis and Passive Microwave Snow Depth. *Journal of Geophysical Research*, *113*. doi: 10.1029/2006JC004085

Mallett, R. D. C., Lawrence, I. R., Stroeve, J. C., Landy, J. C., & Tsamados, M. (2020). Brief communication: Conventional assumptions involving the speed of radar waves in snow introduce systematic underestimates to sea ice thickness and seasonal growth rate estimates. *The Cryosphere*, *14*(1), 251–260. doi: 10.5194/tc-14-251-2020

Markus, T., & Cavalieri, D. (2000). An enhancement of the NASA Team sea ice algorithm. *IEEE Transactions on Geoscience and Remote Sensing*, *38*(3), 1387–1398. doi: 10.1109/36.843033

Marshall, J., & Speer, K. (2012). Closure of the meridional overturning circulation through Southern Ocean upwelling. *Nature Geoscience*, *5*(3), 171–180. doi: 10.1038/ngeo1391

Martinson, D. G., & Iannuzzi, R. A. (1998). Antarctic Ocean-Ice Interaction: Implications from Ocean Bulk Property Distributions in the Weddell Gyre. In *Antarctic Sea Ice: Physical Processes, Interactions and Variability* (pp. 243–271). American Geophysical Union (AGU). doi: 10.1029/AR074p0243

Massom, R. A., Giles, A. B., Fricker, H. A., Warner, R. C., Legrésy, B., Hyland, G., Young, N., & Fraser, A. D. (2010). Examining the interaction between multi-year landfast sea ice and the Mertz Glacier Tongue, East Antarctica: Another factor in ice sheet stability? *Journal of Geophysical Research: Oceans*, *115*(C12). doi: 10.1029/2009JC006083

Massom, R. A., Scambos, T. A., Bennetts, L. G., Reid, P., Squire, V. A., & Stammerjohn, S. E. (2018). Antarctic ice shelf disintegration triggered by sea ice loss and ocean swell. *Nature*, *558*(7710), 383–389. doi: 10.1038/s41586-018-0212-1

Massom, R. A., Stammerjohn, S. E., Lefebvre, W., Harangozo, S. A., Adams, N., Scambos, T. A., Pook, M. J., & Fowler, C. (2008). West Antarctic Peninsula sea ice in 2005: Extreme ice compaction and ice edge retreat due to strong anomaly with respect to climate. *Journal of Geophysical Research: Oceans*, *113*(C2). doi: 10.1029/2007JC004239

Massonnet, F., Vancoppenolle, M., Goosse, H., Docquier, D., Fichefet, T., & Blanchard-Wrigglesworth, E. (2018). Arctic sea-ice change tied to its mean state through thermodynamic processes. *Nature Climate Change*, *8*(7), 599–603. doi: 10.1038/s41558-018-0204-z

Mathiot, P., Jenkins, A., Harris, C., & Madec, G. (2017). Explicit representation and parametrised impacts of under ice shelf seas in the z^* coordinate ocean model NEMO 3.6. *Geoscientific Model Development*, *10*(7), 2849–2874. doi: 10.5194/gmd-10-2849-2017

Maykut, G. A., & McPhee, M. G. (1995). Solar heating of the Arctic mixed layer. *Journal of Geophysical Research: Oceans*, *100*(C12), 24691–24703. doi: 10.1029/95JC02554

Maykut, G. A., & Perovich, D. K. (1987). The role of shortwave radiation in the summer decay of a sea ice cover. *Journal of Geophysical Research: Oceans*, *92*(C7), 7032–7044. doi: 10.1029/JC092iC07p07032

McPhee, M. G. (1992). Turbulent heat flux in the upper ocean under sea ice. *Journal of Geophysical Research: Oceans*, *97*(C4), 5365–5379. doi: 10.1029/92JC00239

Meehl, G. A., Arblaster, J. M., Bitz, C. M., Chung, C. T. Y., & Teng, H. (2016). Antarctic sea-ice expansion between 2000 and 2014 driven by tropical Pacific decadal climate variability. *Nature Geoscience*, *9*(8), 590–595. doi: 10.1038/ngeo2751

Meehl, G. A., Arblaster, J. M., Chung, C. T. Y., Holland, M. M., DuVivier, A., Thompson, L., Yang, D., & Bitz, C. M. (2019). Sustained ocean changes contributed to sudden Antarctic sea ice retreat in late 2016. *Nature Communications*, *10*(1), 14. doi: 10.1038/s41467-018-07865-9

Merchant, C. J., Embury, O., Bulgin, C. E., Block, T., Corlett, G. K., Fiedler, E., Good, S. A., Mittaz, J., Rayner, N. A., Berry, D., Eastwood, S., Taylor, M., Tsushima, Y., Waterfall, A., Wilson, R., & Donlon, C. (2019). Satellite-based time-series of sea-surface temperature since 1981 for climate applications. *Scientific Data*, *6*(1), 223. doi: 10.1038/s41597-019-0236-x

Nakata, K., & Ohshima, K. I. (2022). Mapping of Active Frazil and Sea Ice Production in the Northern Hemisphere, With Comparison to the Southern Hemisphere. *Journal of Geophysical Research: Oceans*, *127*(12), e2022JC018553. doi: 10.1029/2022JC018553

Nihashi, S., & Cavalieri, D. J. (2006). Observational evidence of a hemispheric-wide ice–ocean albedo feedback effect on Antarctic sea-ice decay. *Journal of Geophysical Research: Oceans*, *111*(C12). doi: 10.1029/2005JC003447

Nihashi, S., & Ohshima, K. I. (2015). Circumpolar Mapping of Antarctic Coastal Polynyas and Landfast Sea Ice: Relationship and Variability. *Journal of Climate*, *28*(9), 3650–3670. doi: 10.1175/JCLI-D-14-00369.1

Ocean and Sea Ice Satellite Application Facility. (2023). *OSI SAF Sea ice index 1978-onwards, version 2.2*. OSI SAF. doi: 10.15770/EUM_SAF_OSI_0022

Ohshima, K. I., Yoshida, K., Shimoda, H., Wakatsuchi, M., Endoh, T., & Fakuchi, M. (1998). Relationship between the upper ocean and sea ice during the Antarctic melting season. *Journal of Geophysical Research: Oceans*, *103*(C4), 7601–7615. doi: 10.1029/97JC02806

Oleson, K., Lawrence, M., Bonan, B., Drewniak, B., Huang, M., Koven, D., Levis, S., Li, F., Riley, J., Subin, M., Swenson, S., Thornton, E., Bozbiyik, A., Fisher, R., Heald, L., Kluzek, E., Lamarque, J.-F., Lawrence, J., Leung, R., Lipscomb, W., Muszala, P., Ricciuto, M., Sacks, J., Sun, Y., Tang, J., & Yang, Z.-L. (2013). Technical description of version 4.5 of the Community Land Model (CLM).
doi: 10.5065/D6RR1W7M

Parkinson, C. L. (1994). Spatial patterns in the length of the sea ice season in the Southern Ocean, 1979–1986. *Journal of Geophysical Research: Oceans*, *99*(C8), 16327–16339. doi: 10.1029/94JC01146

Parkinson, C. L. (2014). Spatially mapped reductions in the length of the Arctic sea ice season. *Geophysical Research Letters*, *41*(12), 4316–4322. doi: 10.1002/2014GL060434

Parkinson, C. L. (2019). A 40-y record reveals gradual Antarctic sea ice increases followed by decreases at rates far exceeding the rates seen in the Arctic. *Proceedings of the National Academy of Sciences*, *116*(29), 14414–14423. doi: 10.1073/pnas.1906556116

Parkinson, C. L., & Cavalieri, D. J. (2012). Antarctic sea ice variability and trends, 1979–2010. *The Cryosphere*, *6*(4), 871–880. doi: 10.5194/tc-6-871-2012

Paul, Sallila, H, Hendricks, S., & Rinne, E. (2021). *ESA CCI+ Climate Change Initiative Phase 1, D2.1 Sea Ice Thickness Algorithm Theoretical Basis Document (ATBD), v.3.1* (Tech. Rep.).

Pauling, A. G., Bitz, C. M., Smith, I. J., & Langhorne, P. J. (2016). The Response of the Southern Ocean and Antarctic Sea Ice to Freshwater from Ice Shelves in an Earth System Model. *Journal of Climate*, *29*(5), 1655–1672. doi: 10.1175/JCLI-D-15-0501.1

Pellichero, V., Sallée, J.-B., Chapman, C. C., & Downes, S. M. (2018). The southern ocean meridional overturning in the sea-ice sector is driven by freshwater fluxes. *Nature Communications*, *9*(1), 1789. doi: 10.1038/s41467-018-04101-2

Pellichero, V., Sallée, J.-B., Schmidtko, S., Roquet, F., & Charrassin, J.-B. (2017). The ocean mixed layer under Southern Ocean sea-ice: Seasonal cycle and forcing. *Journal of Geophysical Research: Oceans*, *122*(2), 1608–1633. doi: 10.1002/2016JC011970

Perovich, D. K., Grenfell, T. C., Light, B., & Hobbs, P. V. (2002). Seasonal evolution of the albedo of multiyear Arctic sea ice. *Journal of Geophysical Research: Oceans*, *107*(C10), SHE 20–1-SHE 20–13. doi: 10.1029/2000JC000438

Perovich, D. K., Light, B., Eicken, H., Jones, K. F., Runciman, K., & Nghiem, S. V. (2007). Increasing solar heating of the Arctic Ocean and adjacent seas, 1979–2005: Attribution and role in the ice-albedo feedback. *Geophysical Research Letters*, *34*(19). doi: 10.1029/2007GL031480

Person, R., Vancoppenolle, M., Aumont, O., & Malsang, M. (2021). Continental and Sea Ice Iron Sources Fertilize the Southern Ocean in Synergy. *Geophysical Research Letters*, *48*(23), e2021GL094761. doi: 10.1029/2021GL094761

Polvani, L. M., & Smith, K. L. (2013). Can natural variability explain observed Antarctic sea ice trends? New modeling evidence from CMIP5. *Geophysical Research Letters*, *40*(12), 3195–3199. doi: 10.1002/grl.50578

Prather, M. J. (1986). Numerical advection by conservation of second-order moments. *Journal of Geophysical Research: Atmospheres*, *91*(D6), 6671–6681. doi: 10.1029/JD091iD06p06671

Pringle, D. J., Eicken, H., Trodahl, H. J., & Backstrom, L. G. E. (2007). Thermal conductivity of landfast Antarctic and Arctic sea ice. *Journal of Geophysical Research: Oceans*, *112*(C4). doi: 10.1029/2006JC003641

Purich, A., & Doddridge, E. W. (2023). Record low Antarctic sea ice coverage indicates a new sea ice state. *Communications Earth & Environment*, *4*(1), 1–9. doi: 10.1038/s43247-023-00961-9

Raphael, M. N., & Handcock, M. S. (2022). A new record minimum for Antarctic sea ice. *Nature Reviews Earth & Environment*, *3*(4), 215–216. doi: 10.1038/s43017-022-00281-0

Rathore, S., de Lavergne, C., Madec, G., Sallée, J.-B., Ethé, C., Nasser, A., & Vancoppenolle, M. (*in prep.*). Effects of improved tidal mixing in NEMO one-degree global ocean model (in preparation).

Riihelä, A., Bright, R. M., & Anttila, K. (2021). Recent strengthening of snow and ice albedo feedback driven by Antarctic sea-ice loss. *Nature Geoscience*, *14*, 832–836. doi: 10.1038/s41561-021-00841-x

Roach, L. A., Dörr, J., Holmes, C. R., Massonnet, F., Blockley, E. W., Notz, D., Rackow, T., Raphael, M. N., O'Farrell, S. P., Bailey, D. A., & Bitz, C. M. (2020). Antarctic Sea Ice Area in CMIP6. *Geophysical Research Letters*, *47*(9), e2019GL086729. doi: 10.1029/2019GL086729

Roach, L. A., Eisenman, I., Wagner, T. J. W., Blanchard-Wrigglesworth, E., & Bitz, C. M. (2022). Asymmetry in the seasonal cycle of Antarctic sea ice driven by insolation. *Nature Geoscience*, *15*(4), 277–281. doi: 10.1038/s41561-022-00913-6

Roach, L. A., Mankoff, K. D., Romanou, A., Blanchard-Wrigglesworth, E., Haine, T. W. N., & Schmidt, Gavin. A. (2023). Winds and Meltwater Together Lead to Southern Ocean Surface Cooling and Sea Ice Expansion. *Geophysical Research Letters*, *50*(24), e2023GL105948. doi: 10.1029/2023GL105948

Rockel, B., Will, A., & Hense, A. (2008). The Regional Climate Model COSMO-CLM (CCLM). *Meteorologische Zeitschrift*, 347–348. doi: 10.1127/0941-2948/2008/0309

Rousset, C., Vancoppenolle, M., Madec, G., Fichefet, T., Flavoni, S., Barthélemy, A., Benshila, R., Chanut, J., Levy, C., Masson, S., & Vivier, F. (2015). The Louvain-La-Neuve sea ice model LIM3.6: Global and regional capabilities. *Geoscientific Model Development*, *8*(10), 2991–3005. doi: 10.5194/gmd-8-2991-2015

Saenz, B. T., McKee, D. C., Doney, S. C., Martinson, D. G., & Stammerjohn, S. E. (2023). Influence of seasonally varying sea-ice concentration and subsurface ocean heat on sea-ice thickness and sea-ice seasonality for a 'warm-shelf' region in Antarctica. *Journal of Glaciology*, *69*(277), 1466–1482. doi: 10.1017/jog.2023.36

Sallée, J.-B., Pellichero, V., Akhoudas, C., Pauthenet, E., Vignes, L., Schmidtko, S., Garabato, A. N., Sutherland, P., & Kuusela, M. (2021). Summertime increases in upper-ocean stratification and mixed-layer depth. *Nature*, *591*(7851), 592–598. doi: 10.1038/s41586-021-03303-x

Schloesser, F., Friedrich, T., Timmermann, A., DeConto, R. M., & Pollard, D. (2019). Antarctic iceberg impacts on future Southern Hemisphere climate. *Nature Climate Change*, *9*(9), 672–677. doi: 10.1038/s41558-019-0546-1

Schlosser, E., Haumann, F. A., & Raphael, M. N. (2018). Atmospheric influences on the anomalous 2016 Antarctic sea ice decay. *The Cryosphere*, *12*(3), 1103–1119. doi: 10.5194/tc-12-1103-2018

Schroeter, S., O'Kane, T. J., & Sandery, P. A. (2023). Antarctic sea ice regime shift associated with decreasing zonal symmetry in the Southern Annular Mode. *The Cryosphere*, *17*(2), 701–717. doi: 10.5194/tc-17-701-2023

Semtner, A. J. (1976). A Model for the Thermodynamic Growth of Sea Ice in Numerical Investigations of Climate. *Journal of Physical Oceanography*, *6*(3), 379–389. doi: 10.1175/1520-0485(1976)006<0379:AMFTTG>2.0.CO;2

Shadwick, E. H., Meo, O. A. D., Schroeter, S., Arroyo, M. C., Martinson, D. G., & Ducklow, H. (2021). Sea Ice Suppression of CO2 Outgassing in the West Antarctic Peninsula: Implications For The Evolving Southern Ocean Carbon Sink. *Geophysical Research Letters*, *48*(11), e2020GL091835. doi: 10.1029/2020GL091835

Simpkins, G. R., Ciasto, L. M., & England, M. H. (2013). Observed variations in multidecadal Antarctic sea ice trends during 1979–2012. *Geophysical Research Letters*, *40*(14), 3643–3648. doi: 10.1002/grl.50715

Simpkins, G. R., Ciasto, L. M., Thompson, D. W. J., & England, M. H. (2012). Seasonal Relationships between Large-Scale Climate Variability and Antarctic Sea Ice Concentration. doi: 10.1175/JCLI-D-11-00367.1

Singh, H. A., Polvani, L. M., & Rasch, P. J. (2019). Antarctic Sea Ice Expansion, Driven by Internal Variability, in the Presence of Increasing Atmospheric CO2. *Geophysical Research Letters*, *46*(24), 14762–14771. doi: 10.1029/2019GL083758

Smith, A., Jahn, A., & Wang, M. (2020). Seasonal transition dates can reveal biases in Arctic sea ice simulations. *The Cryosphere*, *14*(9), 2977–2997. doi: 10.5194/tc-14-2977-2020

Smith, W. O., Jr., & Nelson, D. M. (1986). Importance of Ice Edge Phytoplankton Production in the Southern Ocean. *BioScience*, *36*(4), 251–257. doi: 10.2307/1310215

Stammerjohn, S., Massom, R., Rind, D., & Martinson, D. (2012). Regions of rapid sea ice change: An inter-hemispheric seasonal comparison. *Geophysical Research Letters*, *39*(6). doi: 10.1029/2012GL050874

Stammerjohn, S. E., Martinson, D. G., Smith, R. C., Yuan, X., & Rind, D. (2008). Trends in Antarctic annual sea ice retreat and advance and their relation to El Niño–Southern Oscillation and Southern Annular Mode variability. *Journal of Geophysical Research: Oceans*, *113*(C3). doi: 10.1029/2007JC004269

Storkey, D., Blaker, A. T., Mathiot, P., Megann, A., Aksenov, Y., Blockley, E. W., Calvert, D., Graham, T., Hewitt, H. T., Hyder, P., Kuhlbrodt, T., Rae, J. G. L., & Sinha, B. (2018). UK Global Ocean GO6 and GO7: A traceable hierarchy of model resolutions. *Geoscientific Model Development*, *11*(8), 3187–3213. doi: 10.5194/gmd-11-3187-2018

Stroeve, J. C., Crawford, A. D., & Stammerjohn, S. (2016). Using timing of ice retreat to predict timing of fall freeze-up in the Arctic. *Geophysical Research Letters*, *43*(12), 6332–6340. doi: 10.1002/2016GL069314

Stuecker, M. F., Bitz, C. M., & Armour, K. C. (2017). Conditions leading to the unprecedented low Antarctic sea ice extent during the 2016 austral spring season. *Geophysical Research Letters*, *44*(17), 9008–9019. doi: 10.1002/2017GL074691

Su, Z. (2017). Preconditioning of Antarctic maximum sea ice extent by upper ocean stratification on a seasonal timescale. *Geophysical Research Letters*, *44*(12), 6307–6315. doi: 10.1002/2017GL073236

Swart, N. C., & Fyfe, J. C. (2013). The influence of recent Antarctic ice sheet retreat on simulated sea ice area trends. *Geophysical Research Letters*, *40*(16), 4328–4332. doi: 10.1002/grl.50820

Swart, S., Gille, S. T., Delille, B., Josey, S., Mazloff, M., Newman, L., Thompson, A. F., Thomson, J., Ward, B., du Plessis, M. D., Kent, E. C., Girton, J., Gregor, L., Heil, P., Hyder, P., Pezzi, L. P., de Souza, R. B., Tamsitt, V., Weller, R. A., & Zappa, C. J. (2019). Constraining Southern Ocean Air-Sea-Ice Fluxes Through Enhanced Observations. *Frontiers in Marine Science*, *6*. doi: 10.3389/fmars.2019.00421

Talley, L. D., Pickard, G. L., Emery, W. J., & Swift, J. H. (2011). Chapter 3 - Physical Properties of Seawater. In L. D. Talley, G. L. Pickard, W. J. Emery, & J. H. Swift (Eds.), *Descriptive Physical Oceanography (Sixth Edition)* (pp. 29–65). Boston: Academic Press. doi: 10.1016/B978-0-7506-4552-2.10003-4

Tamura, T., Ohshima, K., Nihashi, S., & Hasumi, H. (2011). Estimation of Surface Heat/Salt Fluxes Associated with Sea Ice Growth/Melt in the Southern Ocean. *Scientific online letters on the atmosphere: SOLA*, *7*, 17–20. doi: 10.2151/sola.2011-005

Thompson, D. W. J., Solomon, S., Kushner, P. J., England, M. H., Grise, K. M., & Karoly, D. J. (2011). Signatures of the Antarctic ozone hole in Southern Hemisphere surface climate change. *Nature Geoscience*, *4*(11), 741–749. doi: 10.1038/ngeo1296

Thompson, L., Smith, M., Thomson, J., Stammerjohn, S., Ackley, S., & Loose, B. (2020). Frazil ice growth and production during katabatic wind events in the Ross Sea, Antarctica. *The Cryosphere*, *14*(10), 3329–3347. doi: 10.5194/tc-14-3329-2020

Turner, J., Holmes, C., Caton Harrison, T., Phillips, T., Jena, B., Reeves-Francois, T., Fogt, R., Thomas, E. R., & Bajish, C. C. (2022). Record Low Antarctic Sea Ice Cover in February 2022. *Geophysical Research Letters*, *49*(12), e2022GL098904. doi: 10.1029/2022GL098904

Turner, J., Maksym, T., Phillips, T., Marshall, G. J., & Meredith, M. P. (2013). The impact of changes in sea ice advance on the large winter warming on the western Antarctic Peninsula. *International Journal of Climatology*, *33*(4), 852–861. doi: 10.1002/joc.3474

Turner, J., Phillips, T., Marshall, G. J., Hosking, J. S., Pope, J. O., Bracegirdle, T. J., & Deb, P. (2017). Unprecedented springtime retreat of Antarctic sea ice in 2016. *Geophysical Research Letters*, *44*(13), 6868–6875. doi: 10.1002/2017GL073656

Vancoppenolle, M., Fichefet, T., & Goosse, H. (2009). Simulating the mass balance and salinity of Arctic and Antarctic sea ice. 2. Importance of sea ice salinity variations. *Ocean Modelling*, *27*(1), 54–69. doi: 10.1016/j.ocemod.2008.11.003

Vancoppenolle, M., Rousset, C., Blockley, E., Aksenov, Y., Feltham, D., Fichefet, T., Garric, G., Guémas, V., Iovino, D., Keeley, S., Madec, G., Massonnet, F., Ridley, J., Schroeder, D., & Tietsche, S. (2023). SI3, the NEMO Sea Ice Engine.
doi: 10.5281/zenodo.7534900

Vancoppenolle, M., Timmermann, R., Ackley, S. F., Fichefet, T., Goosse, H., Heil, P., Leonard, K. C., Lieser, J., Nicolaus, M., Papakyriakou, T., & Tison, J.-L. (2011). Assessment of radiation forcing data sets for large-scale sea ice models in the Southern Ocean. *Deep Sea Research Part II: Topical Studies in Oceanography*, *58*(9), 1237–1249. doi: 10.1016/j.dsr2.2010.10.039

Verfaillie, D., Pelletier, C., Goosse, H., Jourdain, N. C., Bull, C. Y. S., Dalaiden, Q., Favier, V., Fichefet, T., & Wille, J. D. (2022). The circum-Antarctic ice-shelves respond to a more positive Southern Annular Mode with regionally varied melting. *Communications Earth & Environment*, *3*(1), 1–12. doi: 10.1038/s43247-022-00458-x

Vialard, J., & Delecluse, P. (1998). An OGCM Study for the TOGA Decade. Part I: Role of Salinity in the Physics of the Western Pacific Fresh Pool. *Journal of Physical Oceanography*, *28*(6), 1071–1088. doi: 10.1175/1520-0485(1998)028<1071:AOSFTT>2.0.CO;2

Vivier, F., Hutchings, J. K., Kawaguchi, Y., Kikuchi, T., Morison, J. H., Lourenço, A., & Noguchi, T. (2016). Sea ice melt onset associated with lead opening during the spring/summer transition near the North Pole. *Journal of Geophysical Research: Oceans*, *121*(4), 2499–2522. doi: 10.1002/2015JC011588

Weeks, W. F., Ackley, S. F., & Govoni, J. (1989). Sea ice ridging in the Ross Sea, Antarctica, as compared with sites in the Arctic. *Journal of Geophysical Research: Oceans*, *94*(C4), 4984–4988. doi: 10.1029/JC094iC04p04984

Wilson, E. A., Riser, S. C., Campbell, E. C., & Wong, A. P. S. (2019). Winter Upper-Ocean Stability and Ice–Ocean Feedbacks in the Sea Ice–Covered Southern Ocean. *Journal of Physical Oceanography*, *49*(4), 1099–1117. doi: 10.1175/JPO-D-18-0184.1

Worby, A. P., Geiger, C. A., Paget, M. J., Van Woert, M. L., Ackley, S. F., & DeLiberty, T. L. (2008). Thickness distribution of Antarctic sea ice. *Journal of Geophysical Research: Oceans*, *113*(C5). doi: 10.1029/2007JC004254

Yuan, X. (2004). ENSO-related impacts on Antarctic sea ice: A synthesis of phenomenon and mechanisms. *Antarctic Science*, *16*(4), 415–425. doi: 10.1017/S0954102004002238

Zhang, J. (2014). Modeling the Impact of Wind Intensification on Antarctic Sea Ice Volume. *Journal of Climate*, *27*(1), 202–214. doi: 10.1175/JCLI-D-12-00139.1

Zhang, L., Delworth, T. L., Cooke, W., & Yang, X. (2019). Natural variability of Southern Ocean convection as a driver of observed climate trends. *Nature Climate Change*, *9*(1), 59–65. doi: 10.1038/s41558-018-0350-3

Zhang, L., Delworth, T. L., Yang, X., Zeng, F., Lu, F., Morioka, Y., & Bushuk, M. (2022). The relative role of the subsurface Southern Ocean in driving negative Antarctic Sea ice extent anomalies in 2016–2021. *Communications Earth & Environment*, *3*(1), 1–9. doi: 10.1038/s43247-022-00624-1

Zunz, V., Goosse, H., & Massonnet, F. (2013). How does internal variability influence the ability of CMIP5 models to reproduce the recent trend in Southern Ocean sea ice extent? *The Cryosphere*, *7*(2), 451–468. doi: 10.5194/tc-7-451-2013